Transition Metal-Free Hydroxylation of (Hetero)aromatic Halides

Patrycja Ubysz

MSc by Research

University of York

Chemistry

December 2021

Abstract

This thesis describes the development of a transition metal-free procedure for hydroxylation of (hetero)aromatic halides. Chapter 1 outlines previous efforts in the areas of arene hydroxylation and substitution through electron transfer. A rationally designed, universal oxime-based nucleophile was synthesised and used as a hydroxide surrogate in the attempted hydroxylation of halides, which was described in Chapter 2. It was demonstrated through an extensive scoping that most of the electron-poor aromatic substrates, in particular the aryl halides bearing an electron-withdrawing group (EWG) in *para*-position to halide, were compatible with the mild conditions proposed and successfully underwent transformation at a temperature as low as 30°C. The reactions of dihalogenated compounds exhibited a level of selectivity. The scope of the proposed transformation was expanded after re-optimisation at higher temperatures (60 and 100°C), and the procedure's performance was significantly improved in substrates such as halides bearing an EWG in *meta*-position and less electron-deficient substrates.

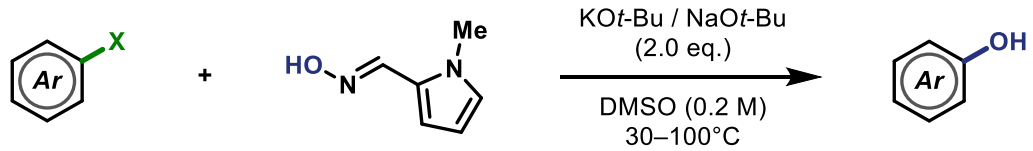

Mechanistic studies involving radical trapping indicated that the process is of at least partially radical nature – participation of $S_{RN}1$ processes is suspected. UV-vis spectroscopy studies were also performed, revealing possible participation of a 1:1 nucleophile to halide charge-transfer complex in the initiation stage. The potential of the developed method for late-stage functionalisation was explored and confirmed through experiments on aryl halide-containing drug molecules.

Table of Contents

List of Tables

List of Figures

Acknowledgments

Firstly, I would like to thank Dr Michael James, my supervisor, for his consistent support, patience, and guidance through this difficult year. Many thanks to my co-supervisor, Prof. Peter O'Brien and the independent panel member Dr Victor Chechik for all the support and insightful comments regarding my research.

Thanks to Heather and Alex for their efforts in NMR centre, Karl for running mass spectrometry, and Mike and Steve for running stores. I would like to thank the group I worked with on a daily basis: Andrew, George, Will, Min, Illya and Zhongzhen, for help and assistance and making my time in the laboratory fun and enjoyable.

Many thanks to The Wild Fund for making my stay in York financially feasible.

Finally, thank you to my family and dear friends who have always provided a shoulder to cry on when needed, and precious advice, these include, in no particular order: Niall, Andy, Rose, Marcus, Benedict, Ryan, Emma, Maja, Kuba, Charlotte, Martin, Zoe, Stefan, Lucille, Dean and Lorna. I am immensely grateful for their presence in my life, as I would not be where I am today without them.

Declaration

I declare that this thesis is a presentation of original work and I am the sole author. This work has not previously been presented for an award at this, or any other, University. All sources are acknowledged as References.

List of Abbreviations

1,1-DPE	1,1-diphenylethylene
A	acceptor
Ac	acyl group
Ad	adamantyl
APS	ammonium persulfate
Ar	aryl
atm	the standard atmosphere unit
BDE	bond dissociation energy
BDFE	bond dissociation free energy
Boc	*tert*-butoxycarbonyl
Bu	butyl group
cat.	catalyst
CTC	charge-transfer complex
D	donor
d	doublet
DCE	dichloroethane
DIPEA	*N*,*N*-diisopropylethylamine
DMF	dimethylformamide
DMI	1,3-dimethyl-2-imidazolidinone
DMPU	*N,N'*-dimethylpropyleneurea
DMSO	dimethyl sulfoxide
dppe	1,2-bis(diphenylophosphino)ethane
E1cB	elimination unimolecular conjugate base
eq.	equivalent
ET	electron transfer
EWG	electron-withdrawing group
h	hour
HOMO	Highest Occupied Molecular Orbital
HPLC	high performance liquid chromatography
HRMS	high resolution mass spectroscopy
kcal	kilocalories
KOt-Bu	potassium *tert*-butoxide
KPS	potassium persulfate
liq	liquid
LSF	late-stage functionalisation
LUMO	Lowest Unoccupied Molecular Orbital
M	metal
m	multiplet
m/z	mass to charge ratio
M+	molecular ion
Me	methyl group
nm	nanometre(s)
NMP	*N*-methyl-2-pyrrolidone
NMR	nuclear magnetic resonance

Nu	nucleophile
Ph	phenyl group
pKa	acid dissociation constant
R	organic group
rt	room temperature
s	second
s	singlet
SCE	saturated calomel electrode
SHE	standard hydrogen electrode
S_NAr	Aromatic Nucleophilic Substitution
SOMO	Singly Occupied Molecular Orbital
$S_{RN}1$	Radical Nucleophilic Substitution
TEMPO	(2,2,6,6-tetramethylpiperidin-1-yl)oxyl
TFA	trifluoroacetic acid
THF	tetrahydrofuran
TMEDA	tetramethylethylenediamine
V	volt
ΔG	Gibbs free energy

Chapter 1. Introduction

1.1. Phenols and Phenol Derivatives

Phenols and their derivatives are incredibly versatile compounds, not only are they a frequent feature of biologically relevant molecules, but they are also a central element of many pharmaceuticals, like aspirin **1**, Masoprocol **2** or epinephrine **3** (Scheme 1a).[1,2] The synthesis of such molecules usually starts with substrates already containing the phenol functionality, which are either obtained from natural sources or via hydroxylation reactions, such as the Hock process (Scheme 1b). It is estimated that the amount of phenol produced by Hock process yearly exceeds 12.7 million tonnes.[3] Whilst clearly this process is of great commercial value, the harsh reaction conditions needed to install the hydroxyl functionality on an aromatic ring limits compatibility with more advanced synthetic intermediates and the possibility of late-stage hydroxylation.

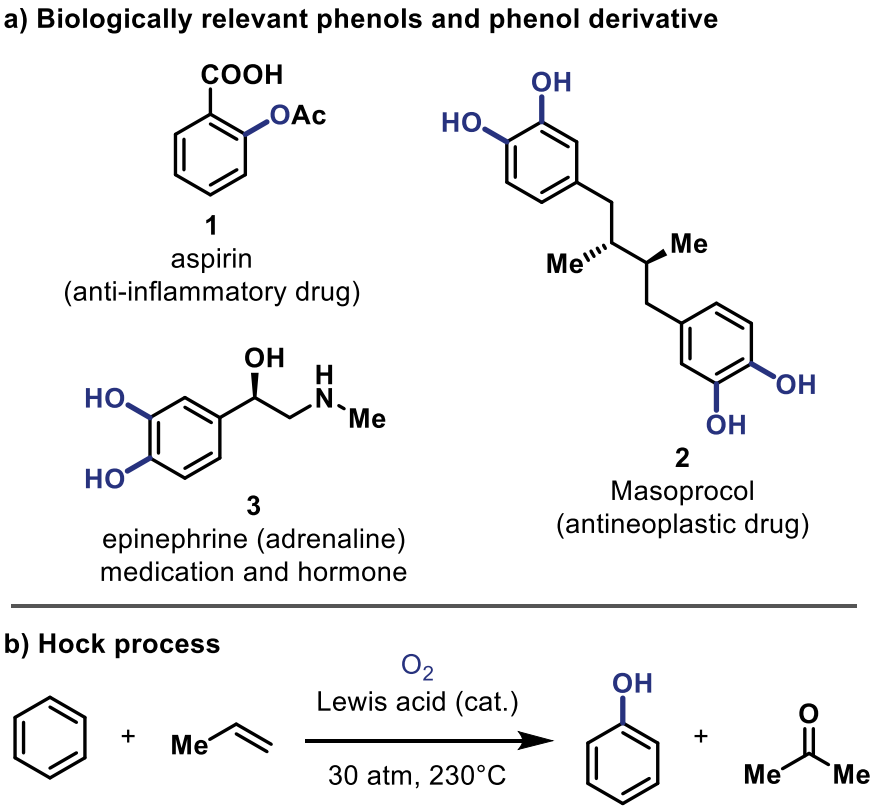

Scheme 1. a) example phenolic drug compounds, b) Hock process scheme.

The development of milder arene hydroxylation reaction conditions has been the target of many research groups. For example, the direct C–H hydroxylation of alkylarylketones **4** has recently been reported by Kwong, Choy and co-workers using catalytic amounts of a

palladium(II) complex (Scheme 2).[4] Importantly, the use of a transition metal catalyst and milder reaction conditions enabled compatibility with a variety of functional groups.

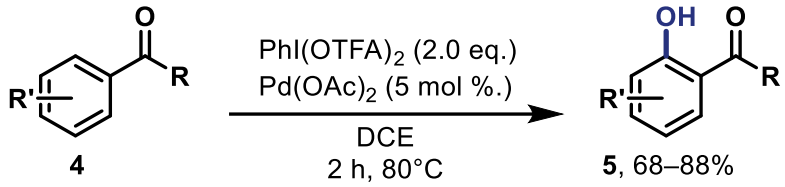

Scheme 2. Palladium-catalysed C–H hydroxylation.

1.2. Synthesis through Functional Group Substitution

Despite the synthetic appeal of direct arene C–H hydroxylation/etherification, the displacement of other functional groups with oxygen-based nucleophiles is one of the most widely used methods in organic synthesis. In this regard, nucleophilic aromatic substitutions (S_NAr) are amongst the most prominent reactions in medicinal chemistry, likely due to the availability and low cost of reagents.[5] Indeed, this class of reaction became so widely used, it became, and remains, a 'go-to method' in the field of drug discovery despite the development of many new synthetic protocols.[6–9] According to a recent review by Brown and Bostrom, aromatic nucleophilic substitution was the second most often used method in medicinal chemistry in 2014, appearing in around 30% of the examined papers.[5]

Nucleophilic aromatic substitution has been well utilised in C–O coupling reactions. For example, Qian and co-workers reported the substitution of aryl fluorides by alkoxides via an S_NAr process.[10] The reactions of *ortho*- substituted fluorobenzenes **6** with cyclopropanol **7** yielded analogous aryl ethers **8** (Scheme 3a), while none of the *meta*-substituted **9** were successfully substituted under these reaction conditions. Fluorobenzenes with electron-donating substituents were not converted to their corresponding ethers, likely due to the repulsive interaction between the electron-rich arene and negatively charged nucleophile.

Stumpf and co-workers used similar conditions in the synthesis of Nav1.7 inhibitor GDC-0310 **14** – a membrane protein taking part in propagating a pain signal.[11] Difluorobenzene derivative **10** was substituted with *N*-Boc-4-piperidinemethanol **11** in the presence of potassium *tert*-butoxide (KO*t*-Bu) to yield the ether **12** (Scheme 3b). Interestingly, the group was able to manipulate the selectivity of this reaction and thus minimise the undesired isomer **13** formation by careful adjustment of the base and solvent combination. Bases like DIPEA,

NaH and KOH in solvents NMP, DMF, DMSO and THF led to high levels of conversion (73–98%), but HPLC analyses showed significant formation of the side product **13**.

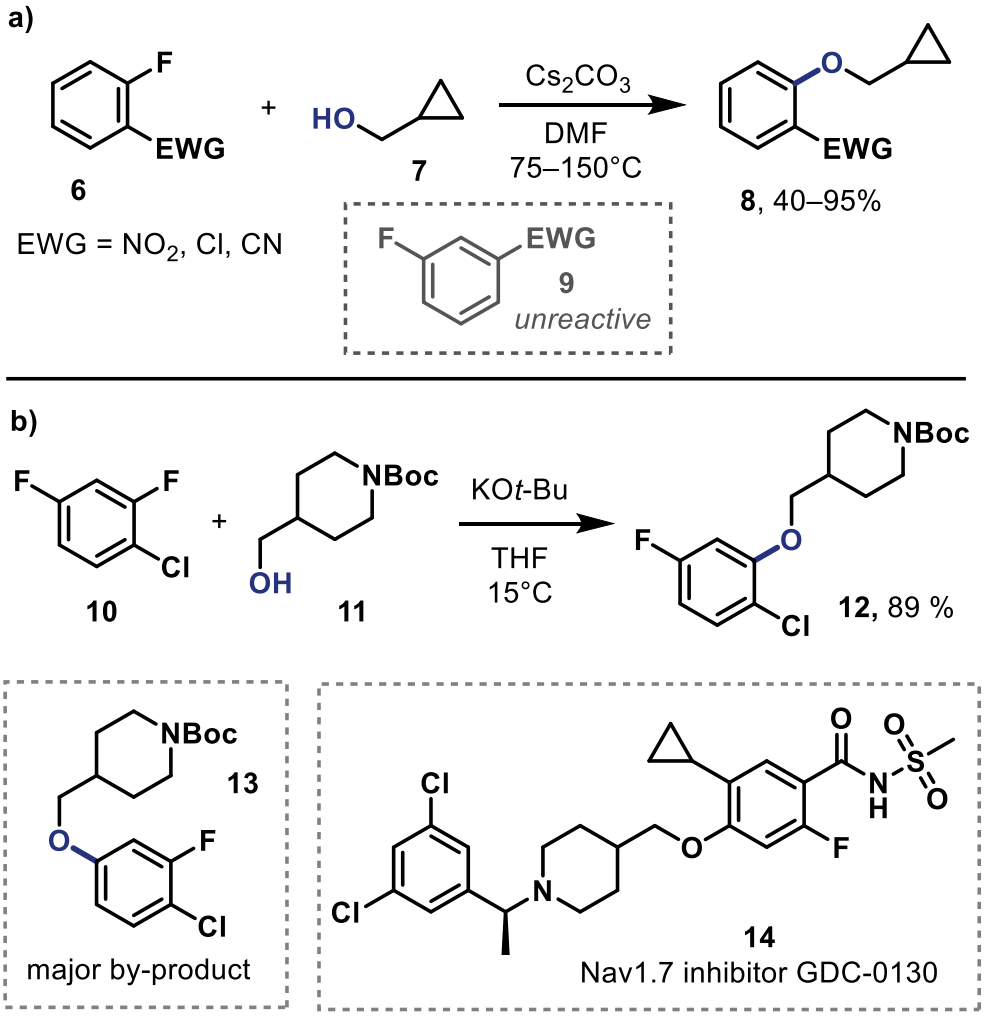

Scheme 3. Examples of alkoxide C–O coupling reactions. a) Quian's proposed substitution of ortho-substituted fluorobenzenes;[10] b) Stumpf's procedure for substitution of a difluorobenzene.[11]

Procedures of substitution with hydroxide, using hydroxide surrogates were also reported. For example, Krapcho and Waterhouse developed a substitution protocol using trimethylsilanoate to substitute anthracenedione derivatives **15**.[12] The resulting silyl ethers **16** are then cleaved by reaction with the liberated fluoride anions to form the unprotected hydroxyl group (Scheme 4a). Rogers and Green developed an alternative strategy for the substitution of electron-poor fluoroarenes **18** using 2-(methylsulfonyl) ethanol.[13] Following substitution, the deprotonation of the intermediate **19** leads to the formation of the phenol product **20** in situ (Scheme 4b). Levin and Du developed a related hydroxylation procedure in which electron-deficient aryl fluorides **21** are substituted by deprotonated 2-butyn-1-ol. The substituted product **22**

undergoes facile isomerisation to afford allenyl ether **23**, which can then be hydrolysed to afford the phenol product **24** (Scheme 4c).[14] Finally, Fier and Maloney showed that hydroxamic acid could also be used as a mild hydroxide surrogate (Scheme 4d).[15] Here, the phenol product **27** is formed *in situ* via Lossen rearrangement of the intermediate **26**.

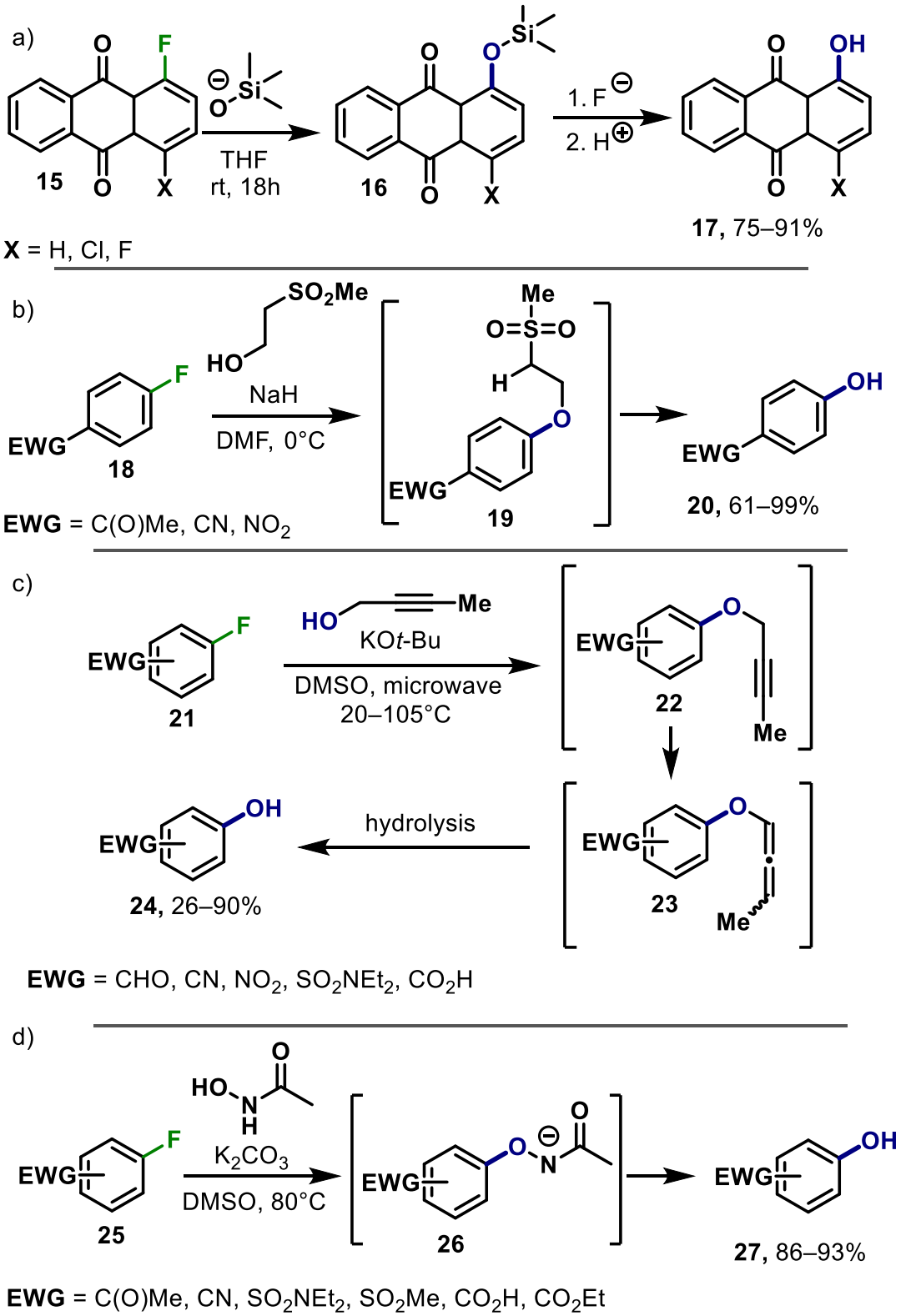

Scheme 4. Substitutions of aryl fluorides with hydroxide via reactions with various hydroxide surrogates: a) trimethylsilanoate; b) 2-(methylsulfonyl) ethanol; c) 2-butyn-1-ol; d) hydroxamic acid.

Interestingly, even though the nucleophilic aromatic substitution was known as early as 1850s,[16] its mechanism has been an area of active interest in recent years.[17] A stepwise addition-elimination mechanism was long assumed to be operative (Scheme 5) due to the isolation and characterisation of anionic intermediates by Meisenheimer and co-workers.[18] In their work, the reaction of 1-methoxy-2,4,6-trinitrobenzene **28** with generated *in situ* sodium ethoxide, as well as the reaction between 1-ethoxy-2,4,6-trinitrobenzene **29** and sodium methoxide, yielded an identical mixtures of products **28** and **29** (Scheme 5). This finding indicated that both reactions proceed through a common intermediate **30**.

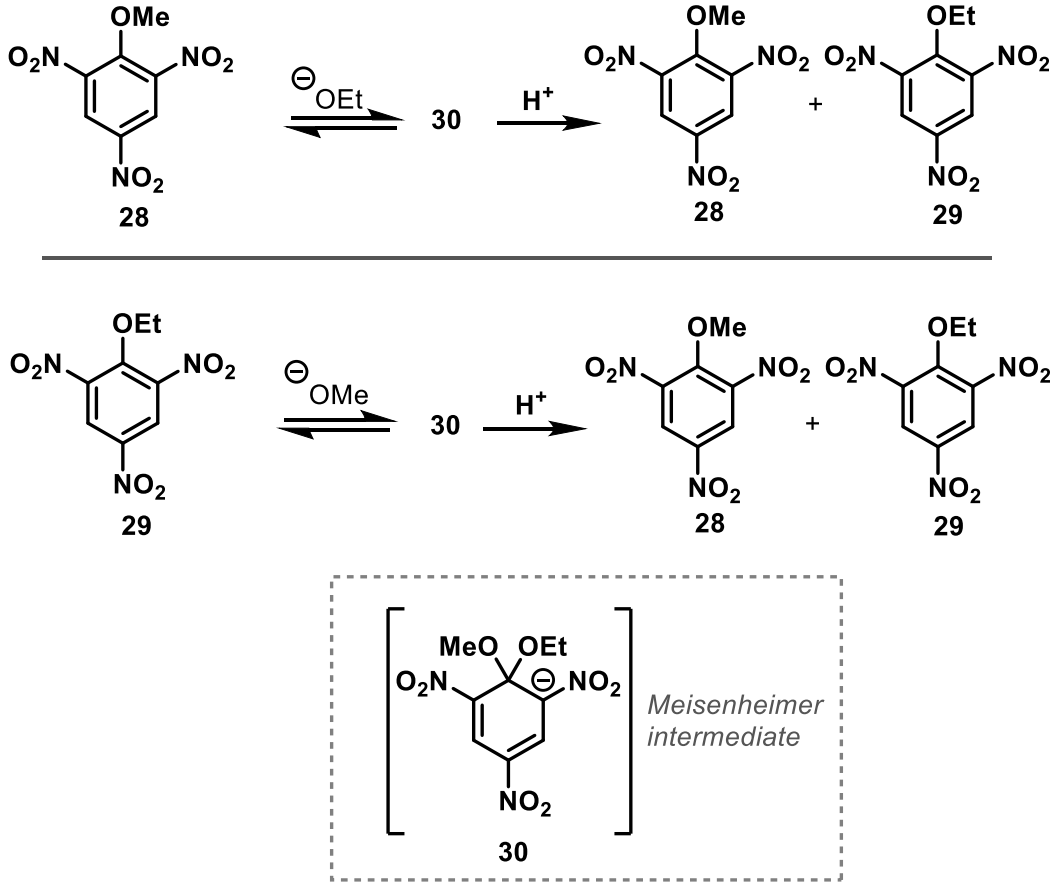

Scheme 5. Meisenheimer's S_NAr experiment.

As the well-established addition-elimination stepwise mechanism involves formation of an intermediate - an anionic Meisenheimer complex (Scheme 6a), the range of substrates is limited to electron-poor aromatic systems with highly polarised bonds to leaving groups such as F^-. Conversely, a concerted process (Scheme 6b) has recently been proposed, which has a lower need for the presence of electron withdrawing groups on the aromatic reactants. Interestingly, there is growing evidence to suggest that a Meisenheimer intermediate is only formed in reactions with nitro-substituted arenes and/or F^- as the leaving group.[19]

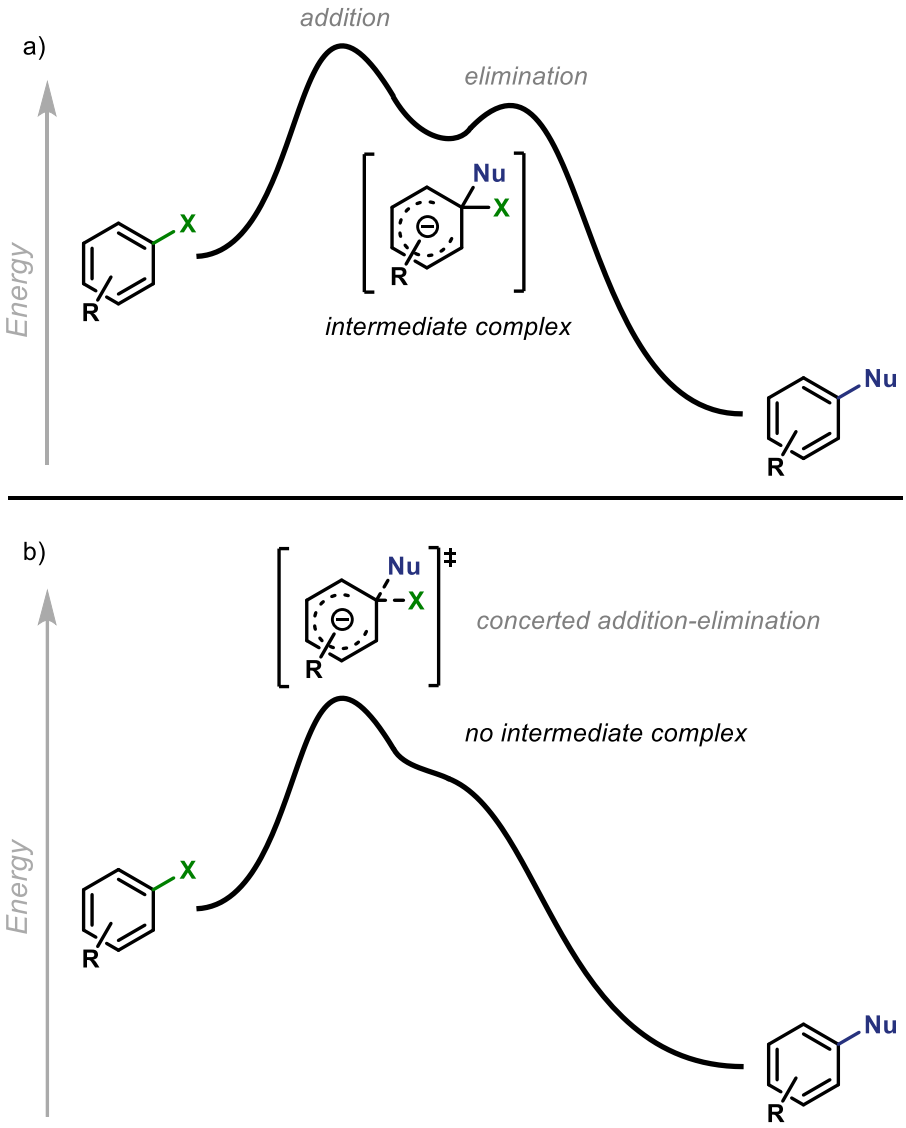

Scheme 6. Energy profile diagrams of a) stepwise S_NAr b) concerted S_NAr.

One of the earliest indications of a concerted mechanism, was observed by Handel and co-workers in 1980,[20] who studied the reaction between halobenzenes **31** and KH in deuterated THF. Analysis of the products led to the conclusion that substituting H in the final product **33** comes from potassium hydride and not the solvent (Scheme 7). Moreover, the order of reactivity of halides was as follows: ArI > ArBr > ArCl > ArF, reverse from a 'standard' stepwise addition-elimination S_NAr. Although no further mechanistic investigation was performed, the authors suggested a concerted mechanism takes place.

The procedure was revisited almost 30 years later, by Tuttle, Murphy, and coworkers.[21] The group provided further evidence for the formation of the concerted 4-membered transition state **32**. Around the same time, Jacobsen and co-workers studied aromatic nucleophilic

substitution reactions and revealed that concerted pathway can be indeed more common than previously anticipated, especially in absence of -NO_2 substituents and poor leaving groups.[22]

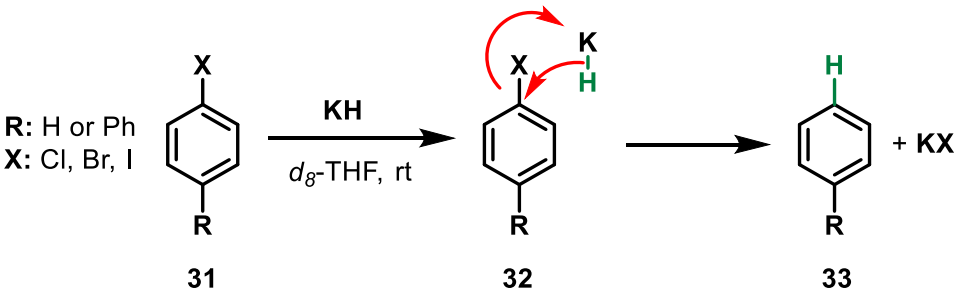

Scheme 7. Concerted S_NAr process with potassium hydride, originally proposed by Handel.

Alongside advances in the development of direct (concerted or stepwise) S_NAr reactions, a number of mild transition-metal-catalysed methods have also been developed which can enable compatibility with wider variety of substrates.

One of the examples of a transition-metal-catalysed hydroxylation reaction was reported by Hansen and co-workers (Scheme 8).[23] First, a diazonium salt is formed in situ from the aniline **34** and later transformed into the corresponding phenol **35** with the addition of copper(II) sulfate and copper(I) oxide. This method is carried out under aqueous conditions and therefore the scope of the reaction might suffer from the low solubility of certain substrates in water.

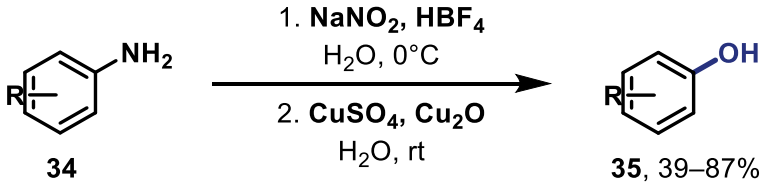

Scheme 8. Copper-catalysed hydroxylation through formation of diazonium salt *in situ*.

Ma and co-workers developed a hydroxylation procedure requiring only small loading (up to 10 mol %) of copper catalyst (Scheme 9) and the organic ligand **40**.[24] They have demonstrated compatibility of the conditions with wide scope of (hetero)aryl chlorides, bromides and iodides.

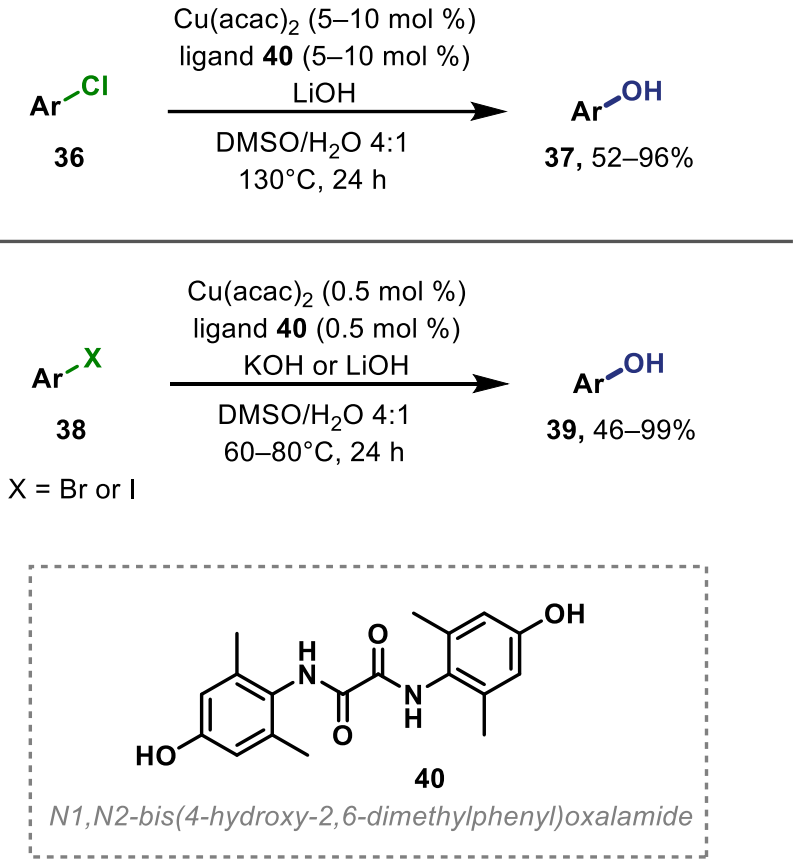

Scheme 9. Hydroxylation procedures for (hetero)aryl chlorides, bromides and iodides with small copper catalyst and ligand loadings.

Fier and Maloney designed a novel nucleophilic hydroxide surrogate, oxime **41**, which could be coupled with a broad range of aryl halides using copper- or palladium catalysis (Scheme 10).[15,25] An oxime was used to ensure: i) oxygen nucleophilicity, and ii) an easy O–N bond cleavage. Oxime ethers **42** are readily degraded in basic conditions, thus removing the need for an additional deprotection step.

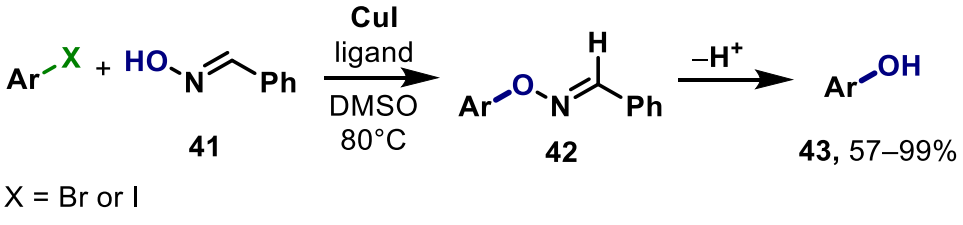

Scheme 10. Aryl halide substitution with benzaldoxime.

Interestingly, Maitra and co-workers also coupled similar oxime derivatives **45** with aryl iodides **44** to afford *O*-aryl oximes **45** (Scheme 11).[26] The authors proposed the involvement of an aryl radical in the reaction mechanism, although did not investigate this further.

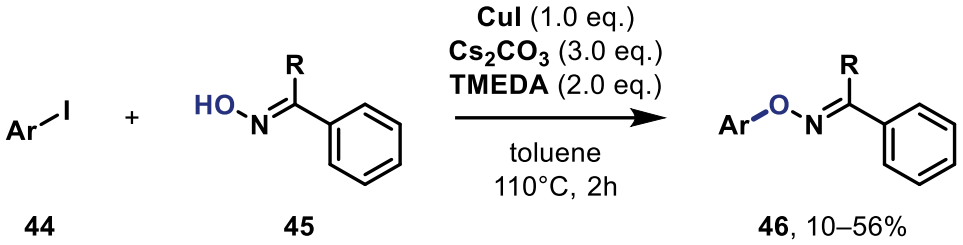

Scheme 11. Coupling reaction between an aryl halide and oxime **45**.

1.3. Substitution through Electron Transfer

If one were to exclude transition metals, there are organic-based radical methods that can also be used to overcome the limitations of polar S_NAr mechanisms whilst avoiding the disadvantages of using transition metals in synthesis, like their cost, toxicity and disposal issues.[27] For example, Cai and co-workers demonstrated that aryl iodides **47** can be converted into phenols **50** via a radical pathway under photochemical, transition-metal-free conditions (Scheme 12).[28] The group used ^{18}O labelling to provide an evidence for the role of molecular oxygen as a source of oxygen in the phenol product.

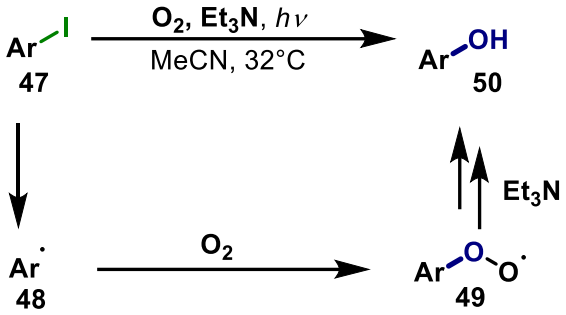

Scheme 12. Proposed mechanism of hydroxylation performed with atmospheric oxygen.

Aryl radical intermediates are also known to couple with anionic nucleophiles in a radical chain process called radical-nucleophilic substitution ($S_{RN}1$). It is worth noting that breaking of a bond in a radical ion is often less energetically demanding than breaking the same bond in the analogous closed-shell molecule.[29] In addition, although this thesis focuses exclusively on aryl halides, the list of substrates and nucleophiles compatible with the radical-nucleophilic substitution mechanism is extensive. Several experiments have been done on aryl halides,[30] nitroarenes,[31] vinyl halides and pseudohalides,[32,33] and even aliphatic nitrates and halides.[34,35]

The general $S_{RN}1$mechanism first proposed by Kornblum, Michel and Kerber in 1966[36] (Scheme 13) typically starts with the one-electron reduction of an Ar–X or alkyl–X coupling partner **51** to form a radical anion **52**. This radical-anion intermediate may then fragment to form a radical species **53**. Alternatively, electron transfer and bond-breaking may occur in a concerted process, which leads directly to the formation of radical **53** from **51**. The radical **53** can then couple with an anionic nucleophile **54** to form a radical anion **55**. The transfer of an electron from **55** to another molecule of the coupling partner **51** affords the neutral, coupled product **56** and radical anion **52** which re-enters the cycle. The number of times the cycle is repeated is also called chain length. Each step of this proposed radical chain will be discussed separately in the following subsections.

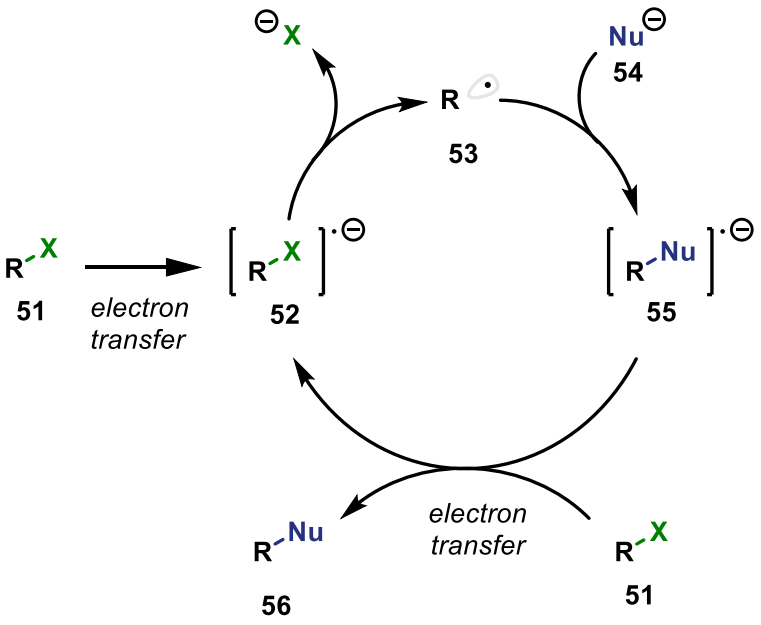

Scheme 13. Overview of the $S_{RN}1$ mechansim.

1.3.1. Initiation

An $S_{RN}1$ chain can be initiated by several ways, and most usually using methods like photoexcitation,[27] microwaves,[37–39] solvated electrons,[40] transition metals,[41] and sonication,[42] to promote an electron transfer event from a donor to the coupling partner.

Initiation through spontaneous thermal electron transfer (Figure 1) between the nucleophile and coupling partner is not uncommon but requires specific conditions and reagents.[43]

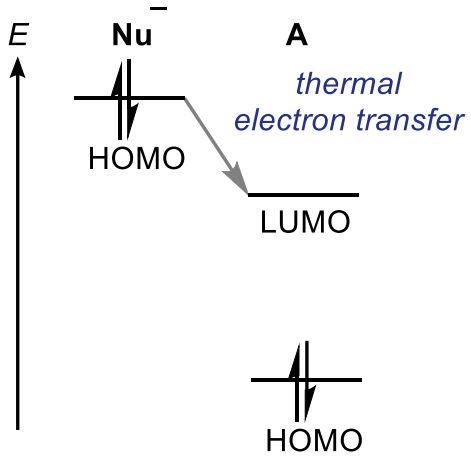

Figure 1. Thermal electron transfer between nucleophile and acceptor molecule.

If the reducing power of the nucleophile is insufficient, it can be replaced with small amount of a sacrificial substance in a process called entrainment (Scheme 14a).[27] An example of

entrainment was recently described by Wang and co-workers, who heated Rongalite **57** to promote the formation of highly reducing sulfur dioxide radical-anions ($SO_2^{\bullet-}$, Scheme 14b), which could be used to entrain various C–C, C–S and C–P $S_{RN}1$ coupling reactions.[30] More recently, Rossi and co-workers also proposed that dimsyl anion **58** may also be an efficient electron donor and could be the species responsible for initiating many $S_{RN}1$ reactions.[44]

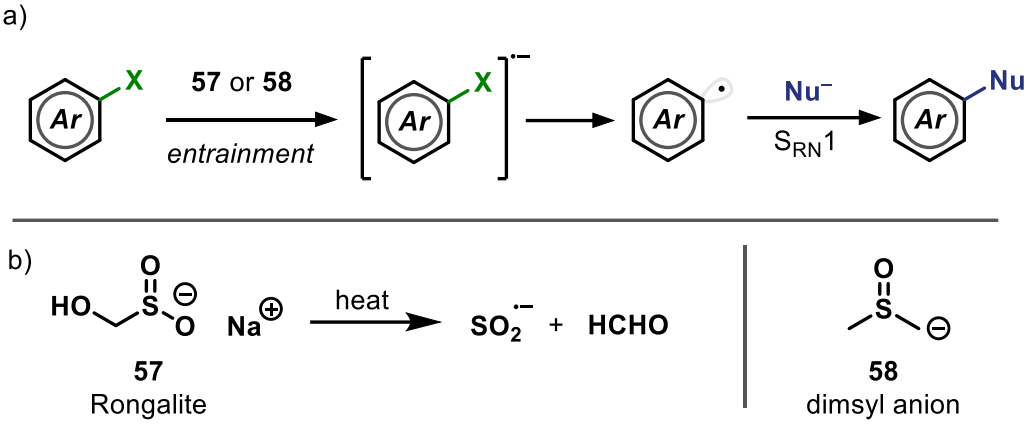

Scheme 14. a) initiation under entrainment conditions, b) examples of electron donors and decomposition of Rongalite.

Alternatively, a photoexcited electron donor (D*) can also be used if its ground-state reducing power is insufficient. The donor may be the nucleophile itself, a photocatalyst, or a sacrificial electron donor.[45–47] For example, Pierini and co-workers photoexcited the thiophenolate anion **59** to promote coupling with iodocubane **60** (Scheme 15b).

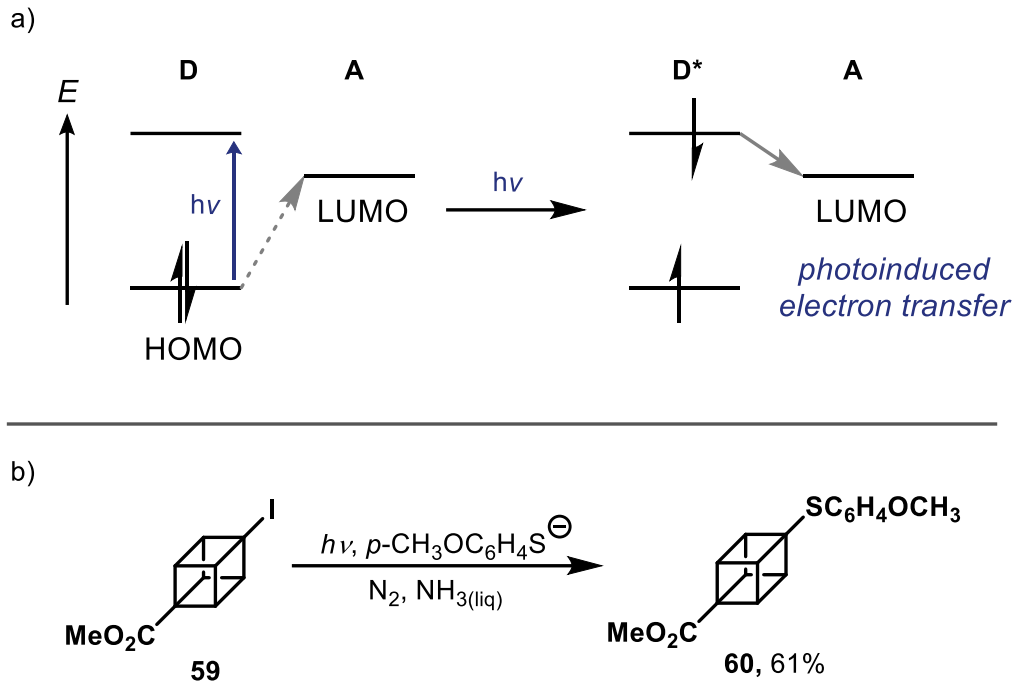

Scheme 15. a) photoinduced electron transfer, b) photoinitiated substitution of an iodocubane.

Additionally, some electron donors can also form charge-transfer complexes (CTCs) with electron acceptors. A CTC is a species formed as a result of a non-covalent association between the donor (D) and the acceptor (A). Such complexes possess different physical properties than D and A separately as new molecular orbitals are formed.[48] The formation of CTCs can be easily identifiable by a change of the reaction mixture's colour, as the newly formed charge-transfer absorption band (the CTC HOMO–LUMO gap) often lies in the visible region (Figure 2). This absorption band can therefore be excited with visible light to promote electron transfer and initiate a radical chain. Interestingly, the formation of a CTC can also greatly reduce the barrier to thermal electron-transfer.[49] Consequently, CTCs have started to receive significant attention for their potential use in the synthesis of new organic molecules.[46]

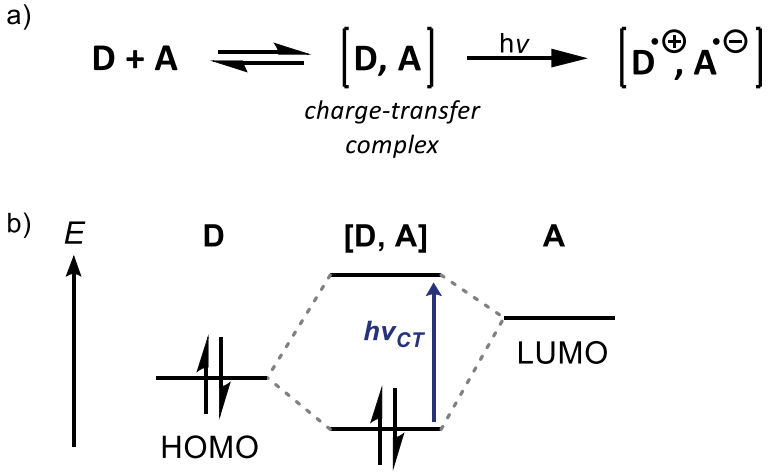

Figure 2. a) general scheme of electron donor-acceptor complex formation; b) ground-state energy levels diagrams. One-sided arrows represent electrons and the green arrow represents the HOMO-LUMO gap equal to the energy required to excite an electron.

Interestingly, such donor-acceptor interactions have also be used to accelerate non-radical reactions through the preorganisation of the reactants as this can reduce the entropic cost of a transition state. This feature was first proposed by Senaweera, Weaver and co-workers who showed that polyfluoroarenes could be substituted to form *para*-chloro-polyfluoroarenes via reverse halogen exchange. No reaction was observed until benzyltributylammonium chloride was added to the reaction mixture, which was proposed to form the 2:1 donor-acceptor complex **61** (Scheme 16).[50]

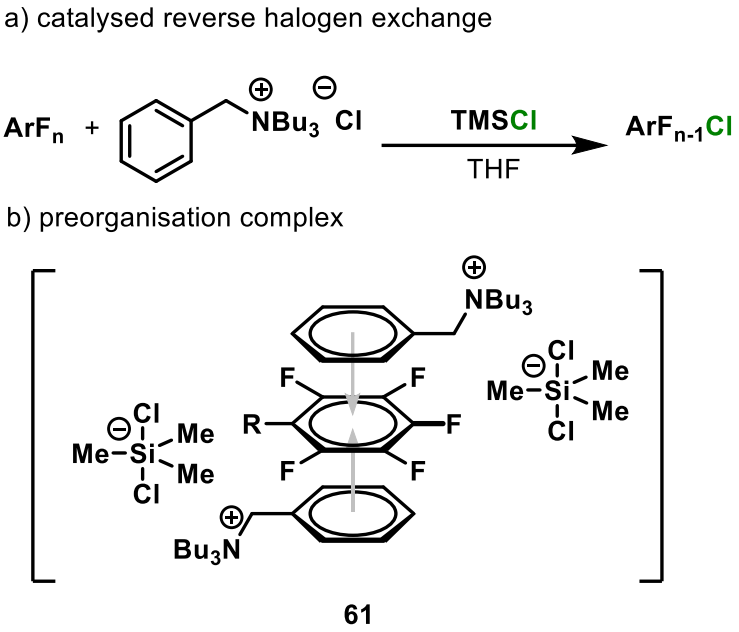

Scheme 16. Substitution aided by a charge transfer complex. a) general reaction scheme, b) preorganisation complex, grey arrows indicate the direction of electron transfer.

Aside from the CTC-related activation, electrochemistry can also be used to promote the one-electron reduction of the coupling partner. For example, aryl iodide **62** can be coupled with a carboxaldehyde imidazole anion **63** under electrochemical conditions (Scheme 17).[51] It was found that the 1-iodo-2-trifluoromethyl benzene radical anion dissociates so fast, the reduction of trifluoromethyl benzene radical occurs immediately on the electrode's surface (Scheme 17a). Therefore, phthalonitrile radical anion was employed as an electron transfer mediator to help generate the aryl radical away from the electrode surface. This approach yielded the *N*-arylated product **64** in 42% yield (Scheme 17b). The use of electrochemical methods can also remove the need for carefully designed electron donor additives, but these methods can suffer from an increased rate of radical–radical dimerization as radicals are often formed and concentrated in the immediate surroundings of the electrode.

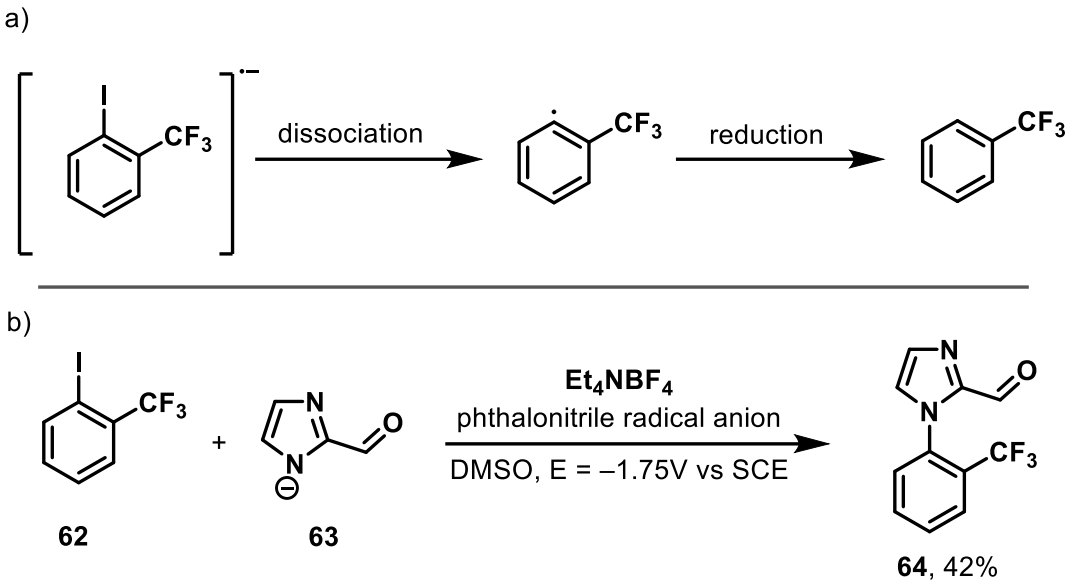

Scheme 17. Electrochemically induced radical nucleophilic substitution. a) Reduction of an aryl radical likely to occur in the immediate surroundings of the electrode; b) An electrochemically induced coupling reaction.

1.3.2. Propagation

Once formed, the radical species R$^{\bullet}$ can enter the radical chain through coupling with an anionic nucleophile (1). This coupled species RNu$^{\bullet-}$ can then propagate the chain by transferring an electron to the substrate RX, resulting in formation of the neutral product RNu and radical anion RX$^{\bullet-}$ (2). For the second propagation step to be fast enough to sustain a radical chain, the standard potential of the $E^0_{RNu|RNu\bullet-}$ couple must be greater than that of the $E^0_{RX|RX\bullet-}$ couple. It is imperative that both of these propagation steps are fast enough that side reactions do not occur to a major extent. If these criteria are satisfied, very efficient radical chains can be realised using only a 'catalytic amount' of a reducing agent.[52]

$$R^{\bullet} + Nu^{-} \rightarrow RNu^{\bullet-} \qquad (1)$$

$$RNu^{\bullet-} + RX \rightarrow RNu + RX^{\bullet-} \qquad (2)$$

The thermodynamic driving force for the coupling of R$^{\bullet}$ and Nu^{-} can be approximated using Savéant's model,[53] and equation (3), which consists of the standard potentials of the $E^0_{Nu\cdot|Nu-}$ and $E^0_{RNu|RNu\cdot-}$ couples, as well as the bond dissociation free energy of the coupled product ($BDFE_{RNu}$).

$$\Delta G^0_{R\cdot + Nu- \rightarrow RNu\cdot-} = E^0_{Nu\cdot|Nu-} - E^0_{RNu|RNu\cdot-} - BDFE_{RNu} \qquad (3)$$

There is a strong relationship between the thermodynamic driving force and the Gibbs free energy of activation $\Delta G^{\neq}$ for radical–anion coupling, which can also be approximated according to Savéant's model[53] and equation (4):

$$\Delta G^{\neq}_{R\cdot + Nu^- \rightarrow RNu^{\cdot -}} = \Delta G_0^{\neq}\left(1 + \frac{\Delta G^0_{A\cdot + Nu^- \rightarrow RNu^{\cdot -}}}{4\Delta G_0^{\neq}}\right)^2 \qquad (4)$$

The intrinsic barrier free energy ($\Delta G_0^{\neq}$) can be calculated with the following formula (5), in which $BDE_{RNu^{\cdot -}}$ is the bond dissociation energy of the radical anion $RNu^{\bullet -}$ and λ_0 is the solvent reorganisation energy.

$$\Delta G_0^{\neq} = \frac{BDE_{RNu^{\cdot -}} + \lambda_0}{4} \qquad (5)$$

1.3.3. Termination

Termination of the radical chain can occur in several ways and result in different products. The radical chains can be controlled to an extent by manipulating the reaction conditions and initiation methods. The main termination pathways are through: i) electron transfer from $ArNu^{\bullet -}$ to the radical species $R^{\bullet}$, which yields a neutral couple product ArNu and the R^- anion (7); ii) radical–radical coupling of two neutral radicals $R^{\bullet}$ to form a dimerised R–R product (8); iii) hydrogen atom abstraction by the neutral radical $R^{\bullet}$ from the solvent SH, which results in the formation of an RH product (9).

$$ArNu^{\bullet -} + R^{\bullet} \rightarrow ArNu + R^- \qquad (7)$$

$$2\ R^{\bullet} \rightarrow R\text{–}R \qquad (8)$$

$$R^{\bullet} + SH \rightarrow RH + S^{\bullet} \qquad (9)$$

As mentioned previously, initiating a reaction electrochemically can cause a concentration gradient and a build-up of $R^{\bullet}$ around an electrode and therefore increase the probability of dimerization. A choice of solvent can alter the frequency of hydrogen atom abstraction events.

1.3.4. Coupling Partner Compatibility

Aryl iodides are some of the most prevalent and attractive starting materials used in $S_{RN}1$ reactions. Most aryl halides are proposed to fragment via the injection of an electron into the π^* orbital, followed by intramolecular electron transfer into the C–X σ^* antibonding orbital (Scheme 18).[54] This process is incredibly fast in unsubstituted halobenzenes, reaching reaction

constant values as large as $7 \times 10^{10}\ s^{-1}$.[54] Fast cleavage, however, is not obligatory for $S_{RN}1$ to proceed: nitro- and cyanosubstituted halobenzenes were observed to fragment in much slower rates, like approximately $0.01\ s^{-1}$ for 2-chloronitrobenzene.[54] Interestingly, radical-nucleophilic substitution is especially favoured with aryl halides bearing electron-withdrawing groups in the *ortho* or *para* positions (similar to the S_NAr mechanism), as these substituents generally increase the size of the singly occupied molecular orbital (SOMO) orbital coefficient on the C–X carbon atom which facilitates π*–σ* orbital mixing. The scope of suitable coupling partners is therefore generally wide and tolerating of various additional functional groups.

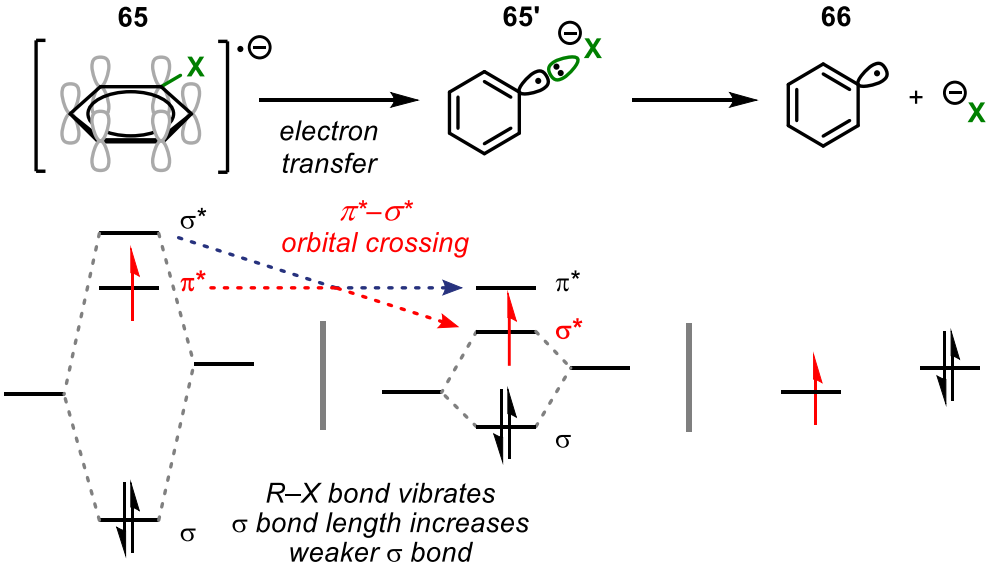

Scheme 18. Scheme and the energy level diagrams of the electron transfer from π* orbital of the radical anion **65** into the σ* orbital, generating 2-centre-3-electron species **65'** that cleaves into the radical **66** and leaving group anion.

Due to the lower C–X σ* bond energy on sp^3 than sp^2 carbon atoms, nucleophilic substitutions with aliphatic substrates usually proceed via polar pathways. The development of aliphatic coupling partners which undergo substitution via the $S_{RN}1$ mechanism has therefore been focused on substrates which do not satisfy the strict geometric requirements for substitution via the S_N2 mechanism, or when their polar transformation would be too entropically costly. Good sp^3 carbon $S_{RN}1$ substrates typically contain electron-withdrawing groups or are polycyclic molecules containing bridgehead atoms.[52] For example, Vanelle and co-workers proposed that α-substituted ketones **67** undergo substitution with nitronate anions via the $S_{RN}1$ mechanism to ultimately form α,β-unsaturated products **69** following an E1cB elimination from **68** (Scheme 19a).[55] For relatively unactivated aliphatic substrates, adamantyl halides

(Ad–X) are particularly prevalent. Rossi and co-workers have described the substitution of halogenated adamantanes **70** using nitronate anion, but a photoexcited acetone enolate ion was required to entrain this reaction (Scheme 19b).[56] Under entrainment conditions, conversion to the product **71** was reported to be 83%. Another instance of radical substitution on adamantanes was reported by Gutierrez and colleagues. $S_{RN}1$ conditions were used in order to achieve substitution of the tetrabromoadamantane **72** (Scheme 19c).[57] The mixture of **72** and sodium cyanate was irradiated for 6 hours resulting in 73% conversion to the tetracyanoadamantane **73**. Overall, the likelihood of an $S_{RN}1$ mechanism being in operation will increase with the electron affinity of the leaving group (e.g. Br < I < SMe_2^+) as this will favour electron transfer and the formation of a radical species.

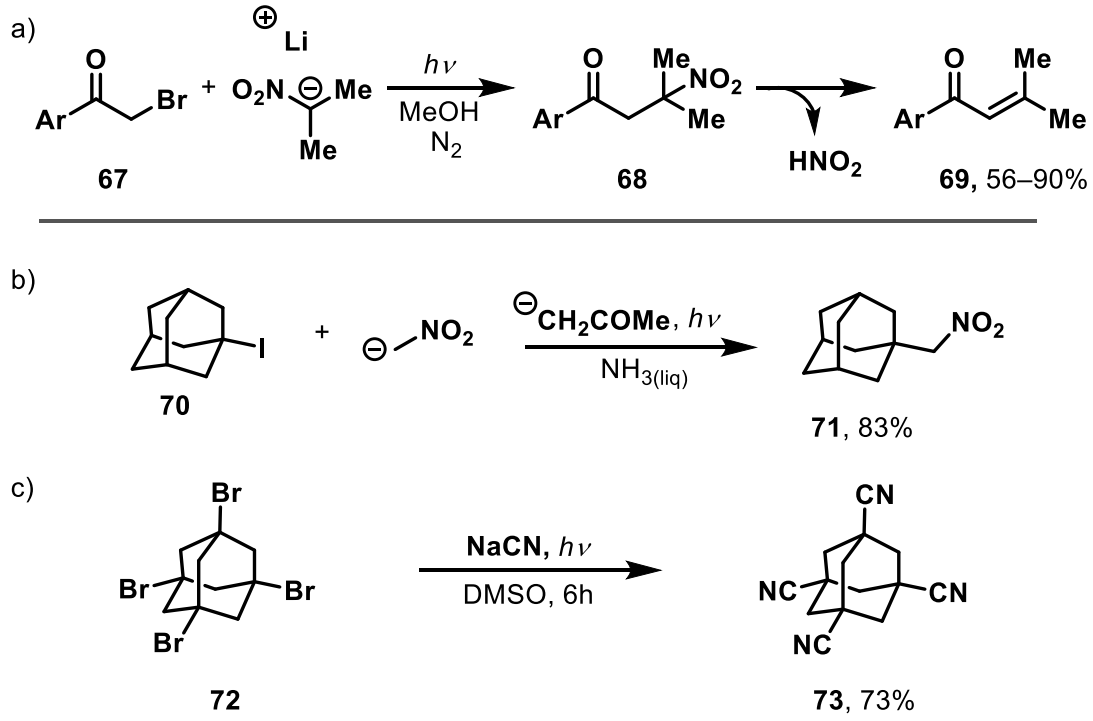

Scheme 19. Radical nucleophilic substitution reactions of: a) α-substituted ketones, b) iodoadamantane **70** c) tetrabromoadamantane **72**.

1.3.5. Compatible Nucleophiles and their Limitations

A variety of nucleophiles have been reported to engage in $S_{RN}1$ coupling reactions, including carbon-based nucleophiles, group 15 atoms (N, P, As) and group 16 (O, S, Se, Te). One of the most prevalent carbanion nucleophiles are enolates.[58–61] For example, Guastavino, Rossi and co-workers described a protocol for the synthesis of benzofused heterocycles **75** using the enolates of **74** (Scheme 20a).[62] However, light irradiation or addition of iron(II) chloride was needed to initiate these reactions. Nitronates are also viable nucleophiles as demonstrated by Vanelle and co-workers, who coupled 2-nitropropane anion **77** with the chloride **76** to achieve C–alkylation **78** in 90% yield (Scheme 20b).[63]

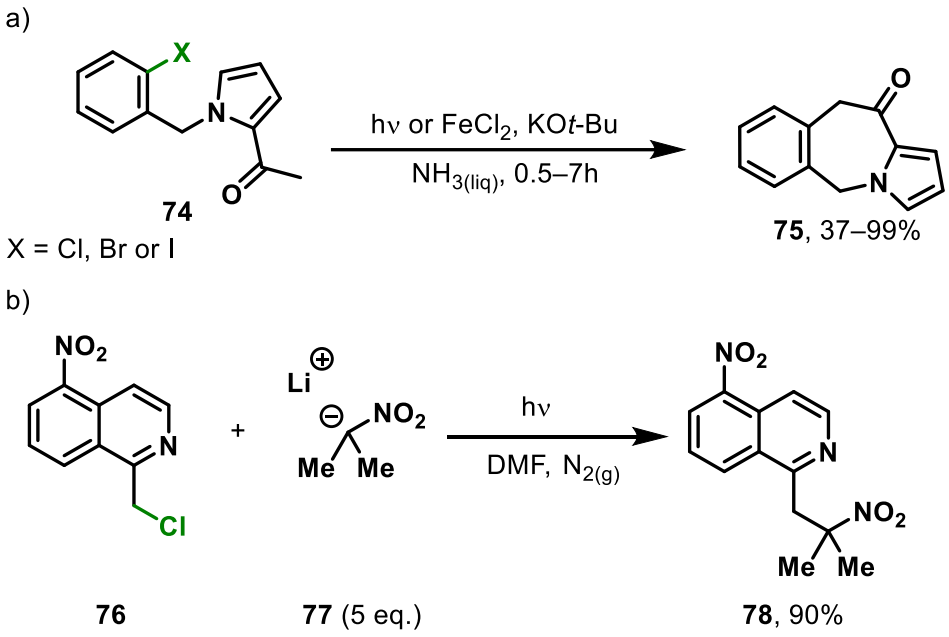

Scheme 20. Radical substitution reactions of C(sp^3) carbanion nucleophiles under photochemical initiation: a) intramolecular; b) intermolecular.

In addition to C(sp^3) carbanions, Grignard reagents have also been used by Hayashi and co-workers as C(sp^2) carbanions and coupled with aryl halides **79** to form biaryls **81** via, as later also supported by Haines and Wiest's computational studies,[64] an $S_{RN}1$ mechanism (Scheme 21).[65]

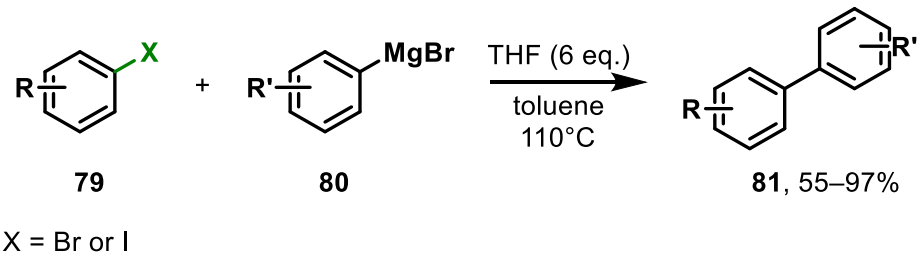

Scheme 21. Grignard reagents in biaryl coupling via a radical nucleophilic substitution.

Nitrogen-based anions can also engage in $S_{RN}1$ coupling reactions, but examples are comparatively rare. The azide anion is perhaps the most prevalent, Creary and colleagues proposed that substitution on arylhalodiazirines **82** with azide anions proceeds via an $S_{RN}1$ mechanism (Scheme 22).[66] Guerra and co-workers have also described the synthesis of dibenzosultams **86** through the intramolecular $S_{RN}1$ coupling of sulfonamide radical anions **85** using photochemical conditions.[67]

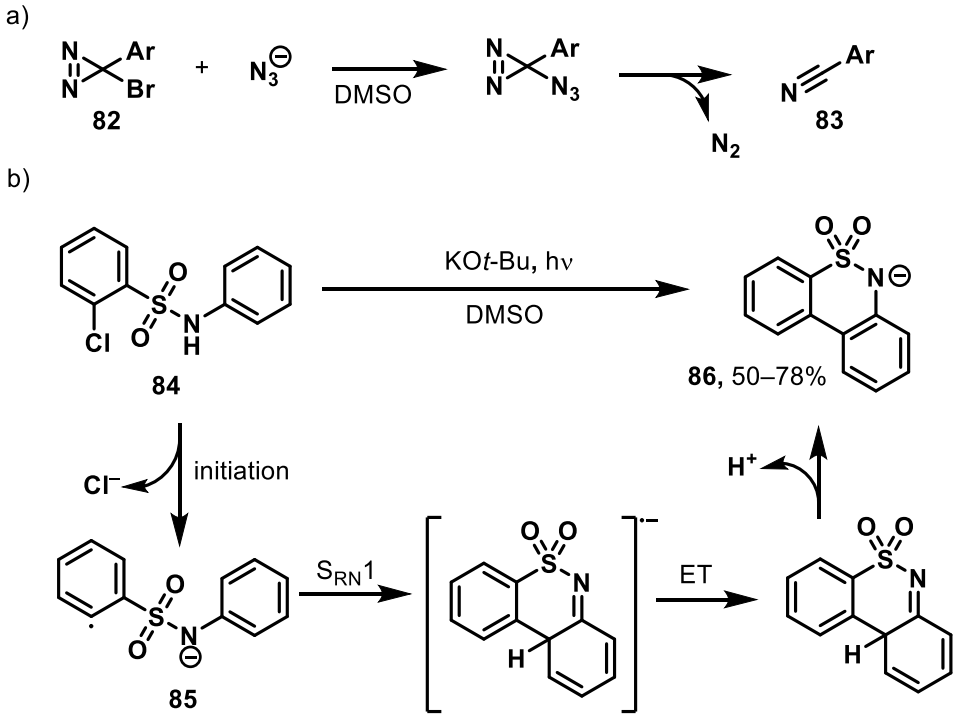

Scheme 22. Intramolecular radical nucleophilic substitution reactions. a) Substitution of arylhalodiazirines; b) intramolecular cyclisation reaction.

Han and co-workers recently developed a procedure for preparation of organophosphines **89** via the $S_{RN}1$ coupling between sodium phosphides **87** and aryl chlorides **88** (Scheme 23a).[68] The mechanism of this process, initiated by the R_2PNa species, was supported and rationalised through extensive scoping, although the reactivity trend (ArI < ArBr < ArCl ≈ ArF) was the

opposite to what is typical for a standard nucleophilic radical substitution. A limited range of vinylic and aliphatic substrates was also found to be compatible with the proposed protocol. Later, a complementary method was developed by Chen and colleagues, who showed that aryl halides **90** will couple with PPh_2H in presence of KOH and that these reactions may proceed through competitive open-shell $S_{RN}1$ and polar S_NAr mechanisms (Scheme 23b).[69]

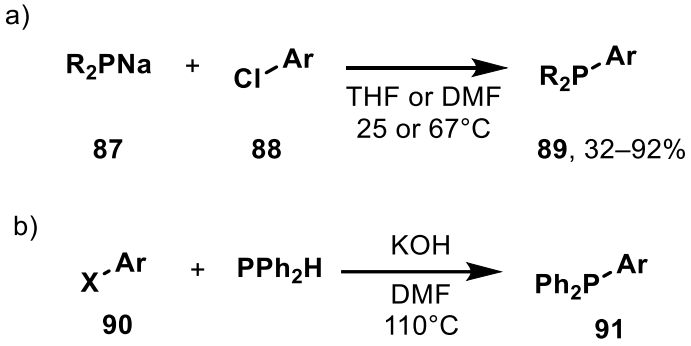

Scheme 23. Use of phosphorus nucleophiles in radical nucleophilic substitution.

Sulfur and selenium nucleophiles are also precedented in nucleophilic radical substitution. PhS^- and $PhSe^-$ anions were recognised as a successful nucleophile in coupling with aryl iodides.[70] Ila and Kumar developed an $S_{RN}1$-based, intramolecular C–S bond formation using isothiocyanate functionality as nucleophile (Scheme 24).[71]

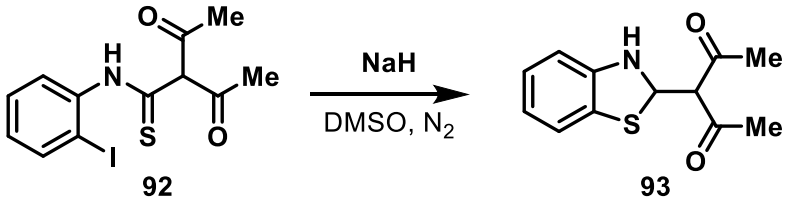

Scheme 24. Intramolecular cyclisation reaction under $S_{RN}1$ conditions with nucleophilic sulfur moiety.

Oxygen-based nucleophiles are very rare in comparison with carbon- and nitrogen-based nucleophiles. [27] This lack of development is likely to be due to the slow coupling of oxygen anions with radicals. Organic oxygen-containing nucleophiles favour a C–C over a C–O coupling, which was studied and demonstrated by Pierini and Rossi for reactions of naphtoxides.[72] Interestingly, as oxygen is replaced with heavier chalcones (S, Se), the C–heteroatom coupling becomes favoured (Scheme 25).

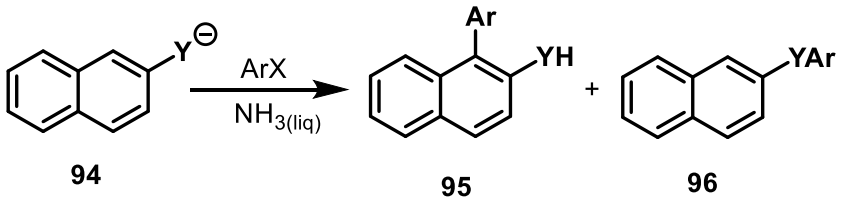

ratios of the detected products:

	95 : 96
Y = O	100 : 0
NH	91 : 9
S	18 : 82
Se	0 : 100

Scheme 25. Selectivity studies on naphthyl nucleophiles with different heteroatoms under $S_{RN}1$ conditions. The table presents ratios in which the products were detected when naphthalene derivatives with different heteroatoms **Y** were used.

1.4. Project Aims

The aim of this project was to develop a mild, transition metal-free hydroxylation method for transforming aryl halides into phenols. Prior studies performed within the James' group revealed potential of the proposed procedure, as bromoacetophenone **108** was transformed into the corresponding phenol $\mathbf{108_{OH}}$ in 85% yield.

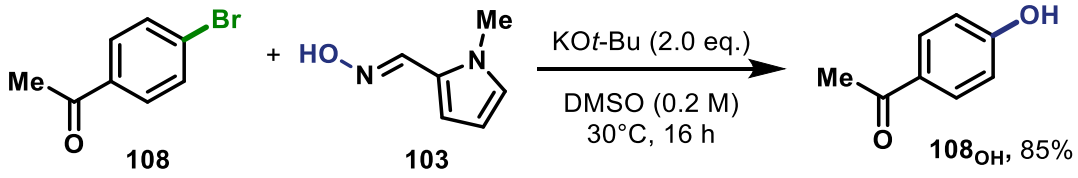

Scheme 26. Preliminary coupling experiment using the rationally designed hydroxide surrogate **103**.

Although the proposed transformation effectively replaces X^- with HO^-, free hydroxide anion is unlikely to substitute the halide on an unactivated sp^2 carbon due to its insufficient nucleophilicity and large, positive reducing potential (1.90 V vs SHE in water), [73] making it unlikely to engage in a radical substitution process. Therefore, building upon Maloney's work on an oxime-based hydroxide surrogate,[25] a versatile nucleophile has been designed and synthesised by the James' group. The oxime functionality is particularly attractive due to its easily manipulated electronics, which depending on the nature of the R group (Scheme 27).

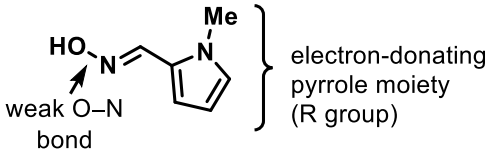

Scheme 27. Oxime **103** scaffold.

Previous research conducted in James' group identified the pyrrole oxime **103** as the optimal nucleophile for the investigated coupling reactions. Pyrrole moiety was discovered to increase the nucleophilicity of the oxime, as it forms electron-rich conjugated system within the molecule, is easily handled, stable under air conditions and easy to prepare.

The design of the nucleophile allowed to remove the need for an additional step for breaking the N–O bond. Once the C–O coupling process has occurred, the intermediate **99** becomes

deprotonated and breaks down into a phenol product **100** and the cyanidete **101** (Scheme 28). The by-product **101** was observed in several crude mixtures via NMR spectra analysis.

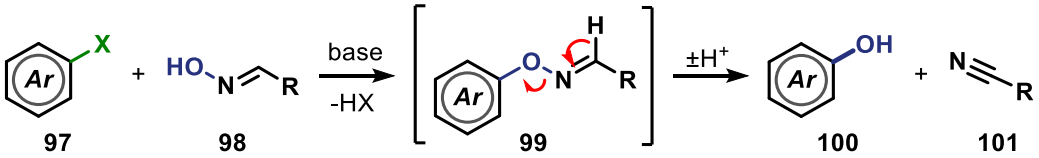

Scheme 28. *In situ* N–O bond cleavage.

Chapter 2. Results and discussion

2.1. Oxime synthesis

Studies began by optimising the synthesis of oxime **103**. Oxime **103** was prepared by condensing aldehyde **102** with hydroxylamine hydrochloride in the presence of a base and a protic solvent under reflux.[74a] First, the condensation was performed with potassium carbonate in methanol for 18 hours, which afforded oxime **103** in 12% isolated yield (Table 1, Entry 1). Increasing the equivalents of hydroxylamine hydrochloride and changing the base to sodium acetate afforded oxime **103** in 34% yield (Entry 2), which could be further improved to 69% by reducing the reaction time to 2 h (Entry 3). Changing the base to sodium carbonate enabled the oxime to be isolated in 89% yield using only 1.2 equivalents of hydroxylamine hydrochloride (Entry 4). However, it should be noted that: i) these reactions displayed some sensitivity to the reaction scale; ii) varying levels of the *Z*-isomer **104** were present in every reaction mixture; and iii) the product was prone to decomposition on acidic silica gel, forming primary amide **105** via a presumed Beckmann rearrangement (Scheme 29).[74b]

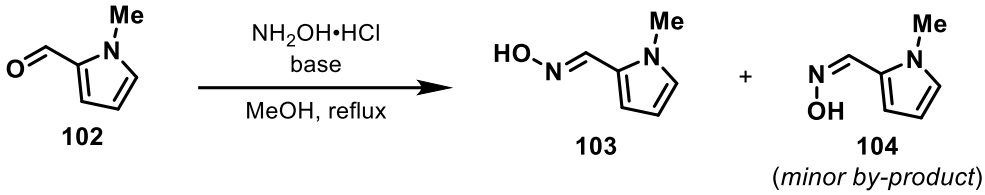

Entry	NH_2OH (eq.)	Base	**102** (mmol)	Time (h)	Yield[a] (%)
1	1.2	K_2CO_3 [b]	5.0	18	12
2	1.6	NaOAc [c]	40.0	18	34
3	1.6	NaOAc [c]	5.0	2	69
4	1.2	Na_2CO_3 [b]	20.0	2	89

Table 1. optimisation of oxime **103** synthesis. [a] isolated yield, [b] 1.2 eq. loading, [c] 2.0 eq. loading.

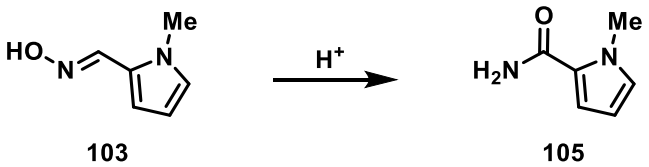

Scheme 29. Degradation of the oxime **103** on silica gel.

The stereochemistry of the major *E*-isomer **103** and the minor *Z*-isomer **104** was confirmed by X-ray crystallography (Figure 3).

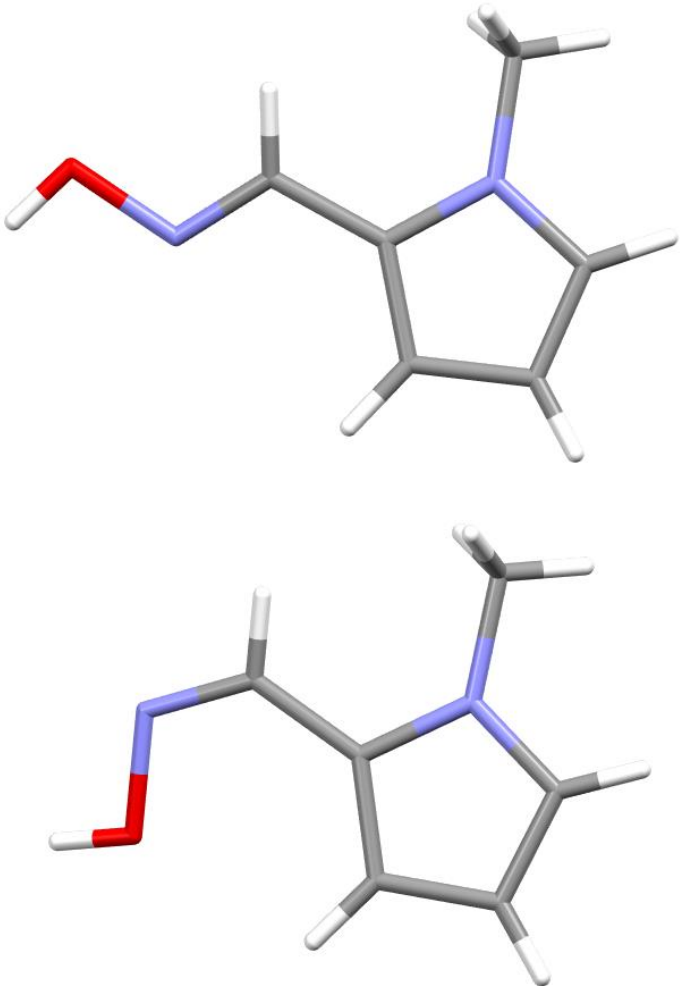

Figure 3. X-ray crystallographic structure of the *E*- (top) and *Z*-oxime isomers (bottom).

In addition, the two isomers could be identified by ^{1}H NMR spectroscopic analysis. For example, the singlets at 8.03 ppm (*E* isomer, Figure 4a) and 7.40 ppm (*Z* isomer, Figure 4b) can be assigned to the aldoxime C–H proton. For the *E*-isomer, this signal is likely to be more deshielded due to the spatial proximity to the electronegative oxygen atom.[75]

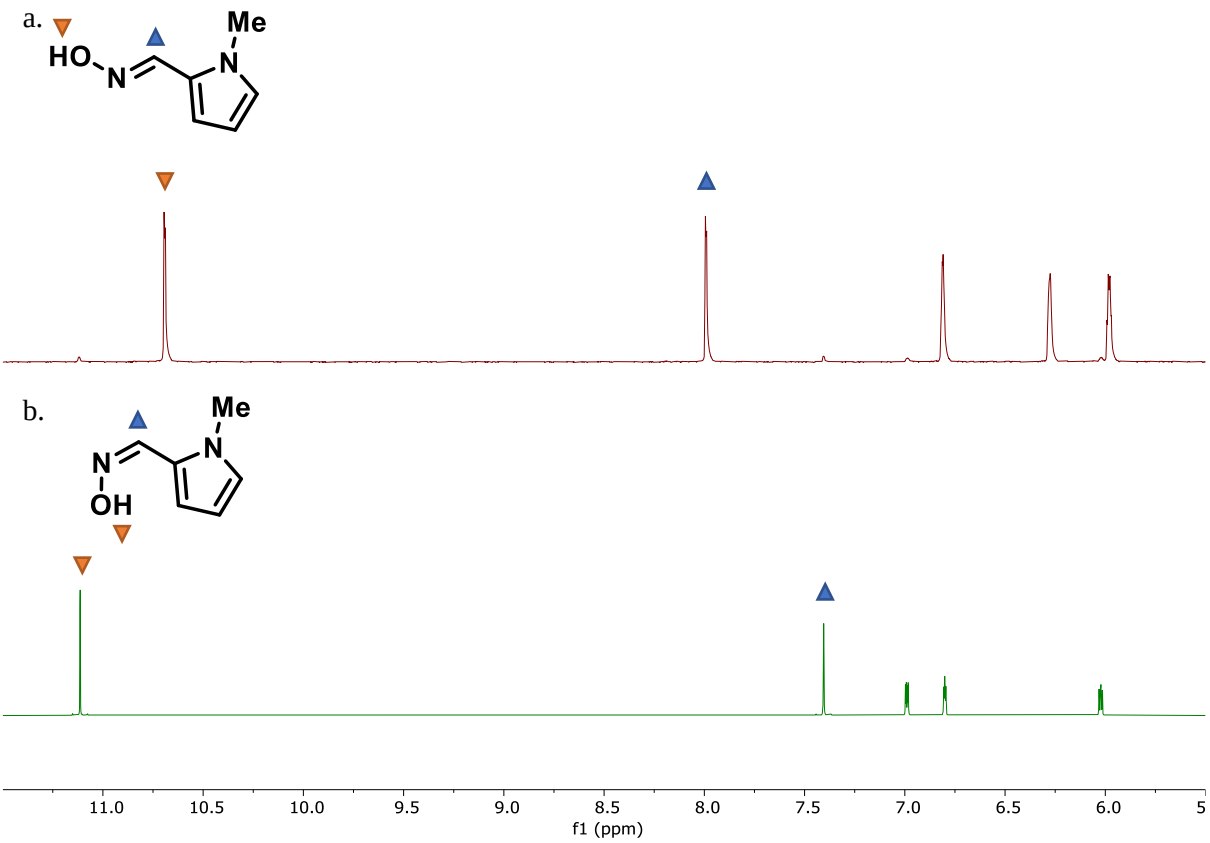

Figure 4. Comparison of the different oxime isomers by ^{1}H NMR spectroscopy. ^{1}H NMR spectra of the E (top) and Z (bottom) isomers in deuterated DMSO. The blue triangle marks the aldoxime proton's signal whilst the orange upside-down triangle marks the placement of O**H** proton in each isomer.

2.2. Initial scoping studies

With oxime **103** in hand, a wide range of aryl halides was examined as coupling partners to investigate the generality of the developed reaction. The yields of these reactions were initially estimated by adding CH_2Br_2 as an internal standard to the reaction mixture after workup which was then analysed by ^1H NMR spectroscopy. The yields were determined by measuring the integration of the phenol product relative to the C**H**$_2$Br$_2$ singlet peak at δ = 4.9 ppm and multiplied by 100%. For example, in Figure 5, the yield was calculated by setting internal standard's signal's integration to 2.00 and noting the integration of product's signals. The broad, deshielded singlet representing the exchangeable O–**H** phenol proton was usually ignored, as its presence and integration was heavily influenced by other components in the reaction mixture. Amongst the rest of the product's signals present, the worst-case scenario (the lowest yield) was assumed. The lowest product's signal integration is equal to 0.96, therefore the approximate NMR yield of this reaction was 96%. Isolation of the phenol products was only attempted when the estimated NMR yields were ≥30%.

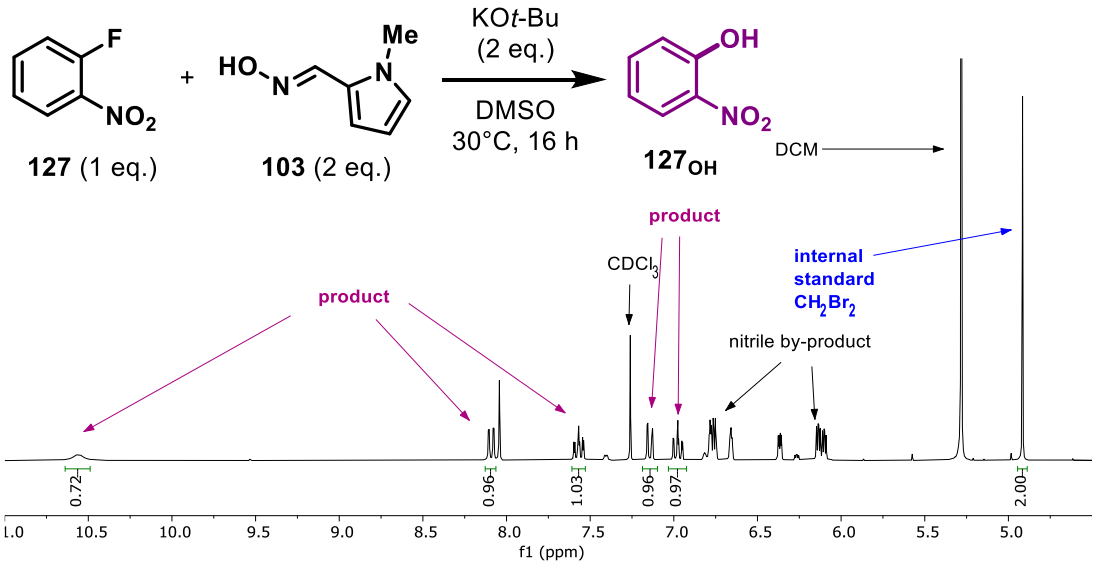

Figure 5. Annotated NMR spectrum of a crude mixture of the reaction between 1-fluoro-2-nitrobenzene **127** and the oxime **103** showing integration of product signals (purple) relative to the internal standard's singlet (blue).

2.2.1. Carbonyl derivatives

The first class of compounds examined for compatibility with the initially developed reaction conditions (using KO*t*-Bu at 30°C) was haloarene carbonyl derivatives. *Para*-substituted aryl fluoride **106**, chloride **107** and bromide **108** acetophenone derivatives were all converted into the corresponding phenols in very good yields. Aryl fluorides are known to favour S_NAr processes and so it is suspected that this complementary substitution mechanism may slightly improve the reaction performance of aryl fluoride **106** (these possibilities are explored further in section 2.4). Ethyl *para*-iodobenzoate **109** was only transformed into the corresponding phenol in 30% yield.

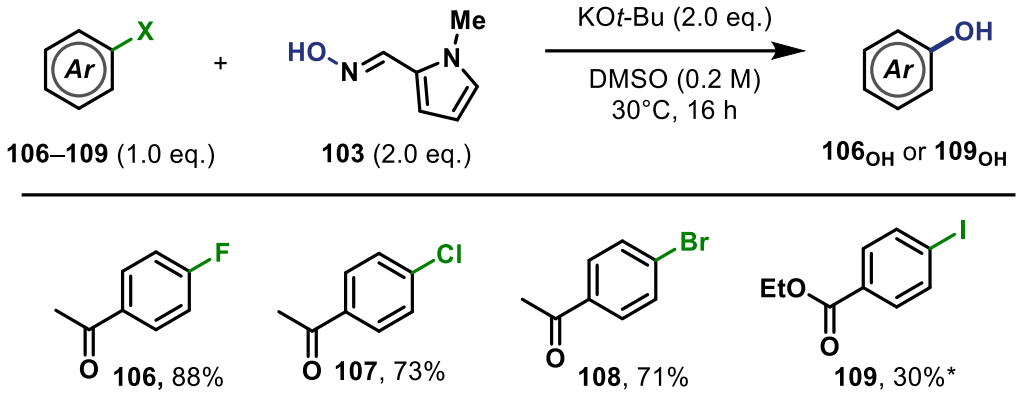

Scheme 30. Substrates and isolated yields of the corresponding phenols. *Yield determined by ^{1}H NMR spectroscopy against an internal standard (dibromomethane).

However, no product was observed when a closely related benzyl ketone derivative **110** was used (Scheme 31), which was tentatively attributed to be due to the enhanced acidity of the α-keto proton (pKa ≈ 20).[76] This ketone would likely be deprotonated to form a negatively charged species **112**, which could potentially repel the deprotonated nucleophile **103**. This process would also be competitive with oxime deprotonation and therefore decrease the quantity of the oxime anion in solution.

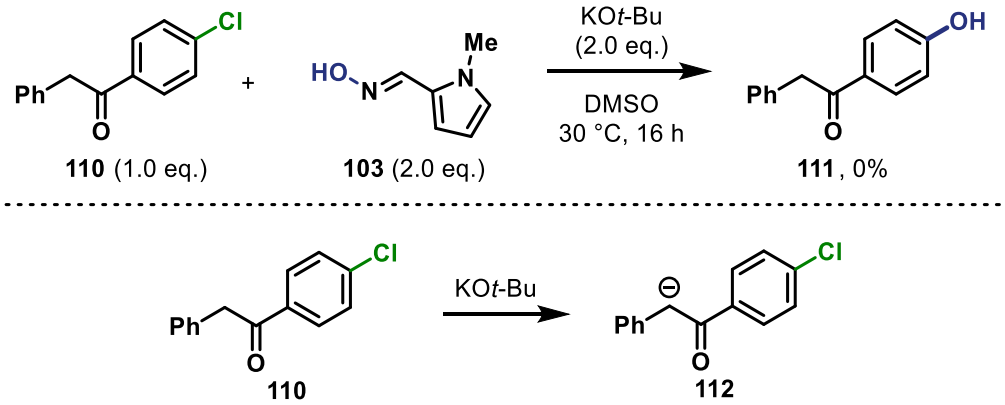

Scheme 31. Attempted coupling reaction between the oxime **103** the benzyl ketone **110** (top), deprotonation of (4-chlorophenyl)benzyl ketone (bottom).

Although the *para*-haloacetophenones generally reacted to form phenols in very good yields, the *meta* isomers examined in this project exhibited limited reactivity. In fact, only 3′-fluoroacetophenone **113$_F$** could be partially converted into phenol **114** (and 3′-chloroacetophenone **113$_{Cl}$** to a lesser extent), which may indicate that this substrate is only compatible with an S_NAr mechanism. However, it is important to note that *meta*-substituents cannot directly stabilise a negative charge via resonance (Scheme 32). Indeed, a recent computational study on S_NAr reactions of haloacetophenones conducted by Trofimov and co-workers indicated that the activation energy of aromatic nucleophilic substitution on the *meta*-fluoroacetophenone can be significantly larger than for the *para*-isomer (e.g. 28.0 kcal/mol vs 21.8 kcal/mol).[77] Interestingly, it has been previously reported that radical anions derived from *meta*-substituted aryl halides fragment considerably slower than their *ortho*- and *para*-analogues due to the relatively small orbital coefficient on the *meta* position of the SOMO (disfavouring π*–σ* orbital mixing). These longer fragmentation times could therefore prevent the efficient initiation and propagation of an $S_{RN}1$ reaction.[54] It is also possible that slower radical-anion fragmentation may also mean that radical–anion coupling is slower, as fragmentation and coupling occur via the same process (they are just opposite signs).

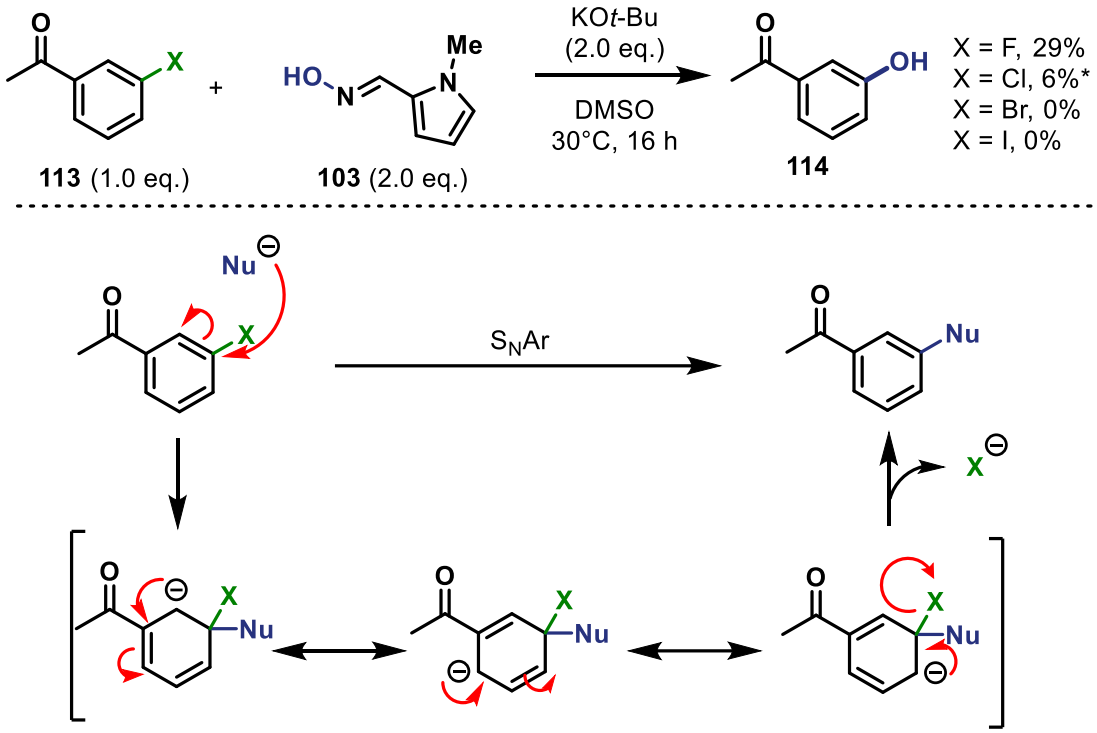

Scheme 32. Coupling reactions of 3'-haloacetophenones (top). Stabilisation of *meta*-substituted halides through resonance (bottom). *Yield determined by ^{1}H NMR spectroscopy against an internal standard (dibromomethane).

The reactivity of benzophenone derivatives was similarly varied (Scheme 33). Whilst *para*-bromobenzophenone **115** could be hydroxylated in 66 % yield, *ortho*-chloro- and bromobenzophenone **116** and **117** respectively, almost completely resisted conversion into the corresponding phenol. It was hypothesised that an S$_{RN}$1 radical chain may be significantly disrupted by an intramolecular radical cyclisation to form fluorenone **119** (Scheme 33), but it could not be detected by HRMS analysis of the reaction mixture. Instead, the low yielding formation of an intermediate suspected to be *O*-aryloxime **118** was detected by HRMS and ^{1}H NMR spectroscopic analysis. The lack of N–O bond cleavage may be due to steric hindrance around the site of substitution.

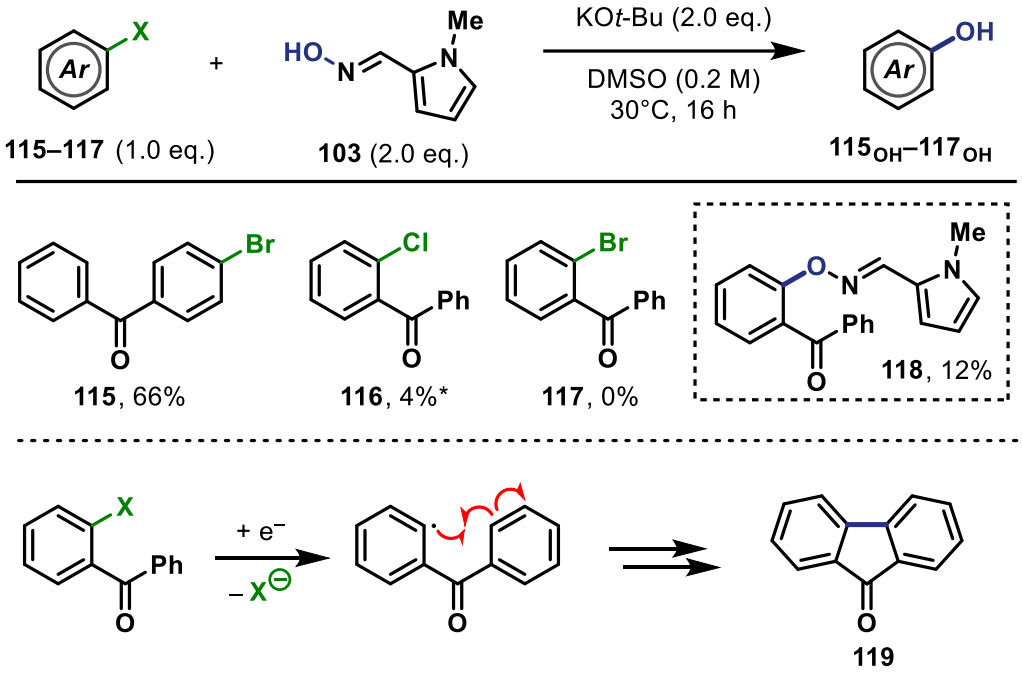

Scheme 33. Screened benzophenone derivatives and yields of the corresponding phenols. *Yield determined by ^{1}H NMR spectroscopy against an internal standard (dibromomethane).

Finally, benzaldehyde derivatives were examined. The coupling reaction of 4-fluorobenzaldehyde **120**$_{F}$ with oxime **103** afforded the phenol product in 82% yield, but the bromo-analogue **120**$_{Br}$ afforded the same phenol product in just 19% yield. This stark difference in reaction performance might indicate an $S_NAr/S_{RN}1$ mechanistic switch. For an $S_{RN}1$ process it is possible that the aldehyde functionality may disrupt the radical chain as the (O)C–H bond is relatively weak and prone to abstraction by other radical species (e.g. an aryl radical).[78,79] Dichlorobenzaldehyde **121** and 2-bromo-4-chlorobenzaldehyde **122** both selectively formed the chloride substituted monohydroxylated product in low yields, indicating that dihalogenated substrates may be resistant to the proposed transformation conditions.

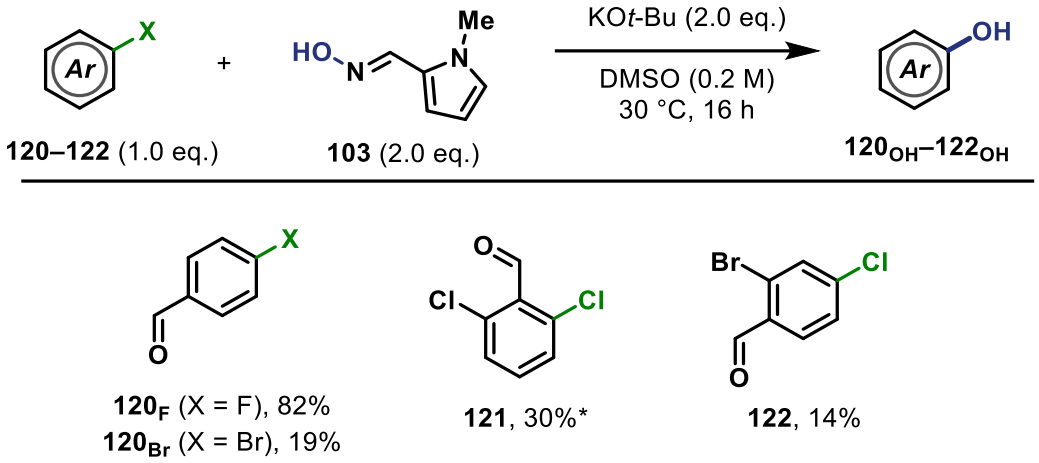

Scheme 34. Benzaldehydes and yields of the corresponding phenols. *Yield determined by ^{1}H NMR spectroscopy against an internal standard (dibromomethane).

2.2.3. Benzonitriles

The compatibility of electron-deficient benzonitriles derivatives was then examined (Scheme 35). Pleasingly, both *para*- and *meta*-bromobenzonitrile (**123, 124**) could be hydroxylated to afford the corresponding phenol products in 67% and 53% yields respectively. Compared to the *meta*-substituted acetophenones **113**, the increased reactivity of *meta*-bromobenzonitrile **124** was intriguing, but it should be noted that this reaction was slow and require an extended reaction time (48 hours). This result might indicate that the fragmentation rate is low, similarly to other *meta*-substituted compounds reported in literature.[80] Interestingly, consistent with previous results, dihalogenated substrate **125** was incompatible with the reaction conditions.

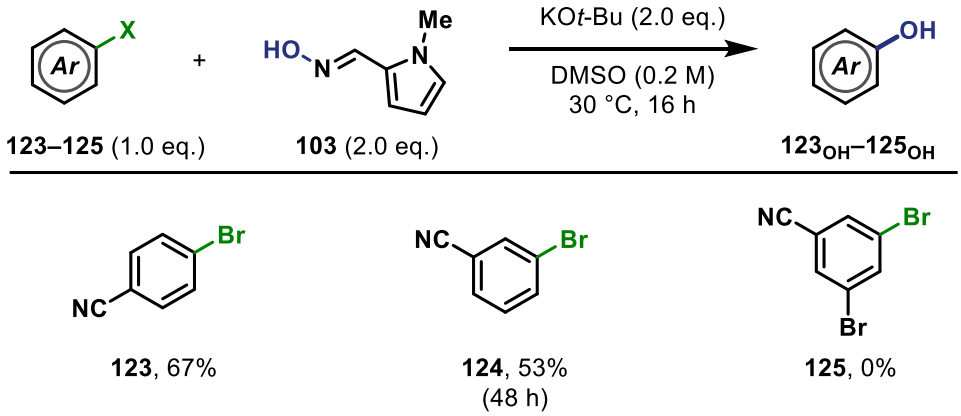

Scheme 35. Benzonitrile derivatives and yields of their conversion into corresponding phenols.

2.2.2. Nitroarenes

Next, strongly electron-deficient halogenated nitroarenes were studied (Scheme 36). Both *para*- and *ortho*-fluoronitrobenzene (**126**, **127**) were converted into the corresponding phenols in high yields, which was unsurprising, considering that fluoro-substituted nitroarenes are model compounds for S_NAr processes (see Chapter 1.2). Methoxy substituted aryl bromide **128** was also compatible with these reaction conditions and converted into phenol in 27% yield. This experiment demonstrates that electron-donating groups can be tolerated if a sufficiently electron-withdrawing group is also present. It should also be noted that all of these reaction mixtures were vividly coloured, which could indicate that strongly interacting charge-transfer complexes are being formed.

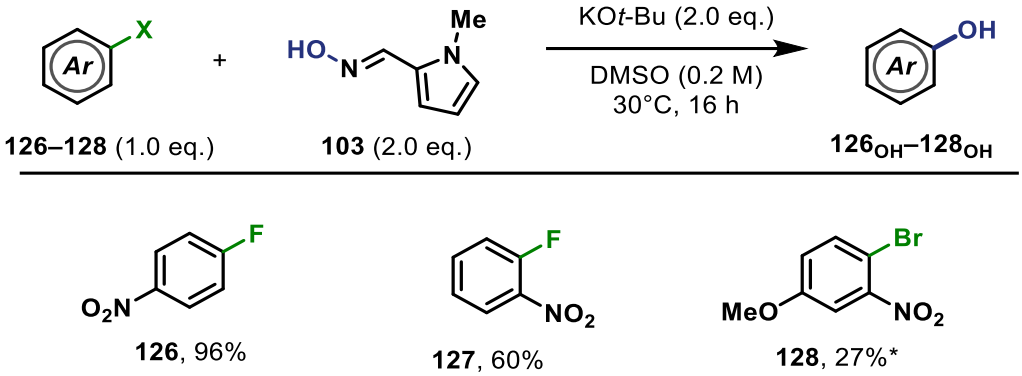

Scheme 36. List of nitro-substituted substrates and the yields of their conversion into phenols. *Yield determined by ^{1}H NMR spectroscopy against an internal standard (dibromomethane).

2.2.4. Heteroarenes

Next, the reactivity of heteroaromatic compounds was briefly examined and pleasingly, 5-bromo-2(trifluoromethyl) pyridine **129** was converted into the corresponding phenol **130** in 76% yield (Scheme 37). Pyridine **129** was chosen as a particularly attractive target due its electron-deficient nature, which could facilitate both S_NAr and $S_{RN}1$ pathways. Importantly, this result also demonstrated that this methodology tolerates heteroarenes, which are privileged scaffolds in drug discovery.[81]

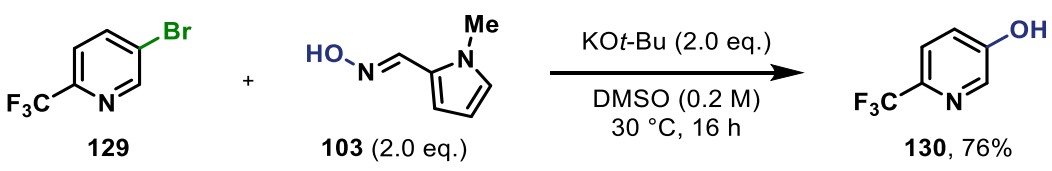

Scheme 37. Coupling reaction of heteoaryl bromide **129** with oxime **103**.

2.2.5. Unactivated haloarenes

Several aryl halides lacking an activating electron-withdrawing group were then examined (**131–142**). In almost all cases no reactivity was observed (only the starting materials were observed by ^{1}H NMR spectroscopic analysis of the crude reaction mixture), which was consistent with the previous results. However, exceptional reactivity was exhibited by 4-bromo-2-fluorobiphenyl **142** which, despite the lack of a strong (−M) electron-withdrawing group, was converted into the corresponding phenol in 78% yield (Scheme 38). The reaction was highly chemoselective as only substitution of the fluorine substituent was observed. This result was surprising in comparison with previous dihalogenated substrates. This increase in reactivity could potentially be rationalised by the bending of the fluorine substituent, which may be forced slightly out of plane by the spatial proximity of the bulky phenyl group (Scheme 39). This distortion could facilitate the substitution processes by bringing the molecule's geometry closer to the desired transition state (S_NAr) or by encouraging the radical–anion π*→σ* orbital mixing required for aryl radical generation.

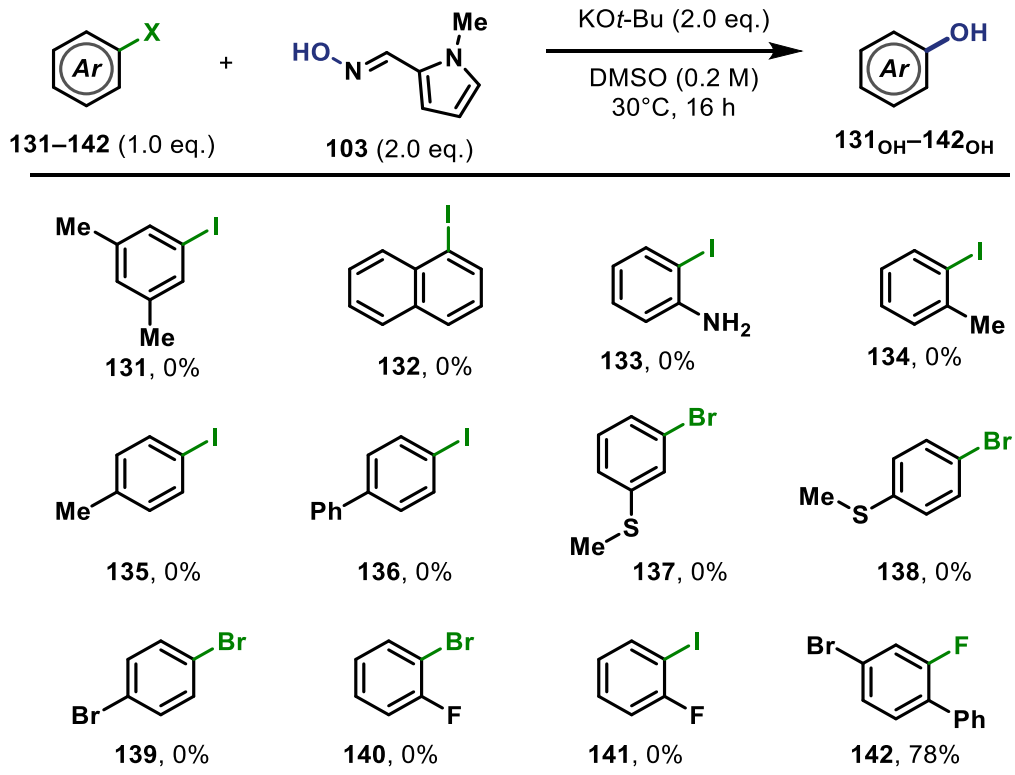

Scheme 38. List of deactivated substrates and the yields of their conversion to phenols.

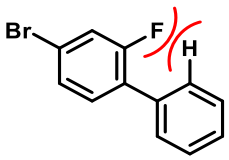

Scheme 39. Potential steric interaction within the halide **142** forcing –F substituent to bend out of plane.

2.3. Reoptimisation of the reaction conditions

The initial scoping studies revealed some promising results, but good yields were limited almost exclusively to haloarenes containing strong electron-withdrawing groups. A series of additional optimisation studies were therefore performed to try to bypass this limitation. First, the influence of the reaction temperature and base was studied using *m*-fluoroacetophenone **113$_F$** as a model substrate due to its partial compatibility with the previously developed reaction conditions (29% yield at 30°C with KO*t*-Bu, see Scheme 32). The reactivity of an anion can be strongly influenced by its counter-cation and alkali metal cations have been previously reported to aid S_NAr and $S_{RN}1$ reactions and therefore bases containing the group I metals were studied (Table 2).[21] First, potassium hydroxide was used as a base at 50°C and 60°C, which afforded phenol **114** in 32 and 48% yield, respectively (Entries 1 and 2). However, potassium *tert*-butoxide once again proved superior as phenol **114** could be isolated in 39% and 62% yield at 50°C and 60°C, respectively (Entries 3 and 4). Conversely, the use of sodium *tert*-butoxide base at 65°C resulted in solubility issues and afforded the phenol product **114** in just 6% yield (Entry 5).

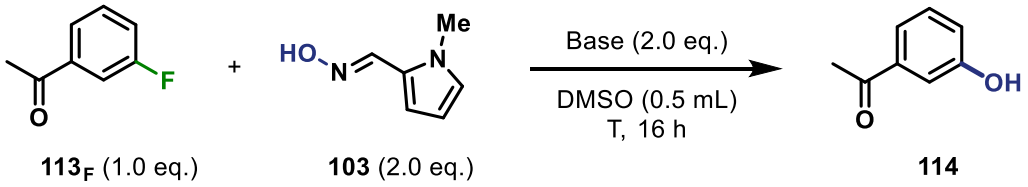

113$_F$ (1.0 eq.) **103** (2.0 eq.) **114**

Entry	Base	Temp (°C)	Yield **114*** (%)
1	KOH	50	32
2	KOH	60	48
3	KO*t*-Bu	50	39
4	KO*t*-Bu	60	62
5	NaO*t*-Bu	65	6

Table 2. Reoptimisation studies at elevated temperatures. *Yield determined by ^{1}H NMR spectroscopy against an internal standard (dibromomethane).

Next, considering the possibility of an $S_{RN}1$ process, potential entrainment conditions using *trans*-1,2-diaminocyclohexane **145** as an electron donor precursor were studied in different solvents.[82] Iodobiphenyl **143** was used as a substrate as it exhibited limited reactivity at 80°C in DMSO (15% yield, Entry 1, Table 3), but the addition of *trans*-1,2-diaminocyclohexane **145** did not significantly improve yield of the transformation into phenol **144** (Entry 2). No improvement in yield was observed when other polar aprotic solvents were used. (DMI,

DMPU, MeCN, Entries 3–5). It was noted that the oxime anion exhibited generally poor solubility in these solvents, which inspired a different approach for optimisation.

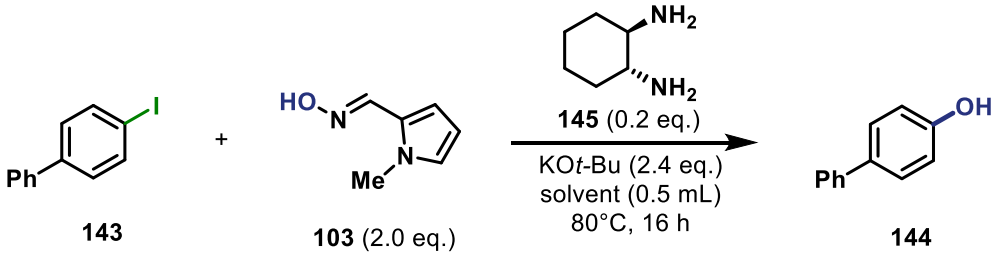

Entry	Solvent	Additive	Yield **144*** (%)
1	DMSO	none	15
2	DMSO[a]	**145** (0.2 eq.)	22
3	DMI	**145** (0.2 eq.)	12
4	DMPU	**145** (0.2 eq.)	10
5	MeCN	**145** (0.2 eq.)	0

Table 3. Optimisation studies in different polar aprotic solvents with and without the additive **145**. *Yield determined by ^{1}H NMR spectroscopy against an internal standard (dibromomethane). *a* – data collected by William Owens-Ward

Instead of entrainment, a range of additives were then tested in an attempt to improve the solubility of the oxime anion in different solvents. Two equivalents of TMEDA were used with a wide range of solvents, which did improve reaction solubility, however, no improvement in reaction performance was observed (Table 4, Entries 5-14). Increasing the equivalents of TMEDA to four was similarly ineffective (results not shown).

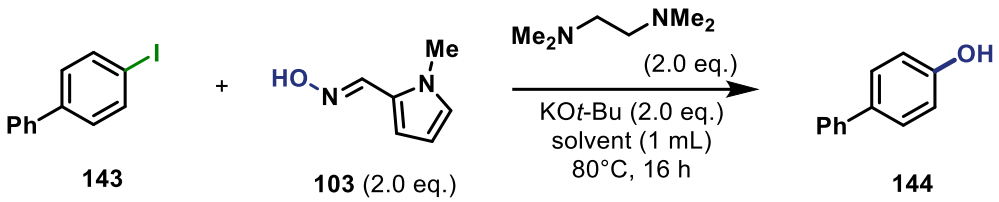

Entry	Solvent	Yield **144*** (%)	Entry	Solvent	Yield **144*** (%)
1	DMSO	18	8	Pyridine	0
2	DMA	11	9	PhCl	0
3	DMPU	12	10	1,4-dioxane	5
4	NMP	13	11	MeCN	0
5	DMF	3	12	THF	0
6	DMI	0	13	Toluene	0
7	DME	0	14	$PhCF_3$	0

Table 4. Solvent screening in presence of 2 eq. of TMEDA. *Yield determined by ^{1}H NMR spectroscopy against an internal standard (dibromomethane).

Considering the lack of improvement using potassium *tert*-butoxide, caesium carbonate was also tested as an alternative base with different solubilising ligands. First, TMEDA was added to the reaction mixtures in the amount of 8 equivalents to ensure 1:2 metal to ligand ratio, which did significantly improve the reaction homogeneity, but the yield of phenol **144** was still very low (Table 5, Entries 1-3). Replacing TMEDA with 4 equivalents of 1,2-bis(diphenylophosphino)ethane (dppe) was attempted, but once again, only trace amounts of the phenol product were found in all cases. Addition of 8 equivalents of dppe was attempted (not shown) but the large volume of the solid reagent exceeded the solution's capacity, which was not an issue posed by liquid TMEDA. As a result, the amount of dppe used was limited to 4 equivalents.

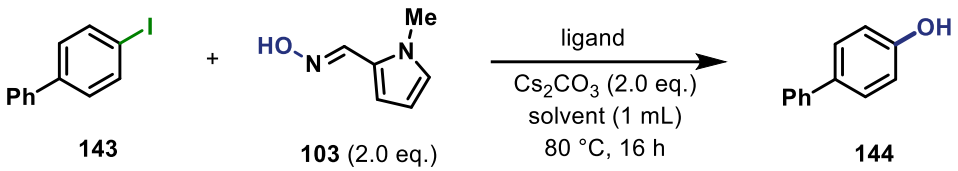

Entry	Ligand	Solvent	Yield **144*** (%)
1	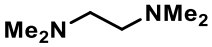	DMSO	4
2	(8 eq.)	DMPU	1
3		NMP	0
4	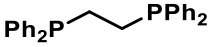	DMSO	1
5	(4 eq.)	DMPU	8
6		NMP	2

Table 5. Solvent screening in presence of caesium carbonate and ligands. *Yield determined by ^{1}H NMR spectroscopy against an internal standard (dibromomethane).

2.3.1. Revisited substrates

Following these re-optimisation studies, the use of ligands/additives to improve reaction performance was discontinued. Instead, previously unreactive haloarenes were re-examined at elevated reaction temperatures.

Simply increasing the reaction temperature to 60°C improved the hydroxylation of *meta*-fluoroacetophenone **113$_F$** from 29% to 61% isolated yield. Similarly, the yield of the phenol product from the substitution of aryl iodide **109** was improved from 30% to 64% yield. Methyl sulfone **146** could also be converted into the corresponding phenol in 62% yield despite the leaving group occupying the *meta* position, although the reaction time was extended to 72 h. Heteroaromatic halides **147** and **148** were also compatible with these new reaction conditions and could be hydroxylated in 44% and 74% yield, respectively. Interestingly, selectivity was observed in the reaction of dihalogenated arene **148**. Not only did the transformation occur in high yield, as opposed to the reactions of other dihalogenated compounds (**121, 122, 125, 139–141**), but also only the fluoride position was substituted. The increase in reaction performance observed when these reactions were carried out at 60°C, and lack of improvement upon addition of electron donors (Table 3), may indicate that there is a greater activation barrier for $S_{RN}1$ radical–anion coupling or the polar S_NAr addition of the anion for *meta*-substituted halides and weakly activated arenes.

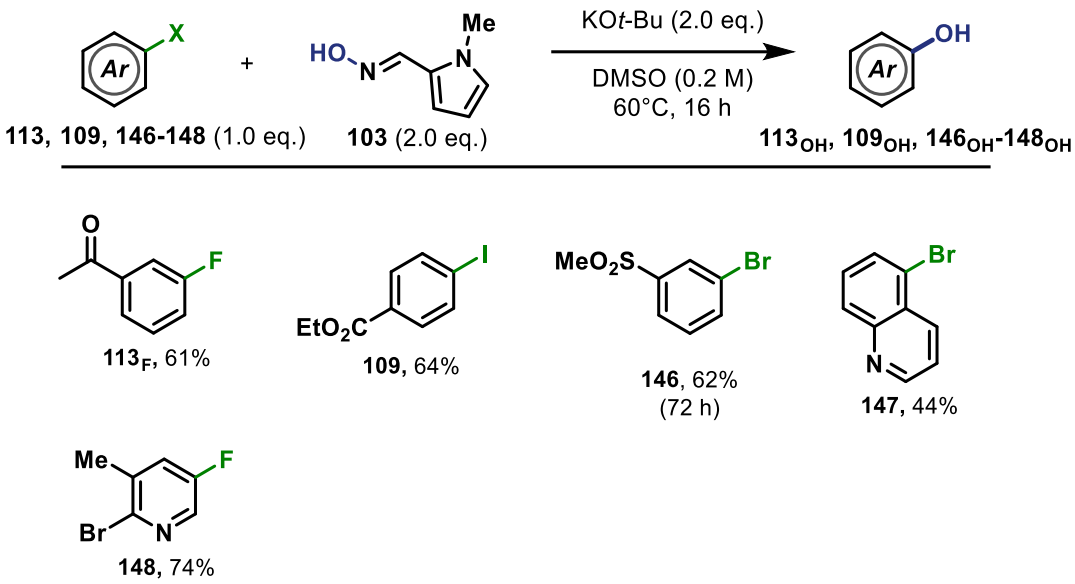

Scheme 40. List of revisited substrates and the yields of their conversion to phenols.

Dihalogenated benzaldehyde **122** also exhibited improved compatibility with oxime **103** at 60°C, forming a mixture of the chloride-substituted product **149** in 27% yield and of the bromide-substituted product **150** in 9% yield (Scheme 41).

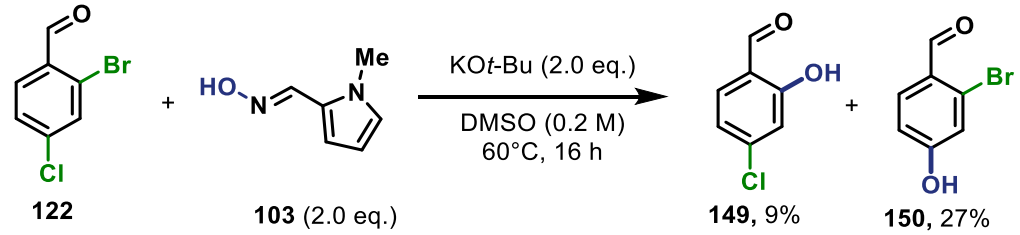

Scheme 41. Reoptimised reaction of the dihalogenated benzaldehyde **122**.

Finally, it was discovered that the hydroxylation of deactivated haloarene **151** could be significantly improved by increasing the reaction temperature to 100°C and using sodium *tert*-butoxide as the base. Unlike the previous studies using sodium *tert*-butoxide (Table 2), the homogeneity/solubility of the reaction mixture was significantly improved under these relatively harsh reaction conditions and phenol **152** could be isolated in 73% yield. This is a promising result revealing the procedure's potential to transform unactivated halides onto the corresponding phenols and encourages future experiments involving polyaromatic systems.

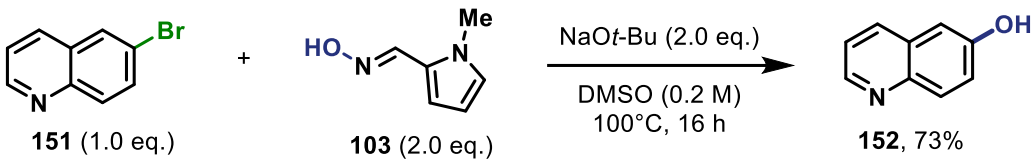

Scheme 42. Reoptimised reaction of 6-bromoquinoline **151**.

2.3.2. Aryl halide-containing drugs

To further probe the functional group compatibility of the developed hydroxylation protocol and its potential use for late-stage functionalisation, the hydroxylation of different aryl halide containing drugs was attempted (Scheme 43). Pleasingly, Fenofibrate **153** (a drug used in lowering lipids levels in human plasma)[83] was smoothly converted into the corresponding phenol product in 76% yield at 30°C. Etoricoxib **154**, used to treat rheumatoid arthritis,[84] could also be hydroxylated in 55% when reacted at 100°C with sodium *tert*-butoxide. Finally, Indomethacin **155**, a nonsteroidal anti-inflammatory drug was examined,[85] but no phenol product was observed (an additional equivalent of base was added to account for the deprotonation of the carboxylic acid). It is difficult to ascertain why this drug was incompatible with the applied conditions as benzoic acid derivatives are known to be compatible with $S_{RN}1$ and S_NAr reactions in literature.[86] It is possible that as previously proposed with benzyl ketone **110** (Scheme 31), acidic α-keto protons and enolate formation could be interfering with the substitution process.

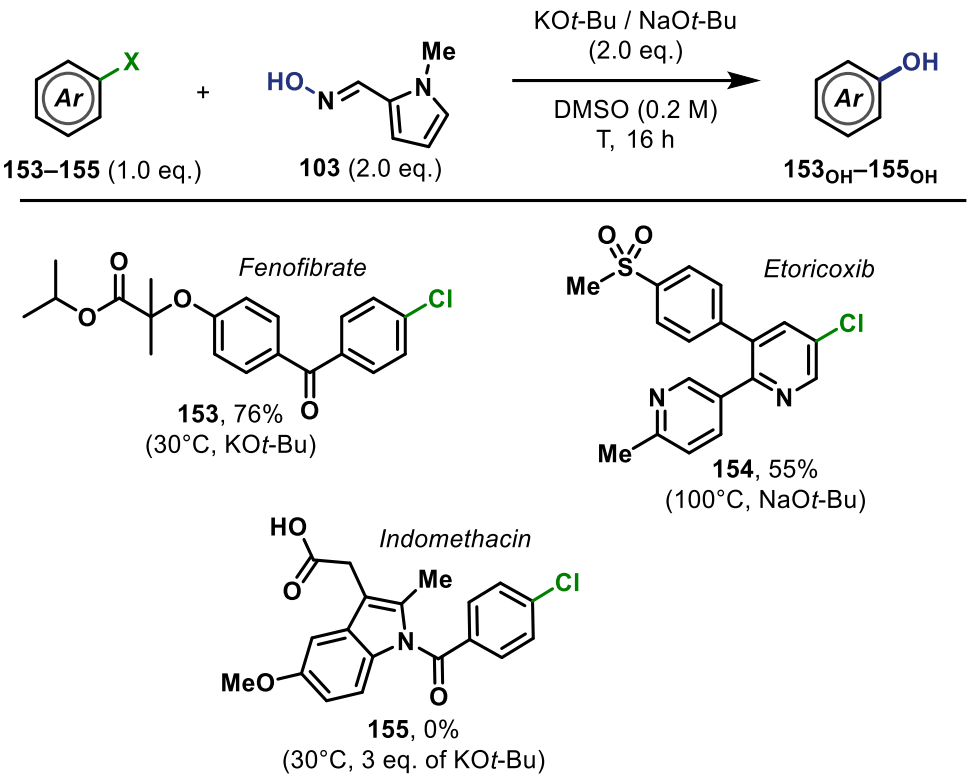

Scheme 43. List of halide-containing drugs, the yields of their conversion to phenols, and the transformation conditions (in brackets).

2.4 Mechanistic studies

2.4.1. Radical inhibition studies

To gain insight into the mechanism of these hydroxylation reactions, selected reactions were performed in the presence of known radical scavengers and oxidants: (2,2,6,6-tetramethylpiperidin-1-yl)oxyl (TEMPO) **156**, Galvinoxyl **157**, and persulfates **158**.

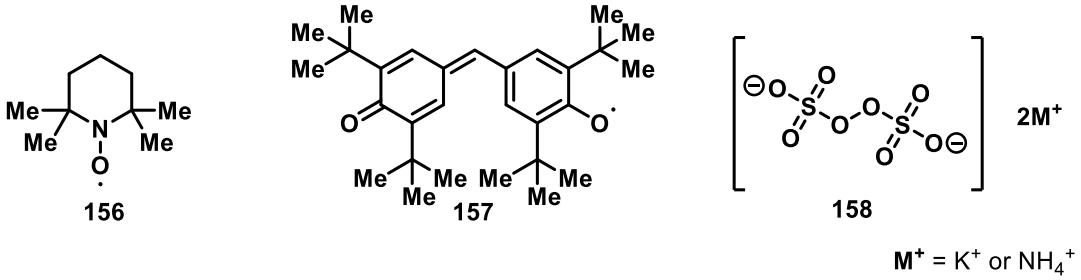

Scheme 44. Radical scavengers and oxidants used in radical inhibition studies.

First, the reactivity of *para*-substituted haloacetophenones **106** and **108** was examined in the presence of the additives. In both cases, the addition of Galvinoxyl **157** significantly decreased the yield of the phenol product (Table 6, Entries 2 and 7), which strongly indicates that these reactions may be radical in nature. Indeed, Galvinoxyl is known to irreversibly bind to free carbon or oxygen radicals (Scheme 45, Equation 3) and it can also be reduced by radical-anion intermediates (Scheme 45, Equations 1 and 2).[87] Conversely, TEMPO **156** exhibited a limited ability to inhibit these reactions,[88] reducing the yields of phenol $\mathbf{106_{OH}}$ to 58% with fluoroacetophenone **106** as the starting material (Table 6, Entry 3), and 49% with bromoacetophenone **108** (Entry 8). Nearly complete inhibition was observed upon addition of ammonium persulfate (APS) $\mathbf{158_{NH4+}}$ (Entries 4 and 9), which was likely due to the acidic ammonium cation protonating the oxime anion. The addition of potassium persulfate (KPS) only partially inhibited the reaction (phenol $\mathbf{106_{OH}}$ formed in 58 and 45% yield, Entries 5 and 10). This reduction in yield may be due to the generation of strongly oxidising $SO_4^{\bullet-}$ species,[89] which would likely oxidise radical-anion intermediates and disrupt an $S_{RN}1$ radical chain. The generally low degree of inhibition observed for all additives could either indicate a polar process is operative, or that radical–anion coupling is very fast and competitive with trapping processes (Scheme 45).

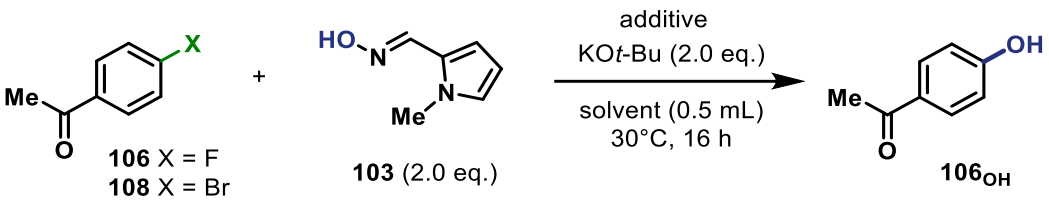

Entry	X	Additive	Yield **106$_{OH}$*** (%)
1		none	82
2		Galvinoxyl (1.0 eq.)	24
3	F	TEMPO (1.0 eq.)	58
4		APS (1.0 eq.)	<5
5		KPS (1.0 eq.)	58
6		None	67
7		Galvinoxyl (1.0 eq.)	10
8	Br	TEMPO (1.0 eq.)	49
9		APS (1.0 eq.)	<5
10		KPS (1.0 eq.)	45

Table 6. Radical inhibition studies of the reactions between *para*-haloacetophenones **106** and **108**, and the oxime **103**. *Yield determined by ^{1}H NMR spectroscopy against an internal standard (dibromomethane).

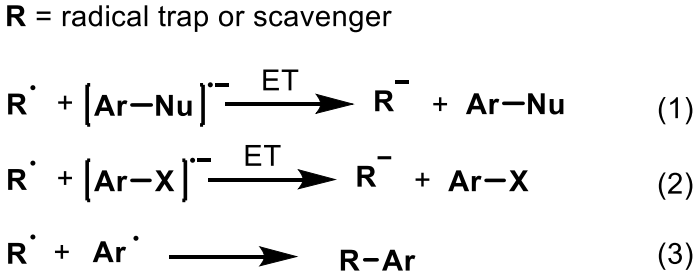

Scheme 45. Potential interactions between radical traps and radical species present in the reaction mixtures.

Using Galvinoxyl as the strongest inhibitor, a similar investigation was performed with *para*-fluoronitrobenzene **126** which was anticipated to act as a model S_NAr substrate. However, the addition of Galvinoxyl still partially inhibited this reaction and reduced the yield of phenol **126$_{OH}$** formation from 96% to 66% (Table 7). This result suggests that the substitution of **126** may proceed at least partially via an open-shell $S_{RN}1$ mechanism.

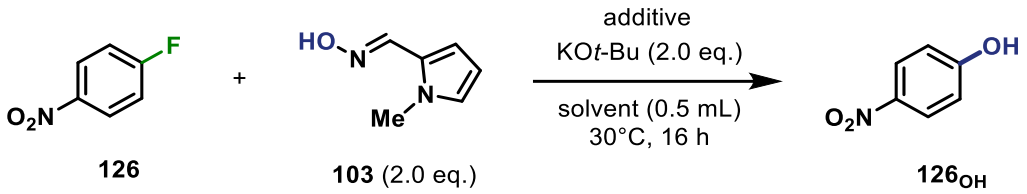

Entry	Additive	Yield **126$_{OH}$*** (%)
1	none	96
2	Galvinoxyl (1.0 eq.)	66

Table 7. Radical inhibition studies of the reactions between *para*-fluoronitrobenzene **126**, and the oxime **103**. *Yield determined by ^{1}H NMR spectroscopy against an internal standard (dibromomethane).

The peculiar reactivity of the unactivated dihalide substrate **142** was also investigated through inhibition studies. Again, a significant inhibition of the reaction was observed by the addition Galvinoxyl **157**, which indicates the involvement of radical processes.

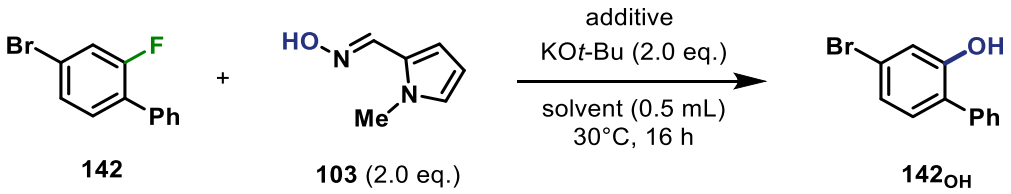

Entry	Additive	Yield **142$_{OH}$*** (%)
1	none	61
2	Galvinoxyl (1.0 eq.)	8

Table 8. Radical inhibition studies of the reactions between dihalogenated biphenyl **142**, and the oxime **103**. *Yield determined by ^{1}H NMR spectroscopy against an internal standard (dibromomethane).

Finally, the reactions with 4-fluoroacetophenone **106**, 4-bromoacetophenone **108** and 4-bromo-2-fluorodiphenyl **142** (which were all strongly inhibited by Galvinoxyl), were repeated in the presence of a 1,1-diphenylethylene **159** (1,1-DPE, 1 equivalent) in anticipation that aryl radical intermediates might rapidly add to 1,1-DPE **159** to form an alkylated product **161** that could be detected by HRMS (Scheme 46).[90] However, no addition products were found from analysis of the crude reaction mixture.

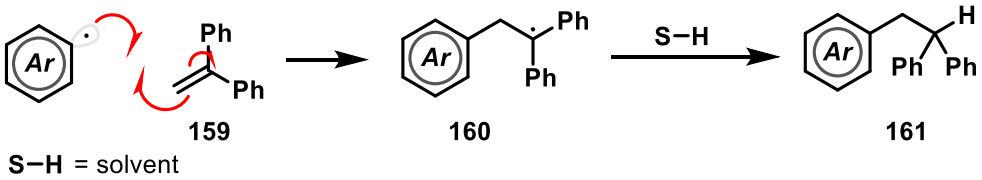

Scheme 46. Potential reaction between 1,1-DPE **159** and an aryl radical.

2.4.2. UV-Vis spectroscopy

Charge-transfer complexes were hypothesised to form under the developed reaction conditions. In collaboration with William Owens-Ward, the formation of such complexes was investigated by UV-vis spectroscopy, which can be used to measure and observe the formation of new (charge transfer) absorption bands.[46]

The absorption spectra of: i) oxime **103** in the presence of KO*t*-Bu (1:1 ratio in DMSO); ii) *para*-bromoacetophenone **108** in the presence of KO*t*-Bu (1:1 ratio in DMSO); and iii) the complete reaction mixture containing *para*-bromoacetophenone **108**, oxime **103** and KO*t*-Bu **162** (1:1:1 ratio in DMSO) were recorded (Figure 6). A new absorption band with a maximum at ~500 nm was observed upon mixing aryl halide **108** and KO*t*-Bu, which was suspected to be due to enolate formation. Signs of a new redshifted absorption band could also be detected in the ternary mixture (**108**, **103** and KO*t*-Bu **162**) as a shoulder observable at ~420 nm, which was presumed to be due to the formation of a charge-transfer complex between deprotonated oxime **103** and the aryl bromide coupling partner.

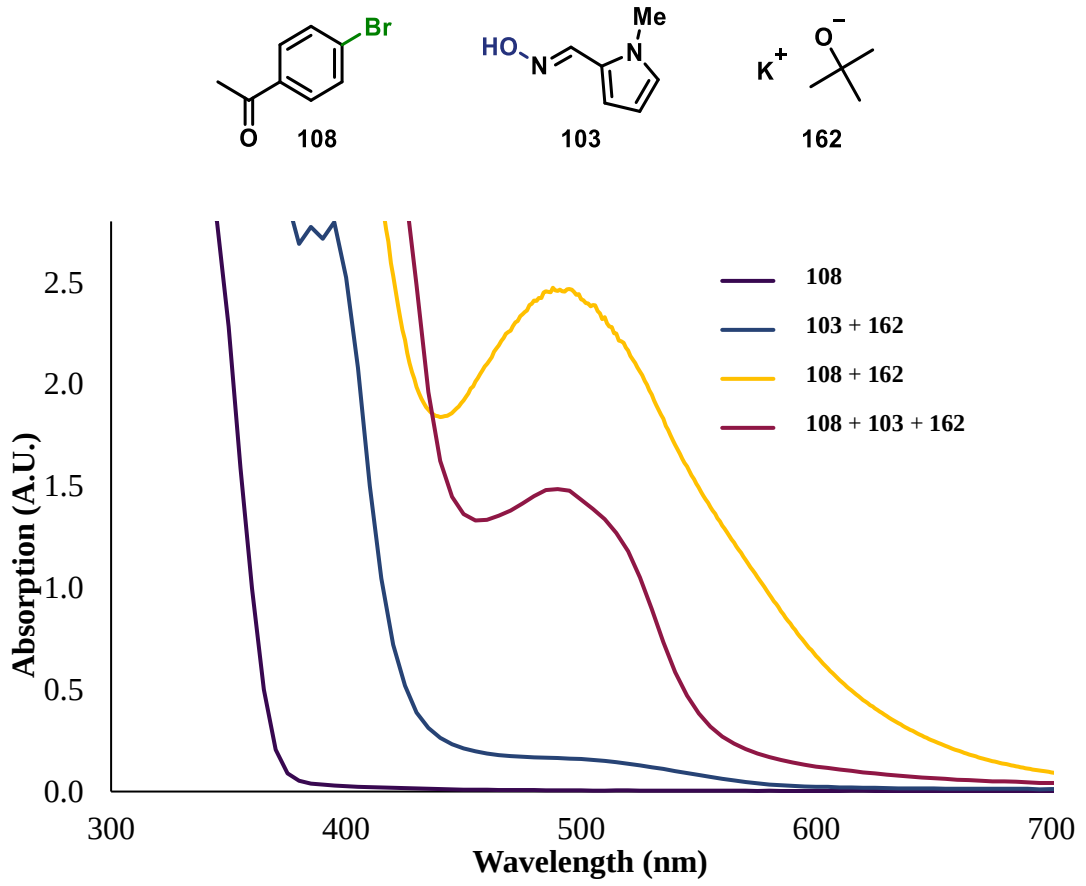

Figure 6. UV-vis absorption spectra overlay. Done in collaboration with William Owens-Ward.

The ratio of acceptor to donor molecules within a charge transfer complex can be determined by mixing acceptor and donor solutions in different proportions. The highest absorption value of the CTC band is indicative of the acceptor to donor ratio within the complex. Stock solutions of deprotonated oxime **103** and 4-bromoacetophenone **108** were therefore mixed in different ratios and the mixtures' absorption spectra were recorded. The highest absorption at around 420 nm is achieved with the components' ratio between 2:1 and 1:1.

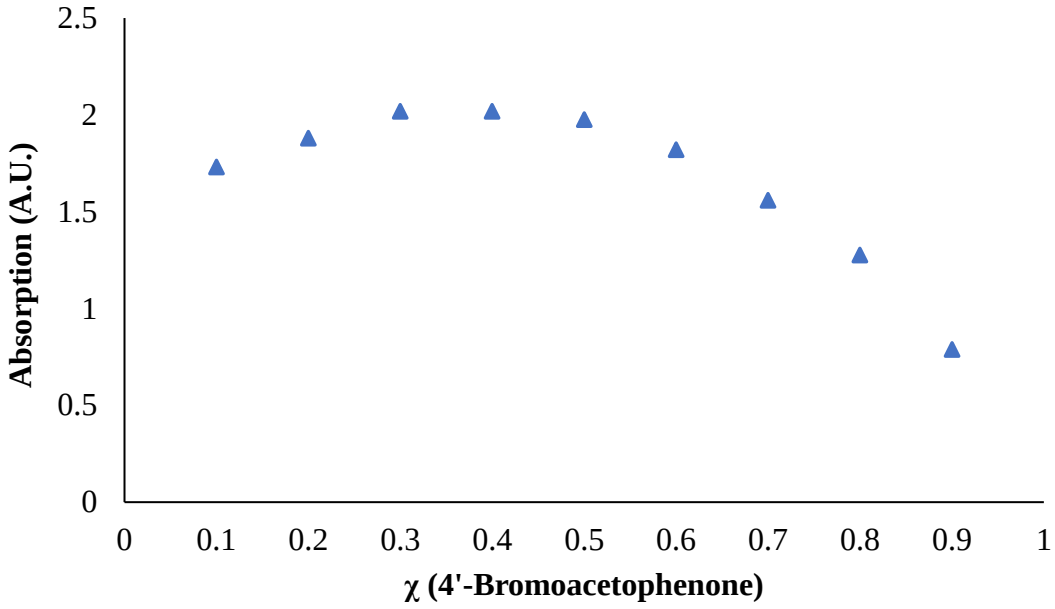

Figure 7. UV vis absorption spectra of oxime **103** and bromoacetophenone **108** solutions mixed in different ratios. Done in collaboration with William Owens-Ward.

From this data the formation of a 1:1 CTC can be assumed within the solution of deprotonated oxime **103** and *p*-bromoacetophenone **108** (Scheme 47). Importantly, as mentioned in Chapter 1, this complex may be activated photochemically (by ambient light in the laboratory) or thermally to form an aryl radical intermediate and initiate a radical chain.

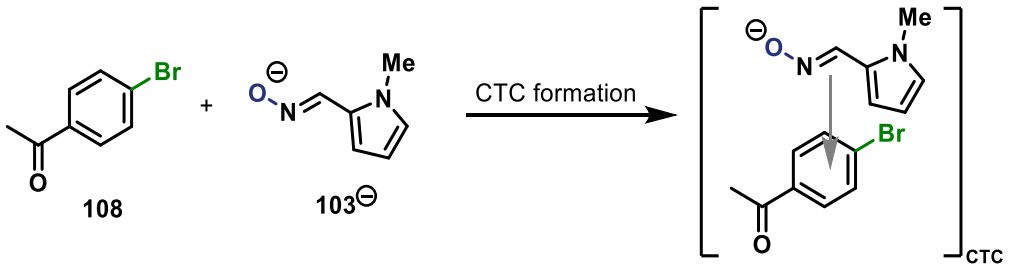

Scheme 47. Scheme of the probable 1:1 CTC formation within the solution of **108** and deprotonated **103**. Grey arrow indicates the direction of electron donation.

2.5. Conclusions and future work

A mild, transition metal-free hydroxylation method was developed. The rationally designed oxime nucleophile was an effective hydroxide surrogate in coupling reactions with electron-deficient aryl halides at 30°C. Re-optimised reaction conditions at 60°C and 100°C successfully accommodated less electron-deficient molecules. Mechanistic investigations indicated participation of radical processes, likely $S_{RN}1$.

Future work may focus on using oxime **103** in late-stage functionalisation (LSF) reactions. LSF is a process which describes a chemoselective, predictable transformation on a complex molecule.[91] Such transformations must tolerate a wide variety of functional groups and therefore mild conditions are highly desirable. LSF processes using sulfonium salts as aryl radical precursors have been recently introduced by Ritter and co-workers,[92–94] and Procter and co-workers [95] (Scheme 48).

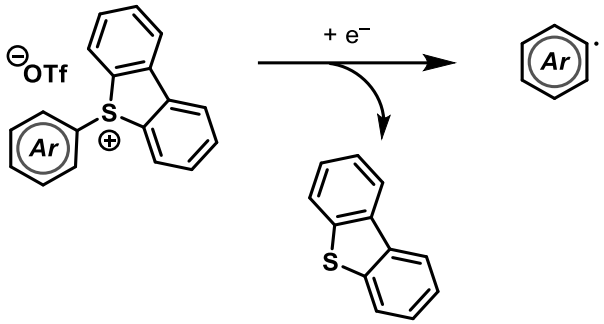

Scheme 48. Mechanism of C–H/C–H coupling enabled by interrupted Pummerer activation.

Initial preliminary studies have been conducted in this area with sulfonium salts **163** and **165**. However, no phenol products could be detected under the standard reaction conditions developed (Scheme 49).

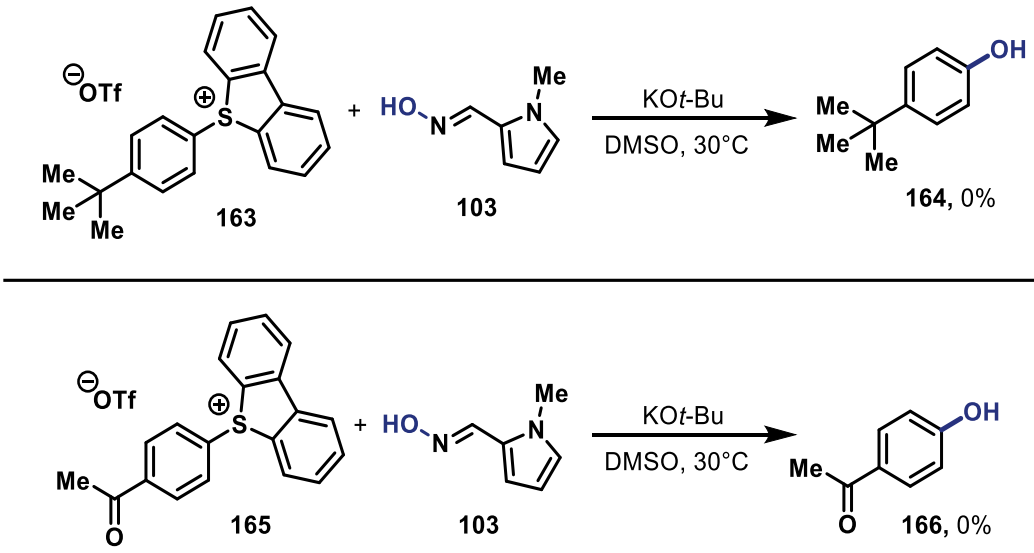

Scheme 49. Coupling reactions between sulfonium salt substrates **163** and **165**, and the oxime **103**.

Chapter 3. Experimental

3.1. General Information

Except where stated, all reagents and anhydrous solvents were purchased from commercial sources and used without further purification. Anhydrous DMSO (99.7 %, Extra Dry over Molecular Sieve) and potassium *tert*-butoxide (98 %) were purchased from Acros Organics.

NMR spectra were recorded on a Bruker AVIII300NB, JEOL ECX400, JEOL ECS400, or Bruker AVIIIHD500 spectrometer. All spectral data was acquired at the stated temperature. Chemical shifts (δ) are quoted in parts per million (ppm). The following residual solvent signals were used as references for ^{1}H and ^{13}C NMR spectra: δ_H 7.26 and δ_C 77.0 for $CDCl_3$, and δ_H 2.50 ppm, δ_C 39.52 ppm for DMSO-d_6. Coupling constants (*J*) are reported in Hertz (Hz) to the nearest 0.1 Hz. The multiplicity abbreviations used are: s singlet, d doublet, t triplet, q quartet, m multiplet. Signal assignment was achieved by analysis of DEPT, COSY, HSQC and HMBC experiments.

Infrared (IR) spectra were recorded on a PerkinElmer UATR 2 spectrometer as a thin film dispersed from CH_2Cl_2 or $CDCl_3$. The wave numbers (*v*) of recorded IR-signals are quoted in cm^{-1}. UV/Vis absorption spectra were recorded on an Agilent Cary 60 spectrometer.

High-resolution mass-spectra were obtained by the University of York Mass Spectrometry Service, using electrospray ionisation (ESI) on a Bruker Daltonics, Micro-tof spectrometer.

EPR spectra were recorded on a Bruker EMX micro spectrometer.

Thin layer chromatography was carried out on Merck silica gel $60F_{254}$ pre-coated aluminium foil sheets and were visualised using UV light (254 nm) and stained with basic aqueous potassium permanganate. Column chromatography was carried out using Fluka silica gel (SiO_2), 35–70 µm, 60 Å under a light positive pressure, eluting with the specified solvent system.

All photochemical reactions were conducted in a fan cooled EvoluChem PhotoRedOx Box reactor using commercial LEDs purchased from HepatoChem Inc.

3.2. Oxime Synthesis

(*E*)-1-Methyl-1H-pyrrole-2-carboxaldehyde oxime (103)

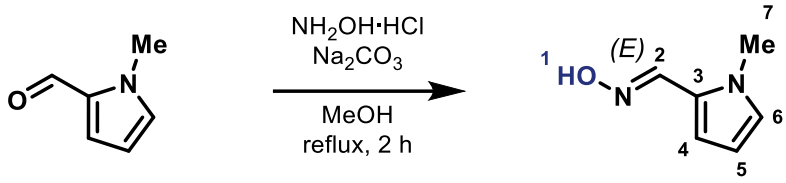

To a stirred solution of $NH_2OH{\cdot}HCl$ (1.67 g, 24.0 mmol), Na_2CO_3 (2.54 g, 24.0 mmol) in MeOH (100 mL) was added *N*-methyl-2-pyrrolecarboxaldehyde (2.15 mL, 20.0 mmol). The mixture was then heated to reflux and stirred for 2 hours. The reaction was allowed to cool to room temperature and MeOH was removed under reduced pressure. The residue was dissolved in EtOAc (50 mL) and H_2O (50 mL). The organic phase was separated and the aqueous phase was extracted with EtOAc (2 × 50 mL). The organics were combined, washed with brine (50 mL), dried ($MgSO_4$), and concentrated under reduced pressure. The crude product was dissolved in a minimum amount of CH_2Cl_2 and purified by column chromatography (30% EtOAc + 3% Et_3N in hexane) to afford the *title compound* **103** (2.12 g, 17.1 mmol, 86%) as a white solid.

Note: Et_3N is added to the column eluent to prevent the decomposition of the oxime reagent.

***R*$_f$** 0.45 (30% EtOAc in hexane);

ATR-FTIR (thin film) ν_{max}/cm^{-1} 3312 (O–H), 1619 (C=N), 1482, 1416, 1309, 1057, 948, 817, 730;

^{1}H NMR (300 MHz, DMSO-D_6) δ_H 10.71 (s, 1H-1), 8.03 (s, 1H-2), 6.85 (dd, *J* = 2.6, 1.8 Hz, 1H-6), 6.32 (dd, *J* = 3.7, 1.8 Hz, 1H-4), 6.02 (dd, *J* = 3.7, 2.6 Hz, 1H-5), 3.73 (s, 3H, H-7);

^{13}C NMR (101 MHz, DMSO-D_6) δ_C 141.5 (CH, C-2), 126.5 (CH, C-6), 125.6 (C, C-3), 112.4 (CH, C-4), 107.8 (CH, C-5), 35.9 (CH_3, C-7).

HRMS (ESI^+) *m/z* calcd. for $C_6H_9N_2O$ $(M + H)^+$ 125.0709, found 125.0712.

3.3. Aryl Halide Hydroxylation

General Procedure A

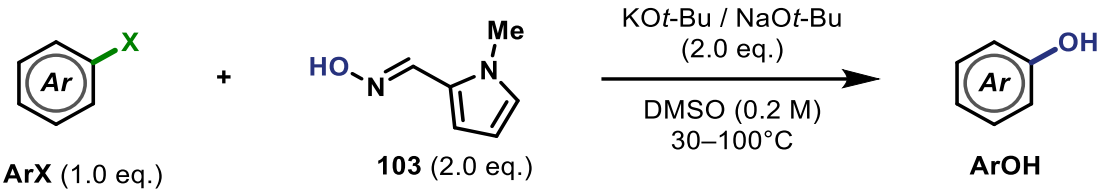

To an oven-dried screw-cap 8 mL reaction vial was charged the appropriate base (2.0 eq.), oxime **103** (2.0 eq.), and if solid, the arene coupling partner **ArX** (0.30 mmol, 1.0 eq.). To the solids was sequentially added a magnetic stir bar, anhydrous DMSO (1.5 mL), and if liquid, the arene coupling partner **ArX**. The vial was closed and the reaction mixture was sparged with N_2 for 15 minutes, then sealed with parafilm. The reaction mixture was stirred and heated at the specified temperature in a metal heating block for the stated time. The mixture was then diluted with CH_2Cl_2 or EtOAc (20 mL), poured into a mixture of water (10 mL) and brine (5 mL), then acidified with 10% aq. HCl (~1 mL). The organic phase was collected and the aqueous phase was extracted with CH_2Cl_2 or EtOAc (3 × 20 mL). The organics were combined, dried ($MgSO_4$), and concentrated under reduced pressure. The crude product was then purified by column chromatography to afford the phenol product **ArOH**.

4′-Hydroxyacetophenone ($\mathbf{106_{OH}}$)

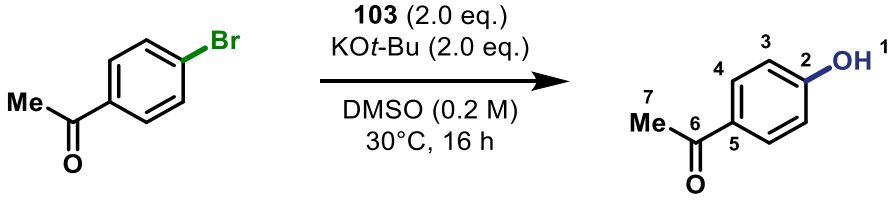

Synthesized using **General Procedure A** with potassium *tert*-butoxide (67.3 mg, 0.60 mmol, 2.0 eq.), oxime **103** (74.5 mg, 0.60 mmol, 2.0 eq.), and 4′-bromoacetophenone **108** (59.7 mg, 0.30 mmol, 1.0 eq.) in DMSO (1.5 mL). The reaction was heated at 30°C and stirred for 16 h. The crude product was dissolved in a minimum amount of CH_2Cl_2, dried onto silica gel, and purified by column chromatography (30% EtOAc in hexane) to afford the *title compound* **$\mathbf{106_{OH}}$** (33.5 mg, 0.246 mmol, 82%) as a white solid.

Lab notebook reference: PU-01-002

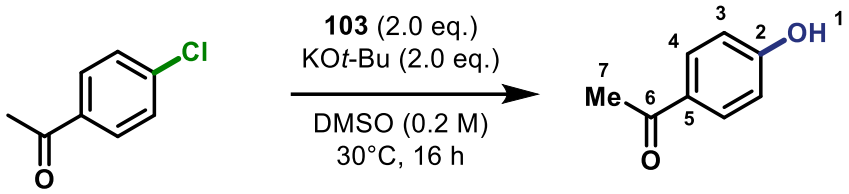

Synthesized using **General Procedure A** with potassium *tert*-butoxide (67.3 mg, 0.60 mmol, 2.0 eq.), oxime **103** (74.5 mg, 0.60 mmol, 2.0 eq.), and 4′-chloroacetophenone **107** (46.4 mg, 0.30 mmol, 1.0 eq.) in DMSO (1.5 mL). The reaction was heated at 30°C and stirred for 16 h. The crude product was dissolved in a minimum amount of CH_2Cl_2, dried onto silica gel, and purified by column chromatography (30% EtOAc in hexane) to afford the *title compound* **106$_{OH}$** (30 mg, 0.22 mmol, 73%) as a white solid.

Lab notebook reference: PU-01-045

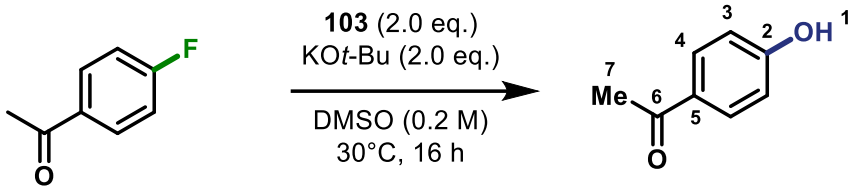

Synthesized using **General Procedure A** with potassium *tert*-butoxide (67.3 mg, 0.60 mmol, 2.0 eq.), oxime **103** (74.5 mg, 0.60 mmol, 2.0 eq.), and 4′-fluoroacetophenone **106** (41.4 mg, 0.30 mmol, 1.0 eq.) in DMSO (1.5 mL). The reaction was heated at 30°C and stirred for 16 h. The crude product was dissolved in a minimum amount of CH_2Cl_2, dried onto silica gel, and purified by column chromatography (30% EtOAc in hexane) to afford the *title compound* **106$_{OH}$** (36.0 mg, 0.265 mmol, 88%) as a white solid.

Lab notebook reference: PU-01-031

R_f 0.51 (50% EtOAc in hexane);

ATR-FTIR (thin film) ν_{max}/cm^{-1} 3303 (O–H), 1660 (C=O), 1602, 1575, 1512, 1357, 1277, 1218, 1166, 963 848, 816, 568;

^{1}H NMR (300 MHz, $CDCl_3$) δ_H 7.91 (d, *J* = 8.8, 2H, H-4), 6.91 (d, *J* = 8.8 Hz, 2H, H-3), 6.37 (br s, 1H, H-1) 2.58 (s, 3H, H-7);

^{13}C NMR (101 MHz, $CDCl_3$) δ_C 198.4 (C, C-6), 161.2 (C, C-2), 131.3 (CH, C-4), 129.9 (C, C-5), 115.6 (CH, C-3), 26.5 (CH_3, C-7);

HRMS (ESI$^-$) *m/z* calcd. for $C_8H_7O_2$ $(M - H)^-$ 135.0452, found 135.0455.

Spectroscopic data matched those reported in the literature.[15]

4′-Hydroxybenzophenone (115_{OH})

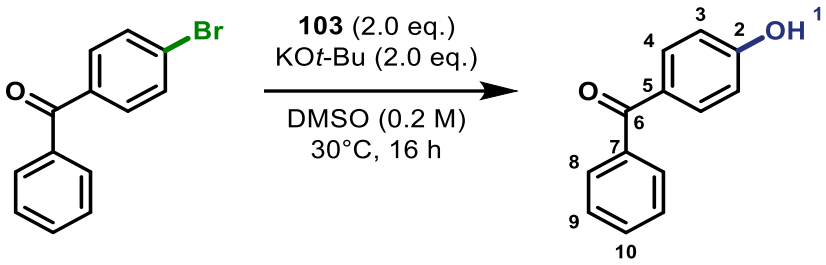

Synthesized using **General Procedure A** with potassium *tert*-butoxide (67.3 mg, 0.60 mmol, 2.0 eq.), oxime **103** (74.5 mg, 0.60 mmol, 2.0 eq.), and 4′-bromobenzophenone **115** (78.3 mg, 0.30 mmol, 1.0 eq.) in DMSO (1.5 mL). The reaction was heated at 30°C and stirred for 16 h. The crude product was dissolved in a minimum amount of CH_2Cl_2, dried onto silica gel, and purified by column chromatography (40% EtOAc in hexane) to afford the *title compound* **115_{OH}** (39.0 mg, 0.197 mmol, 66%) as an off-white solid.

R_f 0.18 (40% EtOAc in hexane);

ATR-FTIR (thin film) ν_{max}/cm^{-1} 3251 (O–H), 1633 (C=O), 1560, 1585, 1572, 1319, 1281, 1150, 699, 606;

^{1}H NMR (400 MHz, $CDCl_3$) δ_H 7.80 (d, *J* = 8.6 Hz, 2H, H-4), 7.76 (d, *J* = 7.6 Hz, 2H, H-8), 7.57 (t, *J* = 7.6 Hz, 1H, H-10), 7.47 (dd, *J* = 7.6, 7.6 Hz, 2H, H-9), 6.92 (d, *J* = 8.6 Hz, 2H, H-3), 5.76 (br s, 1H, H-1);

^{13}C NMR (101 MHz, $CDCl_3$) δ_C 196.8 (C, C-6), 160.7 (C, C-2), 138.2 (C, C-5/7), 133.2 (CH, C-8), 132.3 (CH, C-4/9), 130.0 (CH, C-4/9), 129.8 (C, C-5/7), 128.4 (CH, C-10), 115.5 (CH, C-3);

HRMS (ESI^+) *m/z* calcd. for $C_{13}H_{10}NaO_2$ $(M + Na)^+$ 221.0573, found 221.0572.

Spectroscopic data matched those reported in the literature.[96]

Lab notebook reference: PU-01-079

Ethyl 4-hydroxybenzoate (109_{OH})

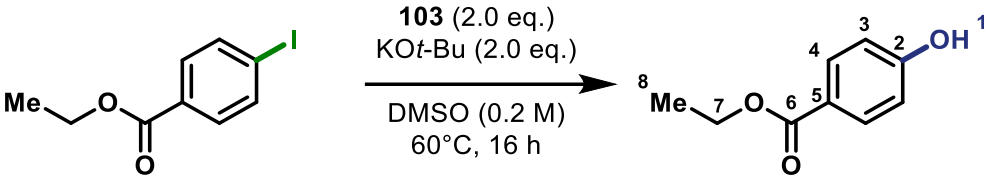

Synthesized using **General Procedure A** with potassium *tert*-butoxide (67.3 mg, 0.60 mmol, 2.0 eq.), oxime **103** (74.5 mg, 0.60 mmol, 2.0 eq.), and ethyl 4-iodobenzoate **109** (82.8 mg, 0.30 mmol, 1.0 eq.) in DMSO (1.5 mL). The reaction was heated at 60°C and stirred for 16 h. The crude product was dissolved in a minimum amount of CH_2Cl_2, dried onto silica gel, and purified by column chromatography (30% EtOAc in hexane) to afford the *title compound* $\mathbf{109_{OH}}$ (32.0 mg, 0.193 mmol, 64%) as an off-white solid.

$\boldsymbol{R_f}$ 0.65 (30% EtOAc in hexane);

ATR-FTIR (thin film) ν_{max}/cm^{-1} 3218 (O–H), 1673 (C=O), 1607, 1592, 1287, 1241, 1169;

^{1}H NMR (400 MHz, $CDCl_3$) δ_H 7.96 (d, J = 8.8 Hz, 2H, H-4), 6.88 (d, J = 8.8 Hz, 2H, H-3), 4.35 (q, J = 7.1 Hz, 2H, H-7), 1.38 (t, J = 7.1 Hz, 3H, H-8);

^{13}C NMR (101 MHz, $CDCl_3$) δ_C 189.1 (C, C-6), 160.0 (C, C-2), 136.0 (C, C-5), 132.0 (CH, C-4), 115.3 (CH, C-3), 61.0 (CH_2, C-7), 14.5 (CH_3, C-8);

HRMS (ESI^-) *m/z* calcd. for $C_9H_9O_3$ $(M - H)^-$ 165.0557, found 165.0557.

Spectroscopic data matched those reported in the literature.[15]

Lab notebook reference: PU-01-075

4-Hydroxybenzaldehyde (120_{OH})

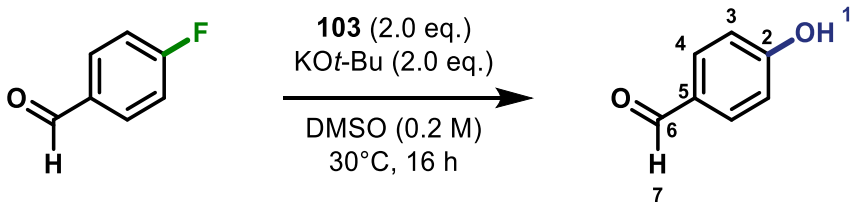

Synthesized using **General Procedure A** with potassium *tert*-butoxide (67.3 mg, 0.60 mmol, 2.0 eq.), oxime **103** (74.5 mg, 0.60 mmol, 2.0 eq.), and 4-fluorobenzaldehyde $\mathbf{120_F}$ (37.3 mg, 0.30 mmol, 1.0 eq.) in DMSO (1.5 mL). The reaction was heated at 30°C and stirred for 16 h.

The crude product was dissolved in a minimum amount of CH_2Cl_2, dried onto silica gel, and purified by column chromatography (30% EtOAc in hexane) to afford the *title compound* **120$_{OH}$** (30.0 mg, 0.246 mmol, 82%) as a peach-coloured solid.

R_f 0.42 (30% EtOAc in hexane);

ATR-FTIR (thin film) ν_{max}/cm^{-1} 3254 (O–H), 1675 (C=O), 1601, 1583, 1216, 1157, 1009;

^{1}H NMR (400 MHz, $CDCl_3$) δ_H 9.88 (s, 1H, H-7), 7.82 (d, *J* = 8.7 Hz, 2H, H-4), 6.95 (d, *J* = 8.7 Hz, 2H, H-3), 5.58 (br s, 1H, H-1);

^{13}C NMR (101 MHz, $CDCl_3$) δ_C 191.5 (CH, C-6), 161.8 (C, C-2), 132.7 (CH, C-4), 123.0 (C, C-5), 116.16 (CH, C-3);

HRMS (ESI$^-$) *m/z* calcd. for $C_7H_5O_2$ $(M - H)^-$ 121.0295, found 121.0298.

Spectroscopic data matched those reported in the literature.[97]

Lab notebook reference: PU-01-078

3'-Hydroxyacetophenone (114)

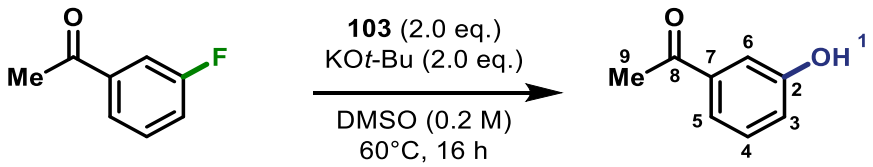

Synthesized using **General Procedure A** with potassium *tert*-butoxide (67.3 mg, 0.60 mmol, 2.0 eq.), oxime **103** (74.5 mg, 0.60 mmol, 2.0 eq.), and 3′-fluoroacetophenone **113$_F$** (41.4 mg, 36.8 µl, 0.30 mmol, 1.0 eq.) in DMSO (1.5 mL). The reaction was heated at 60°C and stirred for 16 h. The crude product was dissolved in a minimum amount of CH_2Cl_2, dried onto silica gel, and purified by column chromatography (20 – 50% EtOAc in hexane) to the *title compound* **114** (25.0 mg, 0.184 mmol, 61%) as an off-white solid.

R_f 0.14 (20% EtOAc in hexane);

ATR-FTIR (thin film) ν_{max}/cm^{-1} 3331 (O–H), 2924, 1668 (C=O), 1585, 1451, 1289;

^{1}H NMR (400 MHz, $CDCl_3$) δ_H 7.55 – 7.47 (m, 2H, H-6 and H-5), 7.35 (dd, *J* = 8.0, 8.0 Hz, 1H, H-4), 7.13 – 7.04 (m, 1H, H-3), 5.75 (br s, 1H, H-1), 2.60 (s, 3H, H-9);

^{13}C NMR (101 MHz, $CDCl_3$) δ_C 198.8 (C, C-8), 156.3 (C, C-2), 138.6 (C, C-7), 130.1 (CH, C-4), 121.3 (CH, C-5/6), 120.8 (CH, C-3), 114.8 (CH, C-6/5), 26.9 (CH_3, C-9);

HRMS (ESI$^-$) *m/z* calcd. for $C_8H_7O_2$ $(M - H)^-$ 135.0452, found 135.0449.

Spectroscopic data matched those reported in the literature.[24]

Lab notebook reference: PU-01-063

4-Hydroxybenzonitrile (123$_{OH}$)

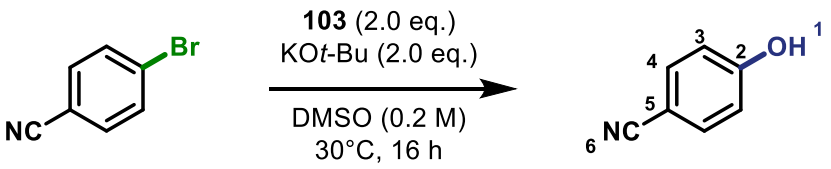

Synthesized using **General Procedure A** with potassium *tert*-butoxide (67.3 mg, 0.60 mmol, 2.0 eq.), oxime **103** (74.5 mg, 0.60 mmol, 2.0 eq.), and 4-bromobenzonitrile **123** (54.6 mg, 0.30 mmol, 1.0 eq.) in DMSO (1.5 mL). The reaction was heated at 30°C and stirred for 16 h. The crude product was dissolved in a minimum amount of CH_2Cl_2, dried onto silica gel, and purified by column chromatography (40% EtOAc in hexane) to afford the *title compound* **123$_{OH}$** (24.0 mg, 0.202 mmol, 67%) as a brown solid.

R_f 0.61 (40% EtOAc in hexane);

ATR-FTIR (thin film) ν_{max}/cm^{-1} 3279 (O–H), 2233 (C≡N), 1612, 1587, 1509;

^{1}H NMR (300 MHz, $CDCl_3$) δ_H 7.56 (d, *J* = 8.8 Hz, 1H, H-4), 6.91 (d, *J* = 8.8 Hz, 1H, H-3), 5.47 (br s, 1H, H-1);

^{13}C NMR (101 MHz, $CDCl_3$) δ_C 160.3 (C, C-2), 134.5 (CH, C-4), 119.4 (CN, C-6), 116.6 (CH, C-3), 103.3 (C, C-5);

HRMS (ESI$^-$) *m/z* calcd. for C_7H_4NO $(M - H)^-$ 118.0298, found 118.0300.

Spectroscopic data matched those reported in the literature.[15]

Lab notebook reference: PU-02-093/094

3-Hydroxybenzonitrile (124_{OH})

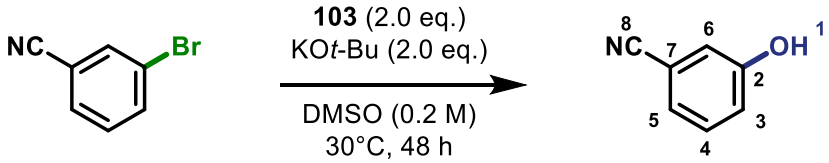

Synthesized using **General Procedure A** with potassium *tert*-butoxide (67.3 mg, 0.60 mmol, 2.0 eq.), oxime **103** (74.5 mg, 0.60 mmol, 2.0 eq.), and 3-bromobenzonitrile **124** (54.6 mg, 0.30 mmol, 1.0 eq.) in DMSO (1.5 mL). The reaction was heated at 30°C and stirred for 48 h. The crude product was dissolved in a minimum amount of CH_2Cl_2, dried onto silica gel, and purified by column chromatography (40% EtOAc in hexane) to afford the *title compound* **124_{OH}** (19 mg, 0.16 mmol, 53%) as an off-white solid.

R_f 0.44 (40% EtOAc in hexane);

ATR-FTIR (thin film) ν_{max}/cm^{-1} 3352 (O–H), 2927, 2238 (C≡N), 1714, 1598, 1583;

^{1}H NMR (300 MHz, $CDCl_3$) δ_H 7.34 (dd, J = 7.9, 7.7 Hz, 1H, H-4), 7.23 (ddd, J = 7.7, 1.3, 1.3 Hz, 1H, H-5), 7.14 – 7.02 (m, 2H, H-6 and H-3), 5.41 (br s, 1H, H-1);

^{13}C NMR (75 MHz, $CDCl_3$) δ_C 156.1 (C, C-2), 130.8 (CH, C-4), 124.8 (CH, H-5), 120.6 (CH, C-3/6), 118.9 (CH, H-3/6), 118.6 (C, C-7/8), 113.4 (C, C-7/8);

HRMS (ESI^-) *m/z* calcd. for C_7H_4NO $(M - H)^-$ 118.0298, found 118.0301.

Spectroscopic data matched those reported in the literature.[98]

Lab notebook reference: PU-01-069

3-(Methylsulfonyl)phenol (146_{OH})

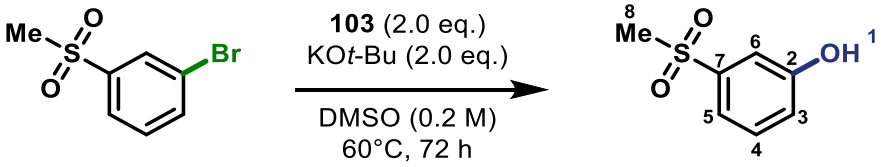

Synthesized using **General Procedure A** with potassium *tert*-butoxide (67.3 mg, 0.60 mmol, 2.0 eq.), oxime **103** (74.5 mg, 0.60 mmol, 2.0 eq.), and 3-bromophenyl-1-methylsulfone **146** (70.5 mg, 0.30 mmol, 1.0 eq.) in DMSO (1.5 mL). The reaction was heated at 60°C and stirred for 72 h. The crude product was dissolved in a minimum amount of CH_2Cl_2, dried onto silica

gel, and purified by column chromatography (60% EtOAc in hexane) to afford the *title compound* **146$_{OH}$** (33.0 mg, 0.192 mmol, 64%) as a bright yellow solid.

R_f 0.61 (60% EtOAc in hexane);

ATR-FTIR (thin film) ν_{max}/cm^{-1} 3384 (O–H), 2927, 1605, 1591, 1447, 1294, 1139 (S=O), 763;

^{1}H NMR (400 MHz, $CDCl_3$) δ_H 7.47 – 7.35 (m, 3H, H-4, H-5 and H-6), 7.16 – 7.09 (m, 1H, H-2), 3.07 (s, 3H, H-8);

^{13}C NMR (101 MHz, $CDCl_3$) δ_C 157.2 (C, C-2), 148.9 (C, C-7), 131.0 (CH, C-4/5/6), 121.7 (CH, C-4/5/6), 118.9 (CH, C-3), 114.0 (CH, C-4/5/6), 44.5 (CH_3, C-8);

HRMS (ESI$^+$) *m/z* calcd. for $C_7H_8NaO_3S$ $(M + Na)^+$ 195.0086, found 195.0090.

Lab notebook reference: PU-02-102

4-Nitrophenol (126$_{OH}$)

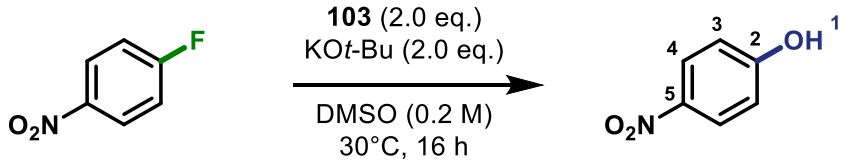

Synthesized using **General Procedure A** with potassium *tert*-butoxide (67.3 mg, 0.60 mmol, 2.0 eq.), oxime **103** (74.5 mg, 0.60 mmol, 2.0 eq.), and 1-fluoro-4-nitrobenzene **126** (42.3 mg, 0.30 mmol, 1.0 eq.) in DMSO (1.5 mL). The reaction was heated at 30°C and stirred for 16 h. The crude product was dissolved in a minimum amount of CH_2Cl_2, dried onto silica gel, and purified by column chromatography (20% EtOAc in hexane) to afford the *title compound* **126$_{OH}$** (40.0 mg, 0.288 mmol, 96%) as a yellow solid.

R_f 0.35 (25% EtOAc in hexane);

ATR-FTIR (thin film) ν_{max}/cm^{-1} 3130 (O–H), 1591, 1513, 1498 (N–O), 1334 (N–O), 1256, 1110, 850;

^{1}H NMR (400 MHz, $CDCl_3$) δ_H 8.18 (d, *J* = 9.1 Hz, 2H, H-4), 6.91 (d, *J* = 9.1 Hz, 2H, H-3), 5.58 (br s, 1H, H-1);

^{13}C NMR (75 MHz, $CDCl_3$) δ_C 161.9 (C, C-2), 141.6 (C, C-5), 126.4 (CH, C-4), 115.9 (CH, C-3);

HRMS (ESI$^-$) *m/z* calcd. for $C_6H_4NO_3$ $(M - H)^-$ 138.0197, found 138.0193.

Spectroscopic data matched those reported in the literature.[15]

Lab notebook reference: PU-01-042

2-Nitrophenol ($\mathbf{127_{OH}}$)

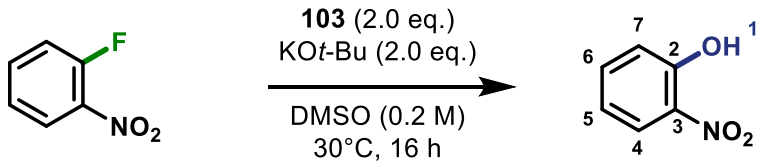

Synthesized using **General Procedure A** with potassium *tert*-butoxide (67.3 mg, 0.60 mmol, 2.0 eq.), oxime **103** (74.5 mg, 0.60 mmol, 2.0 eq.), and 1-fluoro-2-nitrobenzene **127** (42.3 mg, 0.30 mmol, 1.0 eq.) in DMSO (1.5 mL). The reaction was heated at 30 °C and stirred for 16 h. The crude product was dissolved in a minimum amount of CH_2Cl_2, dried onto silica gel, and purified by column chromatography (20% EtOAc in hexane) to afford the *title compound* $\mathbf{127_{OH}}$ (7.0 mg, 0.050 mmol, 17%) as a yellow solid.

$\boldsymbol{R_f}$ 0.49 (20% EtOAc in hexane);

ATR-FTIR (thin film) ν_{max}/cm^{-1} 3252 (O–H), 2924, 1732, 1620, 1591, 1535 (N–O), 1456, 1478, 1333 (N–O), 1257, 1187, 1029, 870, 747, 666;

^{1}H NMR (400 MHz, $CDCl_3$) δ_H 10.60 (s, 1H, H-1), 8.12 (dd, *J* = 8.5, 1.6 Hz, 1H, H-4), 7.59 (ddd, *J* = 8.5, 7.1, 1.6 Hz, 1H, H-6), 7.16 (dd, *J* = 8.5, 1.3 Hz, 1H, H-7), 7.00 (ddd, *J* = 8.5, 7.1, 1.3 Hz, 1H, H-5);

^{13}C NMR (101 MHz, $CDCl_3$) δ_C 155.3 (C, C-2), 137.7 (CH, C-4), 133.8 (C, C-3), 125.2 (CH, C-5/6), 120.4 (CH, C-5/6), 120.1 (CH, C-7);

HRMS (ESI^-) *m/z* calcd. for $C_6H_4NO_3$ $(M - H)^-$ 138.0197, found 138.0196.

Spectroscopic data matched those reported in the literature.[99]

Lab notebook reference: PU-01-022

2-Hydroxy-4-bromobiphenyl (163)

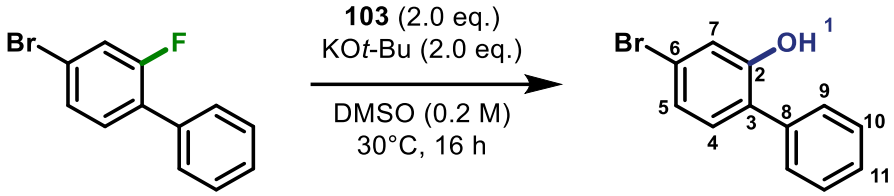

Synthesized using **General Procedure A** with potassium *tert*-butoxide (67.3 mg, 0.60 mmol, 2.0 eq.), oxime **103** (74.5 mg, 0.60 mmol, 2.0 eq.), and 2-fluoro-4-bromobiphenyl **162** (75.3 mg, 0.30 mmol, 1.0 eq.) in DMSO (1.5 mL). The reaction was heated at 30°C and stirred for 16 h. The crude product was dissolved in a minimum amount of CH_2Cl_2, dried onto silica gel, and purified by column chromatography (20% EtOAc in hexane) to afford the *title compound* **163** (58.0 mg, 0.233 mmol, 78%) as a yellow oil.

$\boldsymbol{R_f}$ 0.50 (20% EtOAc in hexane);

ATR-FTIR (thin film) ν_{max}/cm^{-1} 3520 (O–H), 1476, 878, 765, 701;

^{1}H NMR (400 MHz, $CDCl_3$) δ_H 7.55 – 7.46 (m, 2H, H-9), 7.46 – 7.37 (m, 3H, H-4/5/6/10/11), 7.17 (d, J = 1.8 Hz, 1H, H-7), 7.16 – 7.05 (m, 2H, H-4/5/6/10/11), 5.27 (br s, 1H, H-1);

^{13}C NMR (101 MHz, $CDCl_3$) δ_C 153.3 (C, C-2), 136.1 (C, C-6), 131.4 (CH, C-4/5/9/10/11), 129.6 (CH, C-4/5/9/10/11), 129.0 (CH, C-4/5/9/10/11), 128.4 (CH, C-4/5/9/10/11), 127.3 (C, C-8), 124.1 (CH, C-4/5/9/10/11), 122.2 (C, C-3), 119.2 (CH, C-7);

HRMS (ESI$^-$) *m/z* calcd. for $C_{12}H_8O^{79}Br$ $(M - H)^-$ 246.9764, found 246.9761.

Lab notebook reference: PU-01-038

5-Hydroxy-2(trifluoromethyl) pyridine (130)

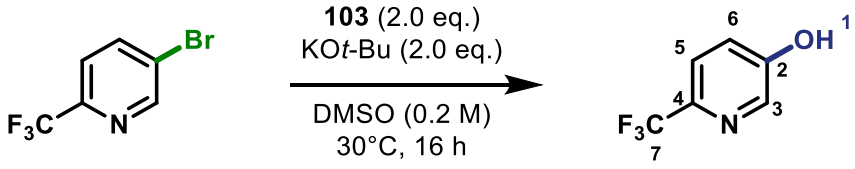

Synthesized using **General Procedure A** with potassium *tert*-butoxide (67.3 mg, 0.60 mmol, 2.0 eq.), oxime **103** (74.5 mg, 0.60 mmol, 2.0 eq.), and 5-bromo-2(trifluoromethyl) pyridine **129** (67.8 mg, 0.30 mmol, 1.0 eq.) in DMSO (1.5 mL). The reaction was heated at 30°C and stirred for 16 h. The crude product was dissolved in a minimum amount of CH_2Cl_2, dried onto silica gel, and purified by column chromatography (30% EtOAc in hexane) to afford the *title compound* **130** (37.0 mg, 0.227 mmol, 76%) as a white solid.

R_f 0.44 (30% EtOAc in hexane);

ATR-FTIR (thin film) ν_{max}/cm^{-1} 3359 (O–H), 1588, 1288, 1138, 1090, 982, 838, 769, 539, 519;

1H NMR (400 MHz, DMSO-D_6) δ_H 10.87 (s, 1H, H-1), 8.26 (d, *J* = 2.7 Hz, 1H, H-3), 7.69 (d, *J* = 8.6 Hz, 1H, H-5), 7.34 (dd, *J* = 8.6, 2.7 Hz, 1H, H-6);

^{13}C NMR (101 MHz, DMSO-D_6) δ_C 156.5 (C, C-2), 138.6 (CH, C-5), 137.2 (q, *J* = 34.1 Hz, C, C-4), 122.8 (CH, C-3), 122.2 (q, *J* = 272.5 Hz, C, C-7), 122.0 (q, *J* = 2.8 Hz, CH, C-6);

^{18}F NMR (282 MHz, $CDCl_3$) δ_F -65.0 (s, 3F, F-7);

HRMS (ESI$^+$) *m/z* calcd. for $C_6H_5F_3NO$ $(M + H)^+$ 164.0318, found 164.0314.

Spectroscopic data matched those reported in the literature.[15]

Lab notebook reference: PU-02-103

5-Hydroxyquinoline (147$_{OH}$)

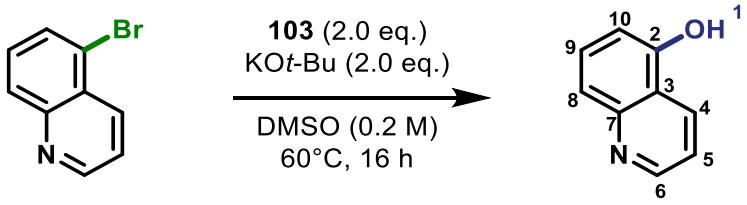

Synthesized using **General Procedure A** with potassium *tert*-butoxide (67.3 mg, 0.60 mmol, 2.0 eq.), oxime **103** (74.5 mg, 0.60 mmol, 2.0 eq.), and 5-bromoquinoline **147** (62.4 mg, 0.30 mmol, 1.0 eq.) in DMSO (1.5 mL). The reaction was heated at 60°C and stirred for 16 h. The crude product was dissolved in a minimum amount of CH_2Cl_2, dried onto silica gel, and purified by column chromatography (60% EtOAc in hexane) to afford the *title compound* **147$_{OH}$** (19.0 mg, 0.131 mmol, 44%) as a white solid.

R_f 0.50 (60% EtOAc in hexane);

ATR-FTIR (thin film) ν_{max}/cm^{-1} 2922 (O–H), 2851, 1982, 1587, 1279, 796;

^{1}H NMR (400 MHz, DMSO-D_6) δ 10.49 (s, 1H, H-1), 8.84 (dd, *J* = 4.2, 1.8 Hz, 1H, H-6), 8.49 (ddd, *J* = 8.5, 1.8, 0.9 Hz, 1H, H-5), 7.54 (dd, *J* = 8.5, 7.5 Hz, 1H, H-9), 7.48 – 7.42 (m, 2H, H-8 and H-4), 6.93 (dd, *J* = 7.5, 1.1 Hz, 1H, H-10);

^{13}C NMR (101 MHz, DMSO-D_6) δ_c 153.3 (C, C-2), 150.5 (CH, C-6), 148.9 (C, C-7), 130.6 (CH, C-5), 129.9 (CH, C-4/8), 120.1 (CH, C-9), 119.6 (C, C-3), 119.4 (CH, C-4/8), 108.4 (CH, C-10);

HRMS (ESI⁻) *m/z* calcd. for C_9H_6NO $(M - H)^-$ 144.0455, found 144.0453.

Spectroscopic data matched those reported in the literature.[98]

Lab notebook reference: PU-01-085

6-Hydroxyquinoline (152)

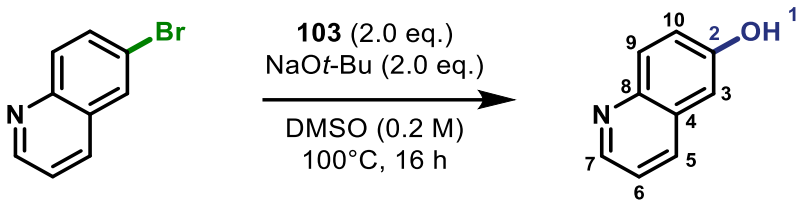

Synthesized using **General Procedure A** with sodium *tert*-butoxide (96.11 mg, 0.60 mmol, 2.0 eq.), oxime **103** (74.5 mg, 0.60 mmol, 2.0 eq.), and 6-bromoquinoline **151** (62.4 mg, 0.30 mmol, 1.0 eq.) in DMSO (1.5 mL). The reaction was heated at 100°C and stirred for 16 h. The crude product was dissolved in a minimum amount of CH_2Cl_2, dried onto silica gel, and purified by column chromatography (80% EtOAc in hexane) to afford the *title compound* **152** (32.0 mg, 0.220 mmol, 73%) as a white solid.

R_f 0.35 (80% EtOAc in hexane);

ATR-FTIR (thin film) ν_{max}/cm^{-1} 3021 (O–H), 1971, 1621, 1506, 1469, 1376, 1315, 1229, 1121, 920, 831;

^{1}H NMR (400 MHz, DMSO-D_6) δ_H 10.05 (s, 1H, H-1), 8.65 (dd, *J* = 4.2, 1.7 Hz, 1H, H-7), 8.13 (ddd, *J* = 8.4, 1.8, 0.7 Hz, 1H, H-5), 7.87 (d, *J* = 9.0 Hz, 1H, H-9), 7.38 (dd, *J* = 8.3, 4.2 Hz, 1H, H-6), 7.32 (dd, *J* = 9.0, 2.7 Hz, 1H, H-10), 7.15 (d, *J* = 2.7 Hz, 1H, H-3);

^{13}C NMR (101 MHz, DMSO-D_6) δ_C 155.5 (C, C-2), 147.2 (CH, C-7), 143.1 (C, C-8), 134.2 (CH, C-5), 130.5 (CH, C-9), 129.4 (C, C-4), 122.0 (CH, C-10/6), 121.4 (CH, C-10/6), 108.4 (CH, C-3);

HRMS (ESI⁻) *m/z* calcd. for C_9H_6NO $(M - H)^-$ 144.0455, found 144.0451.

Spectroscopic data matched those reported in the literature.[24]

Lab notebook reference: PU-02-090

6-Bromo-5-methylpyridin-3-ol (148_{OH})

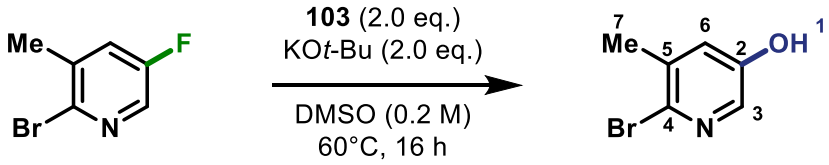

Synthesized using **General Procedure A** with potassium *tert*-butoxide (67.3 mg, 0.60 mmol, 2.0 eq.), oxime **103** (74.5 mg, 0.60 mmol, 2.0 eq.), and 2-bromo-5-fluoro-3-methyl pyridine **148** (57.0 mg, 0.30 mmol, 1.0 eq.) in DMSO (1.5 mL). The reaction was heated at 60°C and stirred for 16 h. The crude product was dissolved in a minimum amount of CH_2Cl_2, dried onto silica gel, and purified by column chromatography (60% EtOAc in hexane) to afford the *title compound* **148_{OH}** (42.0 mg, 0.223 mmol, 74%) as a white solid.

R_f 0.77 (60% EtOAc in hexane);

ATR-FTIR (thin film) ν_{max}/cm^{-1} 2924 (O–H), 1570, 1458, 1403, 1308, 1228, 1158, 1060, 610;

^{1}H NMR (400 MHz, DMSO-D_6) δ_H 10.13 (br s, 1H, H-1), 7.76 (d, J = 3.0 Hz, 1H, H-3), 7.16 (d, J = 3.0 Hz, 1H, H-6), 2.23 (s, 3H, H-7);

^{13}C NMR (101 MHz, DMSO-D_6) δ_C 153.8 (C, C-2), 135.4 (CH, C-3), 135.0 (C, C-4), 132.2 (C, C-5), 126.2 (CH, C-6), 21.3 (CH_3, C-7);

HRMS (ESI^-) *m/z* calcd. for $C_6H_7{}^{79}BrNO$ $(M + H)^+$ 187.9706, found 187.9712.

Lab notebook reference: PU-02-089

Hydroxy-Fenofibrate derivative (153_{OH})

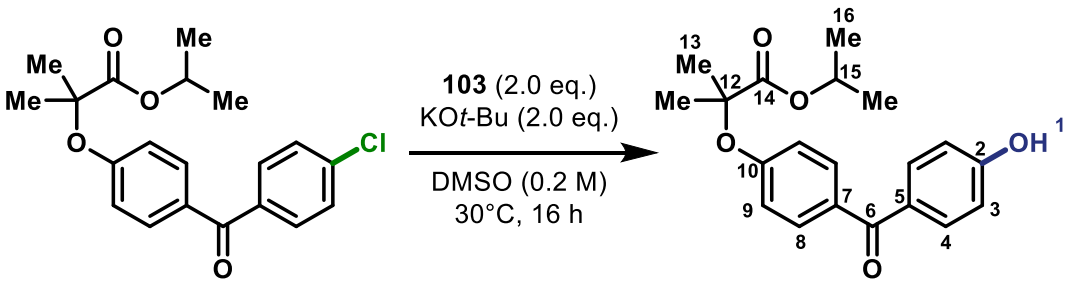

Synthesized using **General Procedure A** with potassium *tert*-butoxide (67.3 mg, 0.60 mmol, 2.0 eq.), oxime **103** (74.5 mg, 0.60 mmol, 2.0 eq.), and Fenofibrate **153** (108.2 mg, 0.30 mmol, 1.0 eq.) in DMSO (1.5 mL). The reaction was heated at 30°C and stirred for 16 h. The crude product was dissolved in a minimum amount of CH_2Cl_2, dried onto silica gel, and purified by

column chromatography (20% EtOAc in hexane) to afford the *title compound* **153$_{OH}$** (78.0 mg, 0.228 mmol, 76%) as an off-white solid.

R_f 0.09 (20% EtOAc in hexane);

ATR-FTIR (thin film) ν_{max}/cm^{-1} 3283 (O–H), 2985, 1730 (C=O), 1600 (C=O), 1285, 1151, 930, 854, 771, 609;

^{1}H NMR (400 MHz, $CDCl_3$) δ_H 7.75 – 7.67 (m, 4H, H-4 and H-8), 6.91 (d, *J* = 8.6 Hz, 2H, H-9), 6.86 (d, *J* = 8.9 Hz, 2H, H-3), 5.09 (septet, *J* = 6.2 Hz, 1H, H-15), 1.66 (s, 6H, H-13), 1.21 (d, *J* = 6.3 Hz, 6H, H-16);

^{13}C NMR (101 MHz, $CDCl_3$) δ_C 195.4 (C, C-6), 173.6 (C, C-14), 160.4 (C, C-2/10), 159.4 (C, C-2/10), 132.8 (CH, C-4/8), 132.0 (CH, C-4/8), 131.2 (C, C-5/7), 130.2 (C, C-5/7), 117.4 (CH, C-3), 115.3 (CH, C-9), 79.5 (C, C-12), 69.6 (CH, C-15), 25.5 (CH_3, C-13), 21.6 (CH_3, C-16);

HRMS (ESI$^-$) *m/z* calcd. for $C_{20}H_{22}NaO_5$ $(M + Na)^+$ 365.1359, found 365.1361.

Spectroscopic data matched those reported in the literature.[100]

Lab notebook reference: PU-01-040

Hydroxy-Etoricoxib derivative (154$_{OH}$)

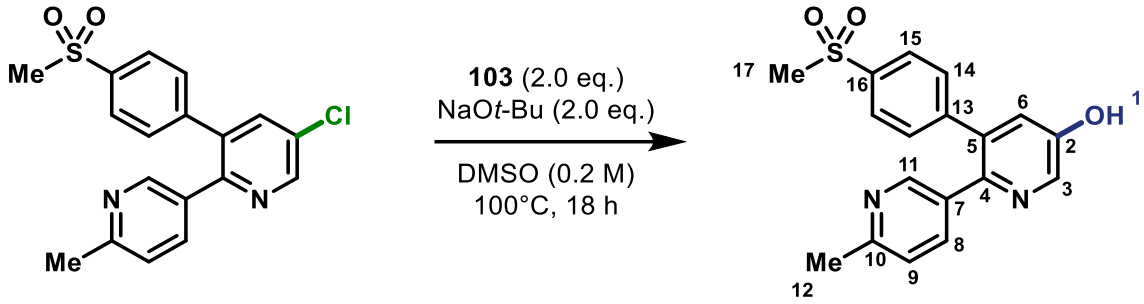

Synthesized using **General Procedure A** with sodium *tert*-butoxide (9.6 mg, 0.14 mmol, 2.0 eq.), oxime **103** (17.4 mg, 0.14 mmol, 2.0 eq.), and Etoricoxib **154** (25.0 mg, 0.07 mmol, 1.0 eq.) in DMSO (0.4 mL). The reaction was heated at 100°C and stirred for 18 h. The crude product was dissolved in a minimum amount of CH_2Cl_2, dried onto silica gel, and purified by column chromatography (5% MeOH in DCM) to afford the *title compound* **154$_{OH}$** (13 mg, 0.04 mmol, 55%) as a white solid.

R$_f$ 0.35 (5% MeOH in DCM);

ATR-FTIR (thin film) ν_{max}/cm^{-1} 2925 (O–H), 2854, 1598, 1441, 1310, 1225, 1151 (S=O), 779, 732, 544;

^{1}H NMR (500 MHz, DMSO-D_6) δ_H 10.47 (s, 1H, H-1), 8.33 (d, *J* = 2.7 Hz, 1H, H-3), 8.27 (d, *J* = 2.3 Hz, 1H, H-11), 7.88 (d, *J* = 8.6 Hz, 2H, H-15), 7.55 (dd, *J* = 8.1, 2.3 Hz, 1H, H-8), 7.48 (d, *J* = 8.6 Hz, 2H, H-14), 7.24 (d, *J* = 2.7 Hz, 1H, H-6), 7.20 (d, *J* = 8.1 Hz, 1H, H-9), 3.24 (s, 3H, H-17), 2.44 (s, 3H, H-12);

^{13}C NMR (126 MHz, DMSO-D_6) δ_C 155.9 (C, C-2), 153.2 (C, C-10), 148.3 (CH, C-11), 144.3 (C, C-4/5/7), 144.0 (C, C-4/5/7), 139.8 (C, C-4/5/7), 138.0 (CH, C-3), 137.9 (CH, C-8), 135.0 (C, C-13/16), 132.7 (C, C-13/16), 130.4 (CH, C-14), 127.2 (CH, C-15), 124.3 (CH, C-6), 122.8 (CH, C-9), 43.4 (CH_3, C-17), 23.2 (CH_3, C-12);

HRMS (ESI^-) *m/z* calcd. for $C_{18}H_{17}N_2O_3S$ $(M + H)^+$ 341.0954, found 341.0955.

Lab notebook reference: PU-02-108

References

1 S. D. Roughley and A. M. Jordan, *Journal of Medicinal Chemistry*, 2011, **54**, 3451–3479.

2 D. Lin, M. Xiao, J. Zhao, Z. Li, B. Xing, X. Li, M. Kong, L. Li, Q. Zhang, Y. Liu, H. Chen, W. Qin, H. Wu and S. Chen, *Molecules*, 2016, **21**, 1374.

3 M. Weber, M. Weber and V. Weber, in *Ullmann's Encyclopedia of Industrial Chemistry*, Wiley, 2020, pp. 1–20.

4 P. Y. Choy and F. Y. Kwong, *Organic Letters*, 2013, **15**, 270–273.

5 D. G. Brown and J. Boström, *Journal of Medicinal Chemistry*, 2016, **59**, 4443–4458.

6 A. R. Surrey and H. F. Hammer, *Journal of the American Chemical Society*, 1946, **68**, 113–116.

7 V. v. Kouznetsov and A. Gómez-Barrio, *European Journal of Medicinal Chemistry*, 2009, **44**, 3091–3113.

8 H. C. Sample and M. O. Senge, *European Journal of Organic Chemistry*, 2021, **2021**, 7–42.

9 A. J. Blacker, G. Moran-Malagon, L. Powell, W. Reynolds, R. Stones and M. R. Chapman, *Organic Process Research and Development*, 2018, **22**, 1086–1091.

10 H. Jin, Z. Gao, S. Zhou and C. Qian, *Synlett*, 2019, **30**, 982–986.

11 A. Stumpf, F. St-Jean, D. Lao, Z. K. Cheng, R. Angelaud and F. Gosselin, *Synthesis (Germany)*, 2020, **52**, 3406–3414.

12 A. P. Krapcho and D. Waterhouse, *Synthetic Communications*, 1998, **28**, 3415–3422.

13 J. F. Rogers and D. M. Green, *Tetrahedron Letters*, 2002, **43**, 3585–3587.

14 J. I. Levin and M. T. Du, *Synthetic Communications*, 2002, **32**, 1401–1406.

15 P. S. Fier and K. M. Maloney, *Organic Letters*, 2016, **18**, 2244–2247.

16 J. F. Bunnett, *Quarterly Reviews*, 1958, **7**, 43–56.

17 S. Rohrbach, A. J. Smith, J. H. Pang, D. L. Poole, T. Tuttle, S. Chiba and J. A. Murphy, *Angewandte Chemie*, 2019, **131**, 16518–16540.

18 J. Meisenheimer, *Justus Liebig's Annalen der Chemie*, 1902, **323**, 205–246.

19 A. J. J. Lennox, *Angewandte Chemie - International Edition*, 2018, **130**, 14898–14900.

20 H. Handel, M. A. Pasquini and Pierre J L, *Tetrahedron*, 1980, **36**, 3205–3208.

21 J. P. Barham, S. E. Dalton, M. Allison, G. Nocera, A. Young, M. P. John, T. McGuire, S. Campos, T. Tuttle and J. A. Murphy, *Journal of the American Chemical Society*, 2018, **140**, 11510–11518.

22 E. E. Kwan, Y. Zeng, H. A. Besser and E. N. Jacobsen, *Nature Chemistry*, 2018, **10**, 917–923.

23 R. Kristianslund, A. Vik and T. v. Hansen, *Synthetic Communications*, 2018, **48**, 2809–2814.

24 S. Xia, L. Gan, K. Wang, Z. Li and D. Ma, *Journal of the American Chemical Society*, 2016, **138**, 13493–13496.

25 P. S. Fier and K. M. Maloney, *Organic Letters*, 2017, **19**, 3033–3036.

26 P. De, Nonappa, K. Pandurangan, U. Maitra and S. Wailes, *Organic Letters*, 2007, **9**, 2767–2770.

27 R. A. Rossi, A. B. Pierini and A. B. Penenory, in *PATAI'S Chemistry of Functional Groups*, John Wiley & Sons, Ltd, 2009.

28 Y. M. Cai, Y. T. Xu, X. Zhang, W. X. Gao, X. B. Huang, Y. B. Zhou, M. C. Liu and H. Y. Wu, *Organic Letters*, 2019, **21**, 8479–8484.

29 N. Zhang, S. R. Samanta, B. M. Rosen and V. Percec, *Chemical Reviews*, 2014, **114**, 5848–5958.

30 F. Yu, R. Mao, M. Yu, X. Gu and Y. Wang, *Journal of Organic Chemistry*, 2019, **84**, 9946–9956.

31 K. H. Chang, W. C. Chao, Y. H. Yang, C. H. Wu, Z. bin Li, H. C. Chen, Y. te Chou, J. an Annie Ho, X. C. Li, Y. C. Peng, Y. C. Liao, K. M. Liu, C. M. Chao and P. T. Chou, *Chemistry - A European Journal*, 2021, **27**, 8040–8047.

32 V. B. Dorn, M. A. Badajoz, M. T. Lockhart, A. B. Chopa and A. B. Pierini, *Journal of Organometallic Chemistry*, 2008, **693**, 2458–2462.

33 T. P. M. Goumans, K. van Alem and G. Lodder, *European Journal of Organic Chemistry*, 2008, **2008**, 435–443.

34 L. B. Jimenez, M. Puiatti, D. M. Andrada, F. Brigante, K. F. Crespo Andrada, R. A. Rossi, R. Priefer and A. B. Pierini, *RSC Advances*, 2018, **8**, 39222–39230.

35 S. I. Al-Khalil, W. R. Bowman, K. Gaitonde, M. A. Marley (née Nagel) and G. D. Richardson, *Journal of the Chemical Society, Perkin Transactions 2*, 2001, **1**, 1557–1565.

36 N. Kornblum, R. E. Michel and R. C. Kerber, *Journal of the American Chemical Society*, 1966, **88**, 5660–5662.

37 D. A. Caminos, M. Puiatti, J. I. Bardagí and A. B. Peñéñory, *RSC Advances*, 2017, **7**, 31148–31157.

38 P. Lidström, J. Tierney, B. Wathey and J. Westman, *Tetrahedron*, 2001, **57**, 9225–9283.

39 M. C. Bagley, V. Fusillo, E. G. B. Hills, A. T. Mulholland, J. Newcombe, L. J. Pentecost, E. L. Radley, B. R. Stephens and C. C. Turrell, *Arkivoc*, 2012, **2012**, 294–313.

40 R. A. Rossi and J. F. Bunnett, *Journal of Organic Chemistry*, 1973, **38**, 2314–2318.

41 T. Niwa, H. Ochiai and T. Hosoya, *ACS Catalysis*, 2017, **7**, 4535–4541.

42 I. Zaborniak and P. Chmielarz, *Materials*, 2019, **12**, 3600.

43 W. Wang, P. Wang, Q. Zhang, P. Du, J. Zhang, H. Deng and H. Jiang, *Tetrahedron*, 2020, **76**, 131477.

44 M. E. Budén, J. I. Bardagí, M. Puiatti and R. A. Rossi, *Journal of Organic Chemistry*, 2017, **82**, 8325–8333.

45 T. Yabuta, M. Hayashi and R. Matsubara, *Journal of Organic Chemistry*, 2021, **86**, 2545–2555.

46 C. G. S. Lima, T. de M. Lima, M. Duarte, I. D. Jurberg and M. W. Paixão, *ACS Catalysis*, 2016, **6**, 1389–1407.

47 N. Petek, H. Brodnik, U. Grošelj, J. Svete, F. Požgan and B. Štefane, *Organic Letters*, 2021, **23**, 5294–5298.

48 G. E. M. Crisenza, D. Mazzarella and P. Melchiorre, *Journal of the American Chemical Society*, 2020, **142**, 5461–5476.

49 S. v. Rosokha and J. K. Kochi, *Accounts of Chemical Research*, 2008, **41**, 641–653.

50 S. Senaweera and J. D. Weaver, *Chemical Communications*, 2017, **53**, 7545–7548.

51 M. Médebielle, J. Pinson and J.-M. Savéant, *Electrochimica Acta*, 1997, **42**, 2049–2055.

52 R. A. Rossi, A. B. Pierini and A. B. Peñéñory, *Chemical Reviews*, 2003, **103**, 71–167.

53 J. M. Saveant, *Journal of the American Chemical Society*, 1992, **114**, 10595–10602.

54 C. Costentin, M. Robert and J. M. Savéant, *Journal of the American Chemical Society*, 2004, **126**, 16051–16057.

55 C. Curti, A. Gellis and P. Vanelle, *Molecules*, 2007, **12**, 797–804.

56 A. N. Santiago, C. A. Toledo and R. A. Rossi, *Journal of Physical Organic Chemistry*, 2003, **16**, 413–419.

57 G. S. Lee, J. N. Bashara, G. Sabih, A. Oganesyan, G. Godjoian, H. M. Duong, E. R. Marinez and C. G. Gutiérrez, *Organic Letters*, 2004, **6**, 1705–1707.

58 R. G. Scamehorn and J. F. Bunnett, *Journal of Organic Chemistry*, 1977, **42**, 1449–1457.

59 R. G. Scamehorn, J. M. Hardacre, J. M. Lukanich and L. R. Sharpe, *Journal of Organic Chemistry*, 1984, **49**, 4881–4883.

60 S. M. Soria-Castro, D. A. Caminos and A. B. Peñéñory, *RSC Adv.*, 2014, **4**, 17490–17497.

61 D. A. Caminos, M. Puiatti, J. I. Bardagí and A. B. Peñéñory, *RSC Advances*, 2017, **7**, 31148–31157.

62 J. F. Guastavino and R. A. Rossi, *Journal of Organic Chemistry*, 2012, **77**, 460–472.

63 P. Vanelle, P. Rathelot, J. Maldonado and M. P. Crozet, *Heterocyclic Communications*, 1994, **1**, 41–46.

64 B. E. Haines and O. Wiest, *Journal of Organic Chemistry*, 2014, **79**, 2771–2774.

65 E. Shirakawa, Y. Hayashi, K. I. Itoh, R. Watabe, N. Uchiyama, W. Konagaya, S. Masui and T. Hayashi, *Angewandte Chemie - International Edition*, 2012, **51**, 218–221.

66 X. Creary, A. F. Sky and G. Phillips, *Journal of Organic Chemistry*, 1990, **55**, 2005–2011.

67 W. D. Guerra, R. A. Rossi, A. B. Pierini and S. M. Barolo, *Journal of Organic Chemistry*, 2016, **81**, 4965–4973.

68 J. Ye, J.-Q. Zhang, Y. Saga, S. Onozawa, S. Kobayashi, K. Sato, N. Fukaya and L.-B. Han, *Organometallics*, 2020, **39**, 2682–2694.

69 Y. Zhou, C. Liu, Z. Shen, B. Dai and J. Chen, *Journal of Organometallic Chemistry*, 2021, **949**, 121932.

70 A. B. Pierini and R. A. Rossi, *Journal of Organometallic Chemistry*, 1978, **144**, C12–C14.

71 Y. Kumar and H. Ila, *Organic Letters*, 2019, **21**, 7863–7867.

72 A. B. Pierini, M. T. Baumgartner and R. A. Rossi, *Journal of Organic Chemistry*, 1991, **56**, 580–586.

73 D. A. Armstrong, R. E. Huie, W. H. Koppenol, S. v. Lymar, G. Merenyi, P. Neta, B. Ruscic, D. M. Stanbury, S. Steenken and P. Wardman, *Pure and Applied Chemistry*, 2015, **87**, 1139–1150.

74 a) J.K. Augustine, R. Kumar, A. Bombrun, A. B. Mandal, *Tetrahedron Letters*, 2011, **52**, 1074-1077.
b) L. de Luca, G. Giacomelli and A. Porcheddu, *Journal of Organic Chemistry*, 2002, **67**, 6272–6274.

75 A. v. Afonin, I. A. Ushakov, D. v. Pavlov, A. v. Ivanov and A. I. Mikhaleva, *Magnetic Resonance in Chemistry*, 2010, **48**, 685–692.

76 M. Arisawa, F. Toriyama and M. Yamaguchi, *Heteroatom Chemistry*, 2011, **22**, 18–23.

77 I. A. Bidusenko, E. Yu. Schmidt, I. A. Ushakov, V. B. Orel, D. Z. Absalyamov, N. M. Vitkovskaya and B. A. Trofimov, *European Journal of Organic Chemistry*, 2020, **2020**, 3480–3485.

78 S. Winstein and F. H. Seubold, *Journal of the American Chemical Society*, 1947, **69**, 2916–2917.

79 Y. L. Liu, Y. J. Ouyang, H. Zheng, H. Liu and W. T. Wei, *Chemical Communications*, 2021, **57**, 6111–6120.

80 N. Takeda, P. v. Poliakov, A. R. Cook and J. R. Miller, *Journal of the American Chemical Society*, 2004, **126**, 4301–4309.

81 Y. Hamada, in *Pyridine*, InTech, 2018.

82 G. Nocera and J. A. Murphy, *Synthesis*, 2020, **52**, 327–336.

83 B. Staels, J. Dallongeville, J. Auwerx, K. Schoonjans, E. Leitersdorf and J.-C. Fruchart, *Circulation*, 1998, **98**, 2088–2093.

84 E. Collantes, S. P. Curtis, K. W. Lee, N. Casas, T. McCarthy, A. Melian, P. L. Zhao, D. B. Rodgers, C. L. McCormick, M. Lee, C. R. Lines and B. J. Gertz, *BMC Family Practice*, 2002, **3**, 10.

85 S. Lucas, *Headache: The Journal of Head and Face Pain*, 2016, **56**, 436–446.

86 S. Joshi, N. Mahanta, D. Fedoseyenko, H. Williams and T. P. Begley, *Journal of the American Chemical Society*, 2017, **139**, 10952–10955.

87 J. F. Areizaga and G. M. Guzmán, *Makromolekulare Chemie. Macromolecular Symposia*, 1988, **20–21**, 77–82.

88 M. R. Heinrich, *Chemistry - A European Journal*, 2009, **15**, 820–833.

89 H. Niehaus and K. Hildenbrand, *Journal of the Chemical Society, Perkin Transactions*, 2000, 947–952.

90 L. R. Hutchings, P. P. Brooks, D. Parker, J. A. Mosely and S. Sevinc, *Macromolecules*, 2015, **48**, 610–628.

91 J. Börgel and T. Ritter, *Chem*, 2020, **6**, 1877–1887.

92 J. Li, J. Chen, R. Sang, W.-S. Ham, M. B. Plutschack, F. Berger, S. Chabbra, A. Schnegg, C. Genicot and T. Ritter, *Nature Chemistry*, 2020, **12**, 56–62.

93 E. M. Alvarez, T. Karl, F. Berger, L. Torkowski and T. Ritter, *Angewandte Chemie - International Edition*, 2021, **60**, 13609–13613.

94 F. Ye, F. Berger, H. Jia, J. Ford, A. Wortman, J. Börgel, C. Genicot and T. Ritter, *Angewandte Chemie*, 2019, **131**, 14757–14761.

95 M. H. Aukland, M. Šiaučiulis, A. West, G. J. P. Perry and D. J. Procter, *Nature Catalysis*, 2020, **3**, 163–169.

96 H. Huang and T. H. Lambert, *Angewandte Chemie - International Edition*, 2021, **60**, 11163–11167.

97 S. You, R. Zhang and M. Cai, *Synthesis*, 2021, **53**, 1962–1970.

98 L. Yang, Z. Huang, G. Li, W. Zhang, R. Cao, C. Wang, J. Xiao and D. Xue, *Angewandte Chemie - International Edition*, 2018, **57**, 1968–1972.

99 Y.-Q. Zou, J.-R. Chen, X.-P. Liu, L.-Q. Lu, R. L. Davis, K. A. Jørgensen and W.-J. Xiao, *Angewandte Chemie - International Edition*, 2012, **51**, 784–788.

100 S. D. Schimler, M. A. Cismesia, P. S. Hanley, R. D. J. Froese, M. J. Jansma, D. C. Bland and M. S. Sanford, *Journal of the American Chemical Society*, 2017, **139**, 1452–1455.